MASTER THESIS

PFAS REMOVAL FROM LEACHATE WATER USING ELECTROCOAGULATION

SANNE SMITH

AFVALZORG

TU Delft

Page left blank intentionally

PFAS removal from leachate water using electrocoagulation

Master Thesis
For the degree of MSc Civil Engineering – Water Management
23-06-2020

Student information:
Sanne Julie Smith
4968883

Committee information:
Prof. dr. ir. T.J. Heimovaara (chair)
Dr. ir. J. Gebert
Dr. ir. S.G.J. Heijman
J. Smit (Afvalzorg)

TU Delft

AFVALZORG

Page left blank intentionally

ABSTRACT

Per- and polyfluoroalkyl substances (PFAS) are common industrial additives that have recently attracted negative attention due to their toxic, bioaccumulative and persistent nature. Discharged wastewater, including landfill leachate, is an important source of PFAS emissions to the environment. Earlier studies suggested that electrocoagulation (EC) is able to reduce aqueous PFAS concentrations by up to 99.6%. In EC, adsorbents are generated in situ by the dissolution of a sacrificial anode, facilitating the removal of various pollutants. However, the effect of additional solutes that are present in leachate on the removal of PFAS was heretofore undetermined. Organic material is an important example of such a co-solute. This thesis therefore aimed to elucidate the effects of dissolved organic matter on the applicability of EC with iron electrodes for PFAS removal from landfill leachate.

The research methodology consisted of an experimental and a computational part. Galvanostatic EC experiments were conducted in an aerated beaker with 500 mL working volume, using iron electrodes with a surface area of 8 cm^2. The pH, voltage and current were measured continuously for 50 minutes. Blank measurements were conducted in a 2 g/L NaCl solution. PFAS removal was tested from 0.25 mmol/L perfluorooctanoic acid (PFOA) and perfluorooctane sulfonic acid (PFOS) solutions at current densities of 12.5 and 25 mA/cm^2, as well as from solutions with a commercial humic acid (HA) source added at 25 mA/cm^2. The removal of HA was also tested separately. Eventually, the removal from real leachate samples was examined. A computer model was constructed in PHREEQC (pH Redox Equilibrium Calculation), a program for modelling chemical processes in water. The model simulates the removal of all tested pollutants based on electrostatic adsorption to a continuously forming surface, associated with the precipitating ferrihydrite.

Model rate constants for O_2 and CO_2 dissolution and Fe(II) oxidation were determined from the results of the blank experiments. Good model fits were obtained for these datasets. HA could be removed completely within 50 minutes at all tested current densities and initial concentrations. PFOA removal was unsuccessful with and without HA as co-solute, with a maximum removal of 17 %. PFOS removal reached 81 % at 25 mA/cm^2, but the removal essentially stagnated after 5 minutes treatment time. The presence of HA did not significantly affect the PFOS removal. Instead, HA removal was retarded by the presence of PFOS. For the real leachate samples, no significant removal of PFAS occurred. Conversely, approximately 20 % PFAS removal was observed after 5 minutes treatment of a leachate sample spiked with 0.15 mmol/L PFOA, perfluorobutane sulfonic acid (PFBS) and perfluorobutanoic acid (PFBA). However, this removal reversed during the remaining treatment time.

The adsorption equilibrium constants were the most important model parameters. These parameters were determined for HA, PFOA and PFOS based on the experimental data. The model fits were good for HA and PFOA removal, indicating that these were indeed mainly removed by electrostatic adsorption. Contrarily, PFOS removal could not be represented accurately by the current model. Instead of stagnating after five minutes, the simulated removal continued to completion. The poor model fit may indicate that the mechanism of PFOS removal extends beyond strict electrostatic adsorption. Instead, charge neutralization of PFOS molecules causing their aggregation or mass transfer limitations in the vicinity of the electrodes could be involved. Further research is needed to explore these possibilities and determine improved equilibrium constants for the relevant adsorption reactions.

In conclusion, this research did not confirm the high PFAS removal efficiency as observed in previous studies. Instead, significant removal of PFOA did not occur and removal of PFOS did not exceed 81 %. Competition effects were not observed in the simultaneous treatment of PFOA and HA. The presence of PFOS impeded the removal of HA, indicating that PFOS was removed preferentially under the current experimental conditions. The established model could simulate most experimental results accurately.

Page left blank intentionally

TABLE OF CONTENTS

Page left blank intentionally

List of Abbreviations

AOX	Adsorbable organic halides
CC	Conventional coagulation
CE	Counter electrode
CFD	Computational fluid dynamics
CMC	Critical micelle concentration
DLCD	Diffusion limited cluster aggregation
DO	Dissolved oxygen
DOC	Dissolved organic carbon
EC	Electrocoagulation
EDL	Electric double layer
EMHS	Electrocoagulated metal hydroxide sludge
HA	Humic acid
Hfo	Hydrous ferric oxide
HPLC-MS-MS	High pressure liquid chromatography – tandem mass spectrometry
LWTP	Leachate water treatment plant
MeFBSAA	Perfluorobutanesulfonylamide(N-methyl)acetate
Nauerna Eff	Effluent water from the Nauerna LWTP
Nauerna Inf	Influent water to the Nauerna LWTP
PFAS	Per- and polyfluoroalkyl substances
PFBA	Perfluorobutanoic acid
PFBS	Perfluorobutane sulfonic acid
PFCAs	Perfluoroalkyl carboxylic acids
PFHpA	Perfluoroheptanoic acid
PFHxA	Perfluorohexanoic acid
PFOA	Perfluorooctanoic acid
PFOS	Perfluorooctane sulfonic acid
PFPeA	Perfluoropentanoic acid
PFSAs	Perfluoroalkane sulfonic acids
PREC	Periodically reversed electrocoagulation
RE	Reference electrode
RLCD	Reaction limited cluster aggregation
rpm	Rounds per minute
TOC	Total organic carbon
WE	Working electrode
Zee. 5	Leachate water from the Zeeasterweg landfill compartment 5
Zee. 8	Leachate water from the Zeeasterweg landfill compartment 8

1. INTRODUCTION

Per- and polyfluoroalkyl substances (PFAS) are a class of highly inert synthetic chemicals that have been widely used in manufactured products[1]. Because they are water and lipid repelling as well as thermally stable, PFAS are common industrial additives[2]. Recently, PFAS have attracted negative attention due to their toxicological effects and bioaccumulative nature. Moreover, monitoring studies have shown that the chemicals are widespread throughout the environment, as PFAS have globally been identified at various concentrations in natural waters, wildlife and human tissue[3]. One of the most important sources for PFAS emissions to the environment is through discharged wastewater[4]. For example, PFAS has been detected in leachate flow from landfills, as PFAS-containing consumer products are subject to degradation in these environments[1,5,6].

Finding an efficient method to remove PFAS from water has become an important quest in the environmental sciences[7]. Existing remediation methods include sorption to activated carbon, membrane filtration and sonochemical destruction[2]. Recently, coagulation has gained interest as an alternative purification method. More specifically, previous studies suggest that electrocoagulation (EC) is able to effectively reduce PFAS concentrations by 99.6%[4]. EC has been applied successfully to remove other pollutants from landfill leachate, such as ammonia and organic matter[8]. Whereas addition of chemical coagulants or flocculants is necessary in conventional coagulation, in EC the adsorbents are generated in situ by the dissolution of a sacrificial anode[9]. Common anode materials include zinc, iron or aluminum and the resultant adsorbents facilitate agglomeration of PFAS molecules by destabilization of their surface charges[4].

Although the three technologies fundamental to EC, namely electrochemistry, coagulation and flotation are well-understood, limited theoretical background is available that describes their integration in EC[9]. Most EC processes are therefore still operated heuristically and a better understanding of the interactions between the underlying mechanisms is essential for designing and operating efficient treatment plants[10]. The development of mathematical models including all involved mechanisms in detail is hard to achieve. Examples of models considering either the detailed electrochemical kinetics,[11] adsorption mechanism[12] or mass transfer[13] exist. However, for most of these models, other processes are simplified or ignored and the inclusion of empirical parameters remains necessary to obtain accurate results. Moreover, mathematical models specific to the removal of PFAS using EC remain to be found.

Another important uncertainty in many PFAS treatment technologies is the effect of co-solutes on the removal[14]. Leachate is a particularly complex matrix that contains an excessive variety of compounds, so a significant effect of co-solutes on the removal is expected[6]. For electrocoagulation, most studies focus on the treatment of demineralized water with added PFAS[4,15]. Herein, PFAS is the only solute and hence competitive removal does not occur. However, research examining the applicability of electrocoagulation for removal of other pollutants has indicated significant competition effects when multiple solutes are present[16]. This leads to the expectation that the presence of additional solutes will affect PFAS removal through electrocoagulation. Particularly the presence of organic compounds may be problematic, as these are structurally similar to PFAS and present in leachate water at high concentrations[17].

The research was conducted in collaboration with Afvalzorg NV, a Dutch waste management company. They manage the storage, treatment and recycling of various types of solid waste[18]. A combination of

various leachate streams and other types of wastewater are treated on their Nauerna site. Part of this water contains high levels of heavy metals and must be treated separately. To this aim, a metal removal unit was constructed, consisting of an aerated electrocoagulation system using iron electrodes and a settling tank[19,20]. The effluent from the electrocoagulation is then treated together with the remaining water in a biological two-stage nitrification-denitrification system. The final effluent water meets all current standards that have been imposed by the responsible government body[21].

Currently, no norms are applied for the discharge of PFAS. Low concentrations of PFAS were detected in the effluent, making it conceivable that discharge limits on the PFAS concentration in the effluent will be introduced in the future. PFAS levels are presently measured by a commercial laboratory using HPLC-MS-MS (high pressure liquid chromatography – tandem mass spectrometry) to enable the possible determination of an appropriate discharge limit[21]. Meanwhile, it is of interest to explore options for PFAS treatment technologies. Possibly, the treatment unit for the removal of heavy metals could also be used to remove PFAS, as electrocoagulation has been applied successfully for PFAS removal from leachate[1]. To assess this option, an improved understanding of the effect of organic material on the electrocoagulation performance is necessary.

This study therefore aimed to assess the effect of dissolved organic material on the removal efficiency of PFAS from landfill leachate. The main research question is *"What is the influence of organic co-solutes in landfill leachate on the mechanism of aqueous PFAS removal by electrocoagulation with iron electrodes and how can this best be represented in a computational model?"* The research aim thus consisted of two parts: to determine the competition effect between PFAS and organic solutes during EC and to simulate this process in a computational model. The main hypothesis was that organic co-solutes compete with PFAS for the generated adsorption sites and thereby impede the PFAS removal. Accordingly, the model focused on the adsorption process and all additional aspects were simplified.

The methodology consisted of an experimental and a computational part. Experimental data were collected to verify the model and determine fits for important model parameters. As this was the first modelling study specific to PFAS removal with electrocoagulation, it was exploratory in nature. The research was intended to contribute to a deeper understanding of the mechanisms involved in PFAS removal through electrocoagulation. The thesis is structured as follows: first, a literature review on the topic is provided. Second, the research objective is outlined together with the followed methodology. Then, the results are presented and discussed, and finally conclusions are drawn.

2. Literature Review

2.1 PFAS

Perfluoroalkyl and polyfluoroalkyl substances (PFAS) have unique properties that make them ideal for certain applications, such as creating water-resistant clothing, stain-free fabric and oil-resistant coatings. PFAS are anthropogenic organic chemicals that consist of a carbon backbone with fluorine functional groups. Typically, PFAS have a charged functional moiety at the end of their long fluoroalkyl chain, making them surface-active. The two most well-known PFAS are perfluorooctanoic acid (PFOA) and perfluorooctane sulfonic acid (PFOS), see Figure 1[3]. However, also aromatic and longer or shorter chain-length compounds exist, such as perfluorobutane sulfonic acid (PFBS) and perfluorobutanoic acid (PFBA)[22]. The desirable properties of PFAS originate from the strong carbon-fluorine bond, which renders the alkyl moiety extremely hydrophobic and thus essentially immune to hydrolysis. Fluorinated hydrocarbons are exceptionally stable, such that PFAS are also highly persistent in the environment[3].

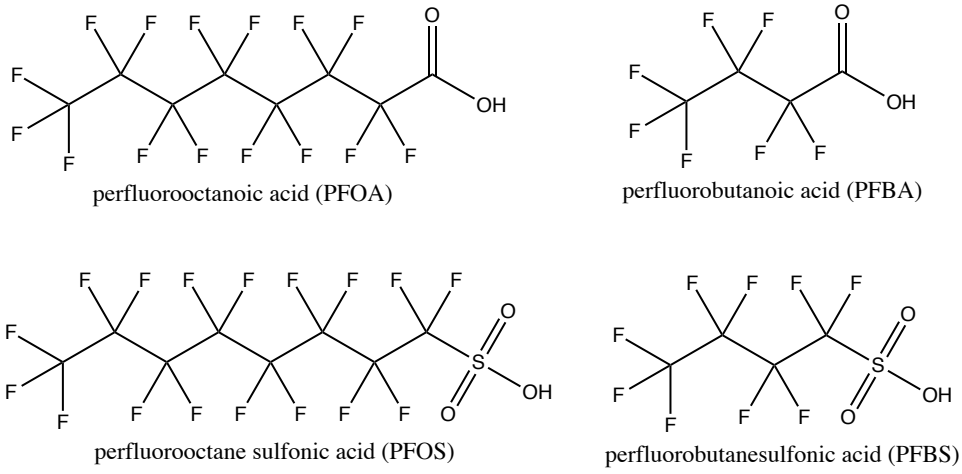

Figure 1: Different types of PFAS. A distinction is commonly made between perfluoroalkane sulfonic acids (PFSAs), such as PFOS and PFBS, and perfluoroalkyl carboxylic acids (PFCAs), such as PFOA and PFBA.

Several types of PFAS have been classified as chemicals of concern, as they are persistent, bioaccumulative and toxic. Based on laboratory animal testing, adverse effects associated with exposure to PFAS include tumor induction, developmental toxicity, immunotoxicity and endocrine disruption[23]. However, an accurate human health risk assessment remains to be completed[24]. The biological half-life of PFAS in the human body is over a factor 100 higher than that in common laboratory animals[25]. Moreover, the fact that the mechanism of toxic action of PFAS has not been identified with certainty constitutes an important issue[26]. Nonetheless, tolerable daily intake doses have been estimated and regulatory guidelines to minimize environmental exposure have been introduced[27].

The chemicals are widespread throughout the environment and have even been found in remote and pristine locations[22]. Treatment methods to effectively remove or degrade PFAS exist, but are often expensive or of limited applicability. Destructive technologies are often unsuccessful due to the high stability of perfluorinated groups. Nonetheless, both biodegradation and physiochemical methods have been reported to achieve (partial) destruction of some PFAS[28,29]. An issue with most destructive methods is their requirement for small volume, highly concentrated waste streams. Therefore, in order to successfully decompose PFAS, pretreatment steps are required[28]. Existing technologies must be

optimized to decrease PFAS concentration in wastewater streams and the environment below their target levels[22].

2.1.1 Aqueous speciation of PFAS

An important property of PFOS and PFOA as compared to regular organic matter is their amphiphilic nature. PFOS and PFOA are surfactants; they have a polar headgroup and an apolar fluorinated carbon tail. Hence, they reduce surface tension at interfaces such as the water-air interface and tend to accumulate there[30]. Moreover, above their critical micelle concentration (CMC) they form micellar structures in water. On mineral surfaces, they can form hemimicelle structures at concentrations as low as 0.001 to 0.01 of their CMC[31,32]. The formation of these surface aggregates may increase the adsorption efficiency of PFAS[28]. The CMC of PFOS depends on solution characteristics such as temperature and ionic strength, but values between 0.8 and 8 mM have been reported[31–33]. If formation of micelles occurs, adsorption of counterions onto the micelle surface or even penetration into the micelle may occur as well[34].

2.1.2 PFAS in landfill leachate

Although the industry has been urged to stop the usage of PFAS in products, it is expected that the presence of PFAS in landfill leachate will continue to be an issue for the foreseeable future. PFAS are persistent molecules and the products will be in circulation for a long time to come. Municipal as well as industrial waste is disposed to landfills, where degradation processes lead to the formation of various byproducts. When rainwater percolates through the landfill, leachate is formed in which these pollutants accumulate. Moreover, waste degradation may lead to liquid formation, thereby also creating leachate[35]. Leachate water is collected and treated before discharge to the environment.

PFAS concentrations may increase in the future because of deliberate disposal of PFAS-rich waste streams to landfills, where the PFAS is contained indefinitely. This method of discharging PFAS is called immobilization and is subject to many regulations on the maximum concentrations in the leachate[14]. Generally, treating PFAS in landfill leachate is considered highly challenging due to the complex background matrix of this solution. In addition to PFAS, leachate contains many other types of pollutants, which makes the water composition extremely diverse[6].

2.2 ELECTROCOAGULATION

Electrocoagulation has been applied for the removal of a variety of compounds from different sources of wastewater. Examples include phosphate[36,37], ammonia[8], humic substances[38], clay particles[10], fluoride[12], arsenic[39] and heavy metals[9,40]. A wide range of water sources has been tested, such as industrial wastewater[9], synthetic wastewater[36], leachate[8], municipal wastewater[37], groundwater[39] and potable water[12,38]. The removal efficiency of EC varies per pollutant and also depends on the background matrix of the removal medium. Recently, electrocoagulation has gained interest as a treatment technology for emerging contaminants such as PFAS[1,4,15,41].

Electrocoagulation may be a cost-effective and efficient mitigation method for PFAS removal, as it is simple to operate and has low maintenance costs[15]. However, EC treatment might be inhibited due to the competition for adsorption sites and complexation between organic matter and PFAS[6]. Electrocoagulation has been used successfully to remove PFAS from deionized water on laboratory scale. These results indicate that EC could potentially be used to remove PFAS from industrial wastewater streams[4,15]. Moreover, bench scale experiments with landfill leachate have confirmed that

EC can be efficient in removing various types of PFAS from this water[1]. To better understand and engineer the effectiveness of EC in PFAS removal, it is essential to gain more insight into the fundamental mechanisms of EC. To this end, a basic understanding of colloidal systems and particle stability is necessary.

2.2.1 Mechanisms of pollutant removal in electrocoagulation

EC removes particles from water by destabilizing the repulsive forces that keep the particles suspended. Larger particles that can be removed more easily will form due to attractive forces. The repulsive forces that keep colloidal particles in suspension originate from similar electrical charges on the particle surface. Oppositely charged particles neutralize this charge. These oppositely charged ions are attracted to the colloid surface, forming an electric double layer (EDL), see Figure 2. The layer of ions closest to the particle is referred to as the Stern layer. The shear plane defines the region where the fluid becomes mobile and is often assumed to be identical to the Stern surface. The potential at the outer limit of the Stern layer is called the zeta potential and gives a measure of the magnitude of repulsion between colloidal particles. Generally, suspended particles with a higher absolute zeta potential than 30 mV are considered stable and thus unsusceptible to coagulation[9].

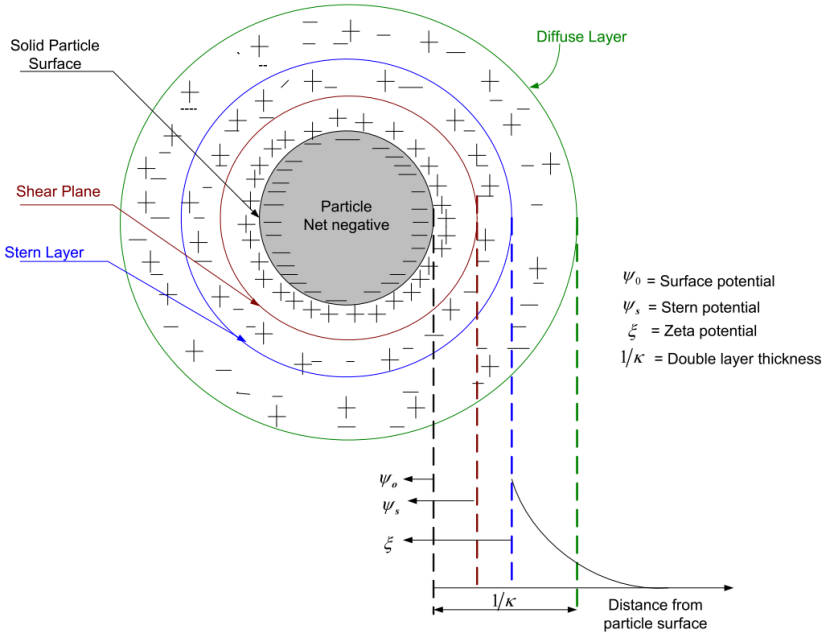

Figure 2: Illustration of the electric double layer[9]. The layer is made up of an inner Stern layer and outer diffuse layer, where the shear plane is often assumed identical to the Stern layer.

To destabilize colloidal particles, the attractive forces must become stronger than the repulsive forces. In electrocoagulation, this is achieved by creating charged ions through oxidation of the metal anode. The anodes thus need to be periodically replaced, as they dissolve in the EC process. Water is reduced into hydrogen gas and hydroxyl ions at the cathode, and these hydroxyl ions can combine with the metal ions to form metal hydroxides. The formation rate of these species is directly related to the applied current intensity, as their formation is limited by electron transfer. After their formation, metal ions and metal hydroxides then act as coagulants in the coagulation process[42,43]. The solution pH is an important factor in EC treatment, as it determines the speciation of the formed metal ion complexes[44]. An overview of the reactions that take place in the EC treatment is given in Figure 3.

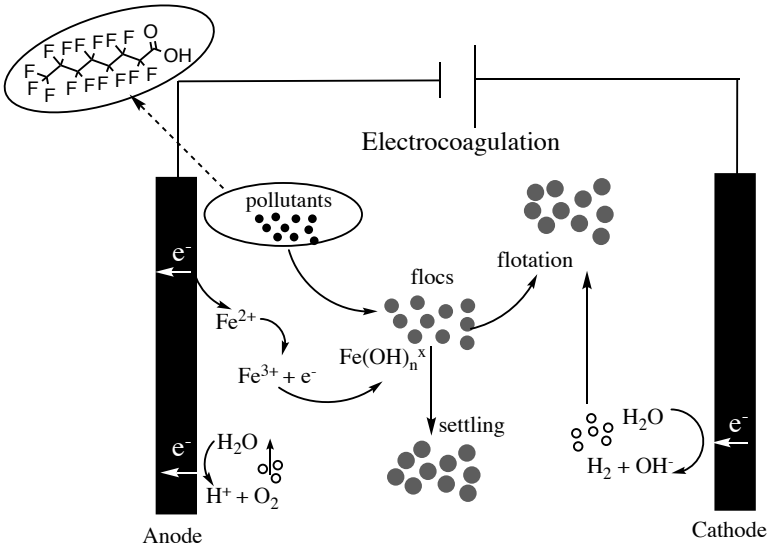

Figure 3: Overview of electrocoagulation process

Metal cations diminish the repulsive forces either by double-layer compression, thereby decreasing the zeta potential, or by neutralization of the surface charges. The particles can hence coagulate to form larger flocs. On the other hand, metal hydroxides are generally poorly soluble and thus precipitate readily by themselves. Water soluble pollutants adsorb to the precipitates, which is referred to as sweep coagulation[42,43]. The formed flocs are subsequently removed by filtration, sedimentation or flotation[9]. Flotation can be promoted by the formation of hydrogen gas at the cathode[16]. The removal rate of these particles is a complex balance between electrochemical kinetics of coagulant formation, mass transfer of the ionic species and fluid dynamics of the reactor[13]. In different systems, different factors may be limiting.

Mass transfer of PFAS molecules to the floc surface or of the flocs towards each other may be limiting in certain regimes and can be improved by altering the stirring speed of stirred systems. However, physical floc breakage occurs at excessively high speeds and hence a balance must be found[4]. Another important factor is the addition of electrolyte to increase conductivity and prevent electrode passivation. This leads to higher rates of anode dissolution and accordingly higher PFAS removal, at the cost of more frequent replacements of the anodes. Finally, the sorption of PFAS onto the metal flocs can be driven by different mechanisms, including electrostatic interaction, hydrophobic interaction, ligand exchange, and hydrogen bonding[4]. Which mechanism occurs depends on the system under investigation[4,15].

The adsorption mechanism may differ depending on which anode material is used. As aforementioned, studies using Zn anodes find hydrophobic interactions to be the main adsorptive driving force. Ligand exchange and electrostatic attraction are deemed less significant[41,45]. Moreover, sweep coagulation and adsorption bridging of zinc hydroxide flocs are mentioned as potential mechanisms[41]. These results are explained by the hydrophobic nature of the $Zn(OH)_2$ flocs on which the PFAS molecules coagulate[15].

Conversely, when iron electrodes are used and ferrihydrite flocs form, hydrophobic interactions and ligand exchange are found unimportant. Here, electrostatic attraction is established as the main driving force for adsorption[4]. Also the presence of co-solutes, the solution pH or other factors may impact the dominant adsorption mechanism[33].

2.2.2 Important factors in the operation of electrocoagulation systems

An important factor in EC design is the electrode arrangement. Generally, EC systems are constructed using a water flow through the space between several plate electrodes. This flow can be either horizontal or vertical, and the electrode arrangement can be monopolar or bipolar. A monopolar arrangement has all anodes connected to each other, as well as all cathodes. In bipolar systems, the power supply is only connected to the outermost electrodes and the current flow polarizes the intermediate electrodes[42]. A schematic overview of these arrangements is given in Figure 4. The current dosage is another example of an important operating parameter that can be controlled directly. Current density affects the rate of coagulant dosage and gas generation, so it impacts mixing as well as mass transfer at the electrodes[42].

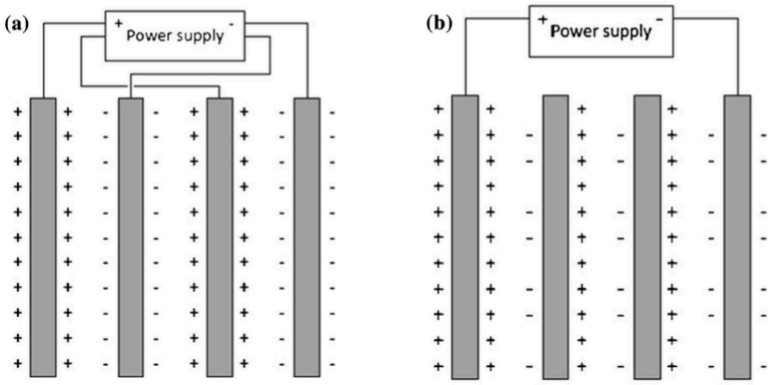

Figure 4: Electrode arrangement in EC. a) monopolar; b) bipolar[42]. Afvalzorg uses a monopolar arrangement in their pilot treatment system.

Although less sludge is formed in electrocoagulation than in conventional chemical coagulation, disposal of this sludge still poses a serious problem. A wide range of toxic compounds is separated from the water and collected in the EC sludge, such as heavy metals and PFAS[42]. Proper management of this sludge is therefore essential. Conventionally, the produced electrocoagulated metal hydroxide sludge (EMHS) is discharged back to the landfill. However, as PFAS originates from the leachate, this would cause accumulation of such substances within the landfill, potentially causing excessive PFAS concentrations in the future. Incineration of the EMHS is another management option[15]. Alternative applications of the EMHS include use as construction material for building blocks, yielding a good quality material[46]. However, also here the remaining presence of PFAS might be problematic.

2.2.3 Research fields related to electrocoagulation

As an understanding of electrochemical processes is crucial to comprehend electrocoagulation, electrochemical research is essential. The performance and treatment efficiency of an electrocoagulation system depends largely on electrochemical factors such as the amount and speciation of dissolved metal[42,47]. An important theoretical control variable is the pe, which is the log of the electron activity and controls the redox conditions in the system[48]. In electrochemical research, the investigated electrochemical process takes place at the working electrode (WE), which can be

placed under potentiostatic or galvanostatic control. In potentiostatic mode, the potential between the WE and a reference electrode (RE) is kept constant. Conversely, under galvanostatic control, the current flow between the WE and the counter electrode (CE) is held constant[49].

In electrocoagulation experiments, the RE and CE are combined in one electrode and galvanostatic electrolysis experiments are used to evaluate the amount of anode material that dissolves, which can be compared to theoretical values calculated from Faradays law[47]. For accurate control of the current density at the working electrode without requiring an excessive voltage, dosing of an electrolyte is necessary. Finally, thorough polishing of the electrodes prior to the experiment, accurate calibration of the cell and identification of the detection limit of the technique are all examples of good practice in electrochemical experiments[49].

In addition to electrochemistry, also colloidal stability and coagulation mechanisms are fundamental in the electrocoagulation process. Conventional coagulation doses metal salts to destabilize colloidal pollutants such that they coagulate. Commonly, jar tests are executed to assess the optimum conditions for conventional coagulation treatment. The coagulation reaction is carried out in a number of stirred jars, each at e.g. a different coagulant concentration or a different pH. Comparisons on the settling efficiency or pollutant removal can be made. Although jar tests are highly useful for finding optimum conditions for practical coagulation, they do not provide detailed mechanistical information[50].

If charge neutralization is the prevailing mechanism of particle destabilization, electrokinetic measurements may be valuable. It can be hypothesized that optimum coagulation regimes occur at the isoelectric point, e.g. at zero zeta-potential. The isoelectric point can be identified using electrophoresis, where suspended charged particles move through a fluid due to the influence of an electric field. Charged colloids move to the positive pole if they are negatively charged and vice versa. The equilibrium position of the particle is a direct indication of its isoelectric point. However, commonly the isoelectric point does not coincide with the optimum conditions as found from jar tests, indicating that destabilization is usually more complex than simple charge neutralization[50]. Instead, hydrophobic interactions or van der Waals interactions may be involved.

2.3 PFAS REMOVAL BY ELECTROCOAGULATION

The removal of PFAS using electrocoagulation has been investigated on bench-scale in five studies. First, a 6 L electrolytic cell with bipolar aluminum electrodes was efficient in the removal of various PFAS from landfill leachate water. The effects of reaction time, plate distance, current density and plate amount were investigated[1], and their relative importance was found to decrease over the order as stated. Second, removal of six types of PFAS from deionized water was achieved using iron, magnesium, aluminum and zinc plates[15]. Of these anode materials, zinc was most efficient and this material was tested further in a 0.4 L cylindrical reactor with a 304 stainless steel cathode. Moreover, sorption mechanism and kinetics were investigated and fitted to a pseudo-second order model in the same study[15].

Third, the efficiency of PFOA and PFOS removal from deionized water in a 0.5 L effective volume electrolytic cell was compared between iron and aluminum electrodes[4]. The iron anode proved to be more effective towards PFAS removal than aluminum. The optimal current density, stirring speed and electrolyte type were determined. Electrostatic adsorption was suggested to be the main removal mechanism under the applied experimental conditions in this study, because a correlation between the

removal efficiency and the pKa values of different PFAS species was found. The removal efficiency decreased with increasing pKa values, and since a lower pKa value implies a higher dissociation degree of the PFAS into ions, electrostatic adsorption was deemed essential in the removal[4].

Finally, periodically reversed electrocoagulation (PREC) was used with mutual combinations of Fe, Al and Zn electrodes in a 0.4 L reactor. In PREC, the roles of the anode and cathode electrode are periodically reversed. This set-up was tested with artificial PFOA solutions to determine optimal conditions, after which these optimal conditions were applied successfully for PFOA removal from contaminated groundwater[41]. Recently, a similar study was carried out to examine the removal of PFSA's, also using different combinations of electrode materials. Both synthetic and natural groundwater samples were tested in this study[51]. No literature describing electrocoagulation for PFAS removal on pilot or industrial scale has been found.

2.4 Electrocoagulation with iron electrodes

As iron electrodes were found most efficient towards PFAS removal by Yang *et al.*[4] and Afvalzorg also uses iron electrodes in their reactor, this was chosen as the electrode material in the current study. The consensus in literature is that ferrous iron (Fe^{2+}) is formed during electrocoagulation with iron electrodes[52–54]. This ferrous iron is subsequently oxidized by dissolved oxygen (DO) to ferric iron (Fe^{3+}), which precipitates as iron hydroxides. The oxidation step is faster at high pH and high DO concentration[55]. Various rate equations for this oxidation step have been described in literature. First, Equation 1 indicates the different rates associated with the various aqueous Fe(II) complexes. Morgan and Lahav presented this as a heuristic model for the oxidation kinetics of Fe(II) by dissolved O_2[55]. It mainly serves to indicate the high sensitivity to pH and the orders of magnitude of the different kinetic constants are indicated to differ by a factor of 10^5.

$$\frac{-dFe^{2+}}{dt} = DO * (k_0[Fe^{2+}] + k_1[Fe(OH)^{+}] + k_2\left[Fe(OH)_2{}^{0}(aq)\right] + k_3[Fe(OH)_3{}^{-}])$$

Equation 1

Lakshmanan *et al.* described the generation rate of $Fe(OH)_3$ from Fe(II) in electrocoagulation as a function of pH and DO and Fe(II) concentration[52]. Here, the oxidation of Fe(II) to Fe(III) and the precipitation of $Fe(OH)_3$ are integrated in one rate law. Finally, Equation 2 is the oxidation rate as used in example 9 of PHREEQC[56] and as described by Singer and Stumm[57]. Here, ACT_i is the activity of species i and p_{O2} is an indication of the partial pressure of O_2. Furthermore, at an oxygen partial pressure of 0.2 atm, k_0 and k_1 are given as 2.91e-9 and 1.33e12, respectively[57]. Which of these equations is most useful in the construction of a PHREEQC model that simulates electrocoagulation remains to be determined.

$$\frac{dFe(III)}{dt} = \left(k_0 + k_1 * ACT_{OH-}{}^{2} * p_{O_2}\right) * ACT_{Fe(II)}$$

Equation 2

The characteristics of metal hydroxide flocs formed in electrocoagulation are different compared to flocs generated via conventional coagulation (CC)[58]. A detailed comparison of floc characteristics from EC and CC has only been found for aluminum, but this indicates that vital differences in the mechanism of floc formation exist between the two techniques[59]. The types of crystal or precipitate formed in EC with iron electrodes depend heavily on solution pH, dissolved oxygen and current dosage[53]. In

electrocoagulation, Fe^{2+} is formed by dissolution of the anode. After the previously described oxidation of Fe^{2+}, Fe^{3+} can form different types of precipitating hydrous ferric oxides. The oxidation step is significantly more probable during EC than during CC[52]. Hence, characterization of the adsorption behavior on flocs formed via CC is most likely less useful towards modelling adsorption on EC flocs.

In addition to micelles and micellar species, PFAS molecules also form aqueous complexes with dissolved metal ions[60]. Both ferrous (divalent) and ferric (trivalent) iron cations can form these complexes, although the effect is greater with ferric iron due to its higher Lewis acidity[61]. The complexation between ferric iron and PFAS is hypothesized to aid its removal in electrocoagulation. Likewise, complexation between divalent ions and a negatively charged PFAS headgroup can lead to a bridging effect with a negatively charged surface. Accordingly, the divalent ferrous iron could promote the adsorption removal of PFOS and PFOA onto ferric hydroxide flocs. This hypothesis is supported by the pH optimum for removal at weakly alkaline conditions, where ferrous and ferric iron coexist[4].

2.5 Competitive adsorption

Generally, most literature research into the mechanism of electrocoagulation for wastewater treatment is based on laboratory scale experiments using synthetic wastewater. The usefulness of these data towards practical applications of EC is limited, as real wastewater is different from pollutant solutions in deionized water. Leachate water contains many different contaminants, including humic acids and anthropogenic compounds[5,62]. The limited information regarding the influence of these dissolved substances on electrocoagulation performance forms an important knowledge gap[63]. However, humic acid has been shown to have a significant retardation effect on the sorption of PFAS on boehmite (AlOOH)[32]. If adsorption is the prevailing removal mechanism, it can hence be hypothesized that organic co-solutes negatively impact removal rates because of competitive adsorption.

Competitive adsorption has been shown to occur in the treatment of metal-bearing wastewaters. The presence of phosphate, silica or humic acids negatively impacts the removal of arsenic in electrocoagulation set-ups[16]. Moreover, also in fluoride removal via electrocoagulation, competition between fluoride and sulfate or chloride for adsorption on aluminum hydroxide has been observed[16]. Competitive sorption experiments with different types of PFAS on zinc hydroxide flocs generated via electrocoagulation showed that molecules having longer C-F chain-lengths were preferentially adsorbed. These results indicate that hydrophobic interaction is determining for the sorption capacity of zinc hydroxide flocs[15].

Because most laboratory scale investigations on the applicability of electrocoagulation for removal of PFAS from water were conducted using deionized water, competition effects are not included in the results[4,15]. As leachate water usually has high concentrations of organic and inorganic compounds, competition for adsorption sites will most probably affect the removal efficiency of PFAS[17]. Specifically, natural organic material such as humic substances could possibly be adsorbed competitively, due to the structural similarity of some of their functional groups to the PFAS headgroups. Competition and complexation between humics and PFAS is expected to significantly limit the applicability of EC for PFAS removal[6]. Moreover, the presence of humic acids reduces iron precipitation[64]. Additionally, applying electrocoagulation to wastewater with high humic acid content may result in the formation of chlorinated compounds such as trihalomethanes, which are toxic[22,42].

On the other hand, the presence of additional pollutants could also benefit treatment performance. Specifically, the removal of arsenic by coagulation processes is generally aided by the presence of calcium ions due to increased iron precipitation[64]. Additionally, the presence of radical-forming compounds may enhance the removal of pollutants in electrocoagulation[65]. The effect of co-solutes present in leachate water on EC performance is currently unknown. This impact must be assessed in order to design an efficient treatment system. As the leachate water is treated biologically for nitrogen removal, the EC unit can be placed either before or after this biological system. Since the water quality of the biologically treated effluent differs from the untreated leachate, the EC removal efficiency is expected to differ as well[66].

2.6 Organic matter and humic substances

Humic substances are a class of organic molecules originating from the decomposition of plant, animal or microbial material[67]. In landfill leachate, humic substances are the major source of dissolved organic carbon[68]. Humic substances are extremely heterogeneous, as their molecular size, chemical functionality and elemental composition vary widely. A classification can be made into humic acids (HA) and fulvic acids. Whereas fulvic acids are soluble at all pH values, humic acids precipitate at low pH. The carbon, oxygen and hydrogen contents of humics are generally around 50 %, 30-40 % and 5 %, respectively, with the rest of the mass made up by nitrogen, sulfur and phosphorus. The chemical structure of humic acid includes various functional moieties[67], as illustrated in Figure 5. As humic substances are mixtures of compounds, their molecular weight is an average value[67].

Humic substances absorb light in the ultraviolet and visible range, hence UV-VIS spectroscopy can be used to approximate humic acid concentrations in a sample. However, absorption is strongly influenced by cation binding and by pH. As the pH increases and protons dissociate, absorption increases. Moreover, binding of some metals, especially iron, intensifies the UV absorption. Complex formation of metal ions with a humic substance as ligand is a well-documented phenomenon and is often defined by at least one shared electron pair between the ligand and the metal. Additionally, also adsorption of humic substances onto metal oxide surfaces is possible, thereby decreasing the UV adsorption. Fluorescence measurements are another method for HA concentration quantification, but also fluorescence is quenched by iron binding[67].

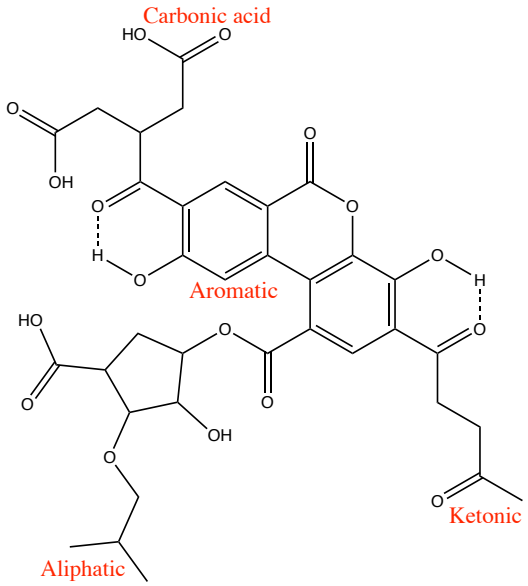

Figure 5: Typical functional moieties in a humic substance

2.7 Modelling of electrocoagulation

As aforementioned, modelling electrocoagulation systems completely and in detail is extremely complex. In literature, different approaches to modelling EC are reported. A distinction is made between statistical models and models based on knowledge. The first class aims at finding optimum operating conditions of an EC system by varying certain design parameters. To this end, a nonlinear regression model is constructed that can be optimized to find the ultimate response. In contrast,

modelling based on knowledge incorporates mechanistical or phenomenological information in the model formulation. Phenomenological models describe the global EC process using kinetics, whereas mechanistical models include the full mechanism of one of the processes contributing to EC[40].

The first class of mechanistical models incorporates the complete electrochemical reactions. The potential difference applied to the electrodes creates an overpotential, which leads to a distortion of the equilibrium and the electrochemical dissolution of the anode. This dissolution rate can be calculated from Faradays law[11,40]. From the reaction rates of the oxidation and reduction reaction, a current density can be calculated. For EC limited by overpotential, the cell potential and current density suffice to give an accurate description of the process rate. However, for large overpotentials, mass transfer in the boundary layer of the electrodes is limiting. This mass transfer relates to diffusion, convection and electronic migration and can be described by the Nernst-Planck equation[40].

Another mechanism involved in EC is adsorption, which can be modeled using either adsorption isotherms or kinetic information. Under thermodynamic control, the Freundlich and Langmuir isotherm models are well-known examples of adsorption models[40]. These isotherm models have successfully been applied to model PFOS adsorption onto different sorbents[69]. Predicting removal efficiency using adsorption kinetics is generally achieved by assuming pseudo first or second order kinetics. Alternatively, variable-order-kinetic models combine isotherm information with Faradays law for metal dissolution over time. This approach is especially efficient for systems where mass transfer is non-limiting[12,40].

$$r_M = \frac{I}{FZV}\varepsilon_c$$

Equation 3: Faradays law[11]

$$N_i = C_i u - Z_i \mu_i F C_i \nabla\varphi - D_i \nabla C_i$$

Equation 4: (Nernst-Planck equation)[40]

Faradays law (Equation 3) represents the dissolution rate (r_m) in mol/(m^3s) of the metal anode, with *I* the applied current intensity (A), *Z* the valence number of the metal, *F* Faraday's constant (94,485C/mol), *V* the solution volume (m^3) and ε_c the current efficiency, which is sometimes neglected[11]. Equation 4 gives the flux of chemical species *i* due to convection, electromigration and diffusion. Here, Z_i is the charge number, *u* the velocity, μ_i the mobility, D_i the diffusion coefficient and ∇C_i and $\nabla\phi$ the concentration and potential gradient, respectively[40]. These equations are fundamental to mechanistic modelling of the electrocoagulation process.

On a molecular scale, electrostatic adsorption models are strongly related to EDL theory. In the vicinity of the surface, ion activities change proportionally to a Boltzmann factor that defines the electrostatic affinity[70]. Equation 5 gives the surface activity (a_i) as a function of the bulk activity ($a_{i,\infty}$), where Ψ(x) is the electrostatic potential at a distance x from the surface, R the gas constant and T the absolute temperature[70,71]. This equation can be substituted in the Poisson-Boltzmann equation (Equation 6, here given in 1 dimension for N different kinds of ions) that describes the gradient in potential. Here, ϵ is the dielectric constant and ϵ_0 the dielectric permittivity of vacuum[71]. Explicit integration of the Poisson-Boltzmann equation is used to calculate the composition of the EDL and hence determine which species are adsorbed[56].

$$a_i(x) = a_{i,\infty} \cdot e^{\frac{-Z_i F \psi(x)}{RT}}$$

Equation 5

$$\frac{d^2\psi(x)}{dx^2} = -\frac{F}{\epsilon\epsilon_0}\sum_{i=1}^{N} Z_i(a_i(x) - a_{i,\infty})$$

Equation 6: Poisson-Boltzmann Equation

In general, chemical equilibria can be described in laws of mass action. For the elementary reaction given in Equation 7a, the equilibrium composition is given by an equilibrium constant K, as defined in Equation 7b, with a_i the activity of species *i*. K can be calculated from the reactions Gibbs energy change according to the second part of Equation 7b[72]. For adsorption reactions, the electrostatic energy change $\Delta_r G_{el}$ is given by Equation 8. Hence, the equilibrium constant describing a strictly electrostatic adsorption equilibrium is given by Equation 9[73]. These equilibrium or mass action law constants are important parameters in surface complexation modelling, as will be explained in section 2.9.1[74]. They are typically determined empirically by fitting experimental data.

a. $A + B \leftrightharpoons C$ b. $K = \frac{a_C}{a_A a_B} = e^{-\frac{\Delta_r G}{RT}}$

Equation 7a and b: Equilibrium constant for a general elementary reaction

$$\Delta_r G_{el} = \sum \frac{\Delta Z_i F}{RT}\psi_i$$

Equation 8

$$K_{el} = e^{-\sum \frac{\Delta Z_i F}{(RT)^2}\psi_i}$$

Equation 9

Flocculation modeling generally makes a distinction between two flocculation regimes: diffusion-limited cluster aggregation (DLCD) and reaction-limited cluster aggregation (RLCD). In DLCD, mass transfer of the smaller flocs towards each other forms the rate limiting step. Conversely, in RLCD the repulsive forces between the particles are still large and many collisions may be required before they coalesce[40]. Flocculation modelling is not widely applied in EC, although the fractal dimension (D_f) that indicates which flocculation regime occurs has been introduced in EC studies to analyze floc growth[40]. Conversely, flotation and settling rates have been included in certain models[10]. Nonetheless, also these models remain too empirical to adequately predict general flocs/sludge removal in EC reactors[40].

Complexation models describe complexation of suspended organic matter by metal hydroxides. From the adsorption equilibrium law and the mass balance of suspended matter, the suspension concentration over time is calculated. These models are especially efficient for simulating mixed effluents by combining multiple single-species effluents, as this gives reasonable results[40]. Alternatively, the interaction between dissolved organic material such as humic acids and metal ions can be evaluated on molecular scale by performing molecular dynamics simulations. These studies provide detailed insights into the mechanism of complex formation between the types of substances[75].

Computational fluid dynamics (CFD) simulations give adequate characterizations of the main local process features of EC reactors, such as velocity profiles, electrode reaction rates and voltage. Mass

and energy conservation laws are combined with reaction rates and equations for ion transport involving an electric field. This system of equations is solved numerically to give a current and potential distribution in the reactor. CFD simulations can successfully describe complex flow patterns in EC cells, and the analysis of mass transfer and reaction kinetics gives valuable information to improve cell design and increase performance. However, CFD is computationally expensive and it requires a high level of expertise for model construction and analysis of simulation results[40].

2.8 Competitive adsorption models

Many methods exist to model the interaction between organic substances and ions. Specifically, the NICA-Donnan model is often used to model the interaction of humic substances with ions[76–79]. The Donnan model includes nonspecific electrostatic adsorption by assuming a 'Donnan volume' that surrounds organic particles. Inside this volume, the charged groups inside the particle are compensated by external ions. The characteristic potential (comparable to the zeta-potential as described above) is equal to the potential within this volume and drops to zero in the bulk. Competition for adsorption sites is included using the NICA (non-ideal competitive adsorption) model, which assumes that each ion has its own stoichiometry with the reference sites, but this stoichiometry is independent of the surface coverage. The occupation of the reference sites affects both the local and the overall binding of ions[70,80].

The NICA-Donnan model is quite successful in modelling metal ion binding to humic substances. As humic acids (HA) are present in landfill leachate,[62] and they can be removed by electrocoagulation,[81] the model could potentially serve to simulate EC treatment of landfill leachate. To this end, it should be realized that in EC the common understanding is that organics adsorb to metal hydroxide flocs, rather than vice versa. Moreover, usages of the NICA-Donnan model to simulate interactions between PFAS and metal ions have not been found in literature. Nonetheless, the ability to include site competition between PFAS and HA or other natural organic matter should be recognized. Accounting for the presence of organic matter in the leachate and including the resulting possible competitive adsorption could create more comprehensive models[80].

Another model describing ion adsorption while considering competition for sites is the CD-Music (charge distribution – multi site complexation) model. Here, surface charges are considered distributed over the interfacial region. Conversely, ion-pair formation in the solution is evaluated using the more conventional framework of point-charges. The CD-Music model enables an accurate description of adsorption and its dependency on pH, concentration and conductivity[73]. Moreover, as it has been applied to adsorption on metal hydroxide surfaces, the applicability to PFAS removal via electrocoagulation is expected to be higher than that of the NICA-Donnan model.

2.9 PHREEQC

Different programs for modelling chemical processes in water exist. Examples include Orchestra (Objects Representing Chemical Speciation and Transport) and PHREEQC (pH Redox Equilibrium Calculation)[56,82,83]. Orchestra, in contrast to conventional chemical modelling packages, does not include model equations in the source code. Instead, equations are defined in text format and entered into the calculation kernel at runtime. This structure makes Orchestra highly adaptable, flexible and extendible[83]. PHREEQC hardcodes diverse aqueous models and uses a keyword-based set-up. Many

options for modelling ion-complexation, adsorption and speciation are included[56,82]. Unless specified in a 'kinetics' keyword, PHREEQC assumes equilibrium in all calculations.

2.9.1 Surface reactions in PHREEQC

Two models for surface complexation are available in PHREEQC. Both are based on the fundamental principles as explained below, but they differ in how they calculate surface charge and potential. The Dzombak-Morel model uses an adapted form of the conventional doubly layer theory relation for relating surface charge to potential. It was originally developed for complexation of heavy metals on hydrous ferric oxide (Hfo). The second option is the aforementioned CD-MUSIC model, which includes more options to fit experimental data. It was developed for sorption on Goethite and the charge, potential and sorbed species can be distributed over the different surface layers. Both include activity corrections in the vicinity of the surface based on the Boltzmann accumulation factor described in section 2.7[56].

As literature mass law constants are more readily available for sorption on Hfo precipitates for the Dzombak-Morel model, the CD-MUSIC model will not be used in the presented model. The minteq.v4 database includes the tabulated mass law constants from Dzombak and Morel[56,74]. Important to notice is that the temperature range in which the tabulated mass law constants from the database are valid is between 20 and 30 degrees. Moreover, their validity is usually limited to systems that contain a low mass of dissolved organic carbon (DOC) relative to oxide solids[74]. As the DOC in landfill leachate is quite high, the applicability of the database surface reactions might be low.

In surface complexation modelling, some fundamental assumptions are made. First of all, sorption on oxides is assumed to take place at specific coordination sites and the sorption reactions are described quantitatively via mass law equations. Any surface charge on the Hfo surface results from sorption reactions themselves, e.g. the surface is initially neutral. Finally, the effect of developed surface charge is included by applying a correction factor to the mass law constants for surface reactions. This Coulombic correction factor is a function of the surface charge and is derived from electrical double layer theory, as touched upon in section 2.7[74].

Conventionally, weak and strong surface sites are defined for sorption of cations, each with different association constants. The weak binding sites have lower sorption constants but a higher site density than strong binding sites. For sorption of anions, one surface site suffices and the mass law constants for anion surface sorption reactions are thus identical for the two surface types[74]. As PFOS is a monovalent anion, two surface reactions are necessary to model its adsorption on Hfo surfaces, analogously to table 10.8 of Dzombak and Morel[74]. The implemented surface reactions are given in Figure 6. Values for the mass law constants remain to be determined experimentally. For other anionic pollutants, such as different PFAS species, analogous mass action laws can be defined.

$$\equiv FeOH^0 + PFOS^- + H^+ = \equiv FePFOS + H_2O \qquad K_2$$

$$\equiv FeOH^0 + PFOS^- = \equiv FeOHPFOS^- \qquad K_3$$

Figure 6: Surface reactions of PFOS on Hfo surface. For PFOA, PFBS and PFBA, analogous adsorption species exist.

The mass law constants K_2 and K_3 determine the affinity of each anion with the surface sites[56]. These constants are commonly reported as *log* values and are calculated as the product of the activities of the products divided by the product of the activities of the reagents at equilibrium, as defined for a

general case in Equation 7. For PFOS sorption, the formal definitions of the equilibrium constants are given in Equation 10a and b. Here, square brackets are used for the definition of the equilibrium activity of each compound. For other anions, such as PFOA or humic acid, analogous reactions can be defined. These equilibrium constants depend on the surface potential at the binding site, as explained in section 2.7. The activity of water is commonly assumed equal to 1 and thus ignored.

$$\text{a.}\quad \log(K_2) = \log\left\{\frac{[\equiv FePFOS]}{[\equiv FeOH^0][PFOS^-][H^+]}\right\} \qquad \text{b.}\quad \log(K_3) = \log\left\{\frac{[\equiv FeOHPFOS^-]}{[\equiv FeOH^0][PFOS^-]}\right\}$$

Equation 10a and b: Definition of equilibrium constants for PFOS sorption. For PFOA, PFBS and PFBA, analogous adsorption reactions apply.

2.10 CONCLUSION

In the research presented in this thesis, a computational model was constructed based on experimental data collected from laboratory-scale galvanostatic EC experiments. The model focused on the adsorption process, whereby double layer theory was used for the calculation of activity corrections in the vicinity of the surface. Hence, mass transfer was ignored and methods such as CFD or flocculation modelling were not selected. Because of its high versatility and extensive documentation, PHREEQC was used for all modeling purposes. Despite its applicability for competitive adsorption modelling, the CD-music approach was not used, because sorption constants were more readily available from Dzombak and Morel[74]. Consequently, the default PHREEQC Hfo surface was applied.

The optimal conditions for PFAS removal as determined by Yang *et al.*[4] were used in the electrocoagulation experiments. Their research suggested that electrostatic adsorption was the main mechanism for PFAS removal under these conditions. Accordingly, as aforementioned, the modelled removal process was based on adsorption. In the research presented in this thesis, it was first attempted to reproduce the experimental results of Yang *et al.*[4] and accurately simulate those in PHREEQC. Subsequently, the effect of adding humic acid to the solution was investigated. Humic acid concentrations were determined based on UV absorption, despite the limitations outlined in section 2.6.

3. METHODOLOGY

3.1 MODELLING AND EXPERIMENTAL APPROACH

The aim of this research was to determine the effect of co-solutes on PFAS removal via electrocoagulation with iron electrodes. To better understand the results and enable generalization to untested co-solutes, a model was constructed that simulates the removal. As mentioned in the literature section, utilization of the PHREEQC software enabled the determination of solution characteristics and iron hydroxide floc formation over time. The main focus of the model is the competition effect between PFAS and organic co-solutes. Therefore, electrode processes; mass transfer and fluid dynamics were largely simplified or ignored in the model. Thorough inclusion of these factors would lead to a more comprehensive model but was deemed too complex for the scope of this research. The generation rate of iron and hydroxide ions was based on Faraday's law.

Laboratory experiments were carried out to generate data for the optimization of the model. As a first step, it was attempted to accurately model the electrocoagulation process in water without pollutants. Once this was achieved, individual solutes were included in the laboratory tests and their removal was evaluated. Eventually, the removal of PFAS with HA was examined. As a final step, also different types of actual leachate water from Afvalzorg were tested. Optimal experimental conditions for PFOS removal using iron electrodes were already identified by Yang and coworkers[4]. The optimal current density, stirring speed and NaCl concentration were determined as 25 mA/cm^2, 180 rounds per minute (rpm) and 2 g/L, respectively. Hence, these optimal conditions were mostly preserved in the currently conducted laboratory experiments.

Preliminary attempts to reproduce literature data on the removal of PFAS in EC with model simulations were also carried out, but it was impossible to obtain consistent pH and concentration results. The number of unknown parameters in the literature data was too high for adequate model optimization. Hence, data for optimization were obtained by performing designated laboratory experiments. Ultimately, the experimental design was such that the empirical results were of the utmost usefulness for the computational model. The model was used to find ranges of experimental conditions where varying certain parameters would lead to a significant change in results, and subsequently the empirical findings in those conditions were used to optimize the relevant model parameters.

3.2 MODEL

3.2.1 Coupling to MATLAB™

PHREEQC was controlled from the MATLAB environment, to enable easy analysis of the results. To run each PHREEQC simulation, an appropriate shell script was executed from the MATLAB environment. Moreover, additional input files were written from the MATLAB environment and included in the PHREEQC input files. Through these additional input files, parameters such as the current density, relevant log(K) values and initial concentrations could be varied easily. All relevant PHREEQC output, such as pH, PFOS concentration, $Fe(OH)_3$ formation and saturation indices were written to a selected output file for each timestep. This output file was read by MATLAB, to compare the model predictions to experimental or literature data and plot the results.

3.2.2 Database modifications

The minteq.v4 database from PHREEQC is used for the calculation of the water composition at each time step during the EC treatment. As PHREEQC assumes full equilibrium, kinetic rate laws were included manually. However, it should be realized that the speciation for all aquatic species not specified in these rate laws is assumed to be at equilibrium throughout the simulation. Moreover, after a reaction or equilibration step, the solution composition has to be saved explicitly, as otherwise equilibration starts from the initial solution composition again in the next calculation. The PHREEQC pseudocode is given in Appendix 1.

An additional PHREEQC database file (Appendix 2, mySolutionSpecies.phr) was constructed wherein the valence states of aqueous iron were manually decoupled, as illustrated in example 9 of the PHREEQC program[56]. Iron(II) was specified as Fe_di and iron(III) as Fe_tri, and all reactions as defined in the minteq.v4 database were included manually. The only omitted reaction was the oxidation of ferrous to ferric iron: $Fe^{2+} = Fe^{3+} + e^-$. This oxidation was included as a kinetic reaction in all relevant input files, with a rate law as in Equation 2.

PFAS and humate solution species were manually defined with appropriate speciation reactions. The PFAS pKa values were found from literature[27]. Humate was included in the database as a divalent weak acid, for which the pKa values were adapted to match the experimental initial solution pH. These parameters were found by minimizing the sum of squared errors between the modelled and laboratory data. Optimization was carried out 100 times from randomly generated seeds via an appropriate MATLAB script utilizing the embedded *fminsearch* function. Finally, adsorption reactions for PFAS and humate onto the ferrous hydroxide surface were included in *mySolutionSpecies* as well. The equilibrium constants for these adsorption reactions were optimized based on the experimental data.

3.2.3 CO_2 and O_2 dissolution rate determination

To obtain accurate pH results during the simulation of the EC experiment, it is important to correctly include the CO_2 and O_2 saturation. It can be assumed that these dissolved gases are not in equilibrium with their atmospheric concentration for the entire duration of the EC treatment. The solubility of both gases is higher at higher pH, but the rate of pH increase is too fast for gas dissolution to compensate. Moreover, dissolved oxygen is depleted in the oxidation reaction of Fe(II). To approximately include the above effect, no equilibration with the atmospheric composition is included in PHREEQC during the EC simulation. Instead, rate laws were defined for the dissolution of CO_2 and O_2. These rate laws (Equation 11, i = CO_2 or O_2) are integrated simultaneously with the oxidation rate and Faradays law in PHREEQC. The values for the rate constants were found from designated experiments, as explained in the experimental section.

$$\frac{dC_i}{dt} = k_{diss,i} * (C_{i,sat} - C_i)$$

Equation 11

3.2.4 Adsorption reactions

An adsorption surface was defined according to the default hydrous ferric oxide surface from the minteq.v4 database. The surface was linked to a ferrihydrite ($Fe(OH)_3$) equilibrium phase, hence precipitation kinetics were not considered in the model. If the solution is supersaturated with respect to $Fe(OH)_3$, it was assumed to precipitate instantaneously. The high stirring rate and constant addition of iron and hydroxide ions ratify this assumption, but its accuracy remains uncertain. The calibrated

Dzombak-Morel adsorption constants were used for the surface composition calculations. The mass law constants for PFOS adsorption on the Hfo surface were included manually in the additional database file. Default site densities of respectively 0.005 and 0.02 mol/mol Fe for strong and weak binding sites were obtained from Dzombak and Morel[74]. These parameters determine the number of binding sites available for pollutant binding.

3.2.5 Electrocoagulation

The initial solution composition was obtained in PHREEQC by adding 2 g/L NaCl and the appropriate solute(s) at a temperature of 20 °C. This solution was equilibrated with an atmospheric composition containing 20 vol% O_2 and 400 ppmv CO_2, after which its composition was saved. The determined rate laws for gas dissolution and iron oxidation were included. Moreover, Faradays law was also included as a kinetics block, to incorporate the continuous electrochemical addition of Fe^{2+} and OH^- to the solution. These rates are integrated simultaneously up to 50 minutes, with an integration timestep of one minute and the tolerance kept at the default (10^{-8}).

3.2.6 Limitations

Certain constants were unavailable in literature and hence model optimization had to be performed to find their values. These constants are listed in Table 1. Moreover, some of the model settings proved to be influential on the simulation results. Examples include, but might not be limited to, the number of steps and integration tolerance in the kinetic calculation. Furthermore, the surface specifications and the log(K) values of $Fe(OH)_3$ precipitation and of all surface reactions other than those involving PFAS are currently all at the default setting of PHREEQC. It is conceivable that these constants are different for $Fe(OH)_3$ formed by EC instead of by chemical coagulation.

3.3 EXPERIMENTAL

Unless mentioned otherwise, a Metrohm Autolab PGSTAT204 with pX1000 pH measurement module and unitrode combined pH electrode and temperature sensor were used for all measurements. A controlled current up to 0.3 A could be supplied with this equipment. pH, temperature, current and voltage were measured every second. When applicable, sampling was executed manually at fixed time intervals to measure aqueous concentrations of solutes. PFAS and total organic carbon (TOC) analyses were carried out by *Eurofins Environment Testing* laboratory. To prevent oxygen limitation in the oxidation of Fe(II) to Fe(III) during EC, the system was aerated using a pressurized air inlet at approximately 1.1 bar and stirred continuously using a magnetic stirrer.

3.3.1 Optimization of kinetic constants for gas dissolution

Experiments were carried out to find values for the rate constants for O_2 and CO_2 dissolution under the current experimental conditions, as well as to confirm the literature oxidation rate. Optimizing these constants together based on the literature data proved to be impossible due to their high interdependencies. All experiments were carried out in triplicate. First, the dissolution rate of CO_2 was determined. 500 mL water was magnetically stirred under aeration vigorously for at least 30 minutes to saturate it with atmospheric O_2 and CO_2. Then, the water was basified with 60 μL 1 M NaOH and the pH was measured for 35 minutes. Due to the dissolution of atmospheric CO_2, the pH dropped over time. By writing a PHREEQC script simulating the aqueous conditions in which the rate constant of CO_2 dissolution could be varied, this constant was determined. The pH was independent of O_2 saturation, hence $k_{diss,CO2}$ could be established independently.

As aforementioned, various rate laws for Fe(II) oxidation have been described in literature. To determine which rate equation best fits the experimental iron oxidation process, iron oxidation tests were carried out in basified water. 0.25 g $Fe(II)SO_4$ and 60 μL 1 M NaOH were simultaneously added to 500 mL atmospherically equilibrated demineralized water. The solution was stirred (without aeration) and the pH was measured over time. The pH change is due to the oxidation of Fe(II) to Fe(III), as well as due to the subsequent precipitation of $Fe(OH)_3$. Oxygen dissolution had no effect on the oxidation process, as the solution remained close to saturated throughout the experiment. An analogous PHREEQC input file was written, from which the oxidation rate constants could be determined.

Finally, the oxygen dissolution rate remained to be determined. 500 mL water was purged with N_2 gas at high pressure for 25 minutes, under constant stirring, to remove the dissolved oxygen. Hereafter, 0.25 g $Fe(II)SO_4$ and 60 μL freshly prepared 1 M NaOH were added simultaneously to the solution, which was now aerated at similar conditions as in the EC experiments. Under constant stirring, the pH was measured for 50 minutes. Due to the dissolution of atmospheric O_2, analogously to the previous experiment, Fe(II) oxidation and $Fe(OH)_3$ precipitation cause a pH change. This pH change was again modeled with a PHREEQC input file that included the previously found Fe(II) oxidation rate, as well as the CO_2 dissolution. From this model, a kinetic constant for O_2 dissolution under Fe(II) oxidizing conditions could be determined.

3.3.2 EC runs without pollutants

To determine the agreement of the electrocoagulation model with reality, EC runs were performed without any pollutants in the initial solution. Preliminary experiments without aeration showed the eventual formation of black, ferromagnetic magnetite precipitate due to oxygen depletion, hence an aerated system was chosen. To this aim, 500 mL 2 g/L NaCl solution was stirred while being aerated through a subsurface air inlet at approximately 110 kPa. Iron electrodes (>99%, Appendix 6) with a submerged surface area of 8 cm^2 and the Metrohm pH electrode were inserted in the solution.

A controlled current was supplied for 50 minutes, while the pH, voltage and temperature were followed. The electrodes were cleaned with 0.1M HCl and weighed before and after each run. The formed iron hydroxide precipitate was filtered under vacuum through a Büchner funnel, dried to air for at least 24 hours, and weighed. Then, the precipitate was dried in an oven at 140 ^oC for at least 4 hours and weighed again. Current densities of 6.25, 12.5, 25 and 37.5 mA/cm^2 were tested.

3.3.3 EC runs with phosphate (PO_4^{3-})

As mentioned in section 3.2.4, the site density of the PHREEQC surface is an important parameter. Although site densities for both weak and strong surface sites on Hfo have been reported extensively in literature, their validity depends on the surface area of the specific ferrihydrite precipitate[74]. Conversely, the ratio between the densities of the two site types is independent of the area. Conventionally, surface area is determined by measuring nitrogen gas adsorption using the BET technique[74]. Because the surface area of EC flocs changes over the course of the reaction, in the current research phosphate removal was used as proxy to test the validity of the literature values. Binding constants for phosphate on the PHREEQC surface are already available in the database, so theoretically, the surface site density was the only unknown.

A 0.25 mmol/l (24 mg/l) PO_4^{3-} solution was made by dissolving the appropriate amount of K_2HPO_4, purchased from Sigma-Aldrich, in 1 L 2 g/L NaCl solution. 500 mL solution was treated at 25 mA/cm^2 current density under identical conditions as all other EC tests. Phosphate concentrations were

determined after 0, 5, 15, 30 and 50 minutes of treatment. 2 mL sample was taken from the reaction flask, centrifuged at 3000 rpm for 4 minutes, and 1 mL supernatant was diluted 6 times to obtain the appropriate concentration range for analysis. 2 mL of the obtained solution was analyzed for PO_4^{3-} using Hach-Lange LCK 349 test kits, following the instructions from the provider[84].

3.3.4 EC runs with dissolved organic matter

To determine the removal rate of humic acid (HA) with electrocoagulation, EC runs with organic material at an initial concentration of 30 mg/L at 6.25 and 12.5 mA/cm^2 were performed in triplicate. Additionally, an initial concentration of 60 mg/L was tested at 12.5 and 25 mA/cm^2. These tests were carried out in duplicate, since the variability in earlier results was low. All other conditions were as aforementioned for the tests without pollutants. HUMIN-P 775 was used as organic matter, which is a water soluble commercially available humic acid source. Its mass-based composition was determined at the University of Amsterdam as roughly 42 % Carbon, 52 % Oxygen, 4 % hydrogen, 1 % Nitrogen and 1 % Sulphur (CNHS analysis, based on unpublished data).

A novel approach based on quadrupole time of flight mass spectrometry was used at the university of Amsterdam to analyze the molecular mass distribution of HUMIN-P 775[85]. The median, minimum and maximum molecular weights were found to be 198, 118 and 572 Da, respectively (based on unpublished data). An important limitation of these results is that the used approach has a bias towards lower molecular weights. Moreover, the number of identified molecular formulas in HUMIN-P 775 was low. Nonetheless, these data give an impression of the approximate average molecular weight of HUMIN-P 775. The molar mass of humic acid that is implemented in the model is an important variable, as it determines the initial molar concentration used by PHREEQC. The high uncertainty in this value increases the uncertainty in the determined log(K) values for HA adsorption.

In reality, the HUMIN-P 775 used in this research consists of a mixture of various compounds with different molar masses. In the model, this is represented by an average compound with one molar mass. Using the median molecular weight in PHREEQC resulted in removal rates that were too low, hence a slightly higher average molar mass of 332.11 Da was assumed. This mass corresponds to an average composition of $C_{10}H_{11.54}O_{10.89}S_{0.09}N_{0.23}$, which is in accordance with the CNHS composition as determined at the University of Amsterdam. The use of a higher-than-median molar mass is ratified by the preference for lower mass compounds of the Q-TOF technique, as well as by the significantly higher molar masses for other humic substances reported in literature[67,75,80].

To determine the concentration of humic acid over time, 5 mL sample was extracted from the EC reaction after 5, 10, 15, 20, 30 and 50 minutes. The samples were centrifuged for four minutes at 3000 rpm, after which the UV absorption (λ=254 nm, as is commonly used for determination of HA concentrations[86]) of 1 mL of the supernatant acidified with 20 μL 0.1 M HCl was measured. A calibration curve in the relevant concentration range was constructed to calculate the HA concentration from the UV absorption. To generate blanks for the absorption measurements, identical experiments at each tested current density without HA acid in solution were carried out in triplicate and the absorption due to iron (hydroxides) was measured at the relevant timesteps. The mean values were subtracted from the absorption measured in the HA experiments.

TOC concentrations were determined to verify the results obtained by UV-spectrophotometry. A sample volume of 100 mL was required for this analysis, and the detection limit was 2 mg/l. Hence, each run was split into two, to enable withdrawal of higher sampling volumes, and an initial

concentration of 120 mg HA/l was used to remain above the detection limit. 1100 mL 120 mg/l HA solution was prepared by dissolving 132 mg HA and 2.2 g NaCl in 1.1 L water. 50 mL of this solution was diluted to 100 mL (2 times) uncentrifuged. Another 50 mL was centrifuged at 3000 rpm for 8 minutes, 40 mL supernatant was extracted and diluted to 100 mL (2.5 times). These samples give the initial TOC concentration and indicate the effect of centrifugation. The sample collection bottles contained 1 g H_2SO_4 solution to conserve the samples.

Electrocoagulation runs were performed with the remainder of the solution at 12.5 and 25 mA/cm^2. First, 500 mL was treated for 15 minutes and 50 mL sample was extracted after 5 minutes and after 15 minutes. Then, the remaining 500 mL was treated for 50 minutes and 50 mL sample was extracted after 30 minutes and after 50 minutes. The sample handling again consisted of centrifugation for 8 minutes, extraction of 40 mL supernatant and dilution to 100 mL. In total, the TOC concentration was thus determined at timesteps of 5, 15, 30 and 50 minutes. Of all samples, the UV-absorption was measured immediately after their collection.

3.3.5 EC runs with PFAS

Perfluorooctanoic acid (PFOA) 96%, perfluorooctanesulfonic acid (PFOS) potassium salt, perfluorobutanoic acid (PFBA) 98 % and perfluorobutanesulfonic acid (PFBS) 97 % were purchased from Boom laboratories. For PFOS and PFOA, stock solutions with a concentration of respectively 1.25 and 2.5 mmol/l were made by dissolving 1 g pure substance (1.858 mmol; 2.415 mmol) in 1487 and 966 mL water, respectively. In the EC runs, 50 mL PFOA or 100 mL PFOS stock solution was diluted up to 500 mL with demineralized water and 1 g NaCl was added, such that the initial PFAS concentration in each sample was 0.25 mmol/l. PFBA and PFBS were measured volumetrically and added directly at a concentration of 0.15 mmol/L each, by dissolving 20 µL (33 mg) PFBA, 26 µL (46 mg) PFBS and 2 g NaCl in 1 L demineralized water.

In each EC run, 500 mL PFAS solution was treated for 50 minutes. 5 mL sample for PFAS analysis was extracted after 5, 10, 15 and 30 minutes. This was centrifuged for 4 minutes at 3000 rpm, after which 2 mL supernatant was diluted 10 times and sent in for analysis. After the end of the run, 25 mL solution was centrifuged, and 20 mL undiluted supernatant was sent in for analysis. 20 µL 2 M HCl was added to acidify each sample and thereby prevent further precipitation of iron hydroxides. PFOS and PFOA removal was tested at 12.5 and 25 mA/cm^2 current density, whereas PFBS and PFBA removal was only tested at 25 mA/cm^2. All tests were performed in duplicate, except for PFOA removal at 12.5 mA/cm^2, which was carried out in triplicate. For PFBS and PFBA removal, the sampling after 10 minutes was omitted.

Initial concentrations were not measured for all samples, as in principle, the concentration was known. For two of the runs with PFOA at 12.5 mA/cm^2, initially 5 mL sample was extracted, centrifuged, and 1 mL supernatant was diluted 20 times and acidified as described previously. The remaining 4 mL were added back to the solution to maintain an initial volume close to 500 mL. For the final run at 12.5 mA/cm^2, 1 mL of the initial solution was simply diluted 20 times without centrifugation, to enable a comparison of the effect of centrifuging and acidifying. The UV absorption at 254 nm of the final diluted samples was measured before sending them out for analysis.

To assess the reliability of the concentration measurements, samples with known PFAS concentrations were sent in for analysis. A stock solution containing approximately 0.15 mmol/L PFOA, PFBS and PFBA and 0.25 mmol/L PFOS was made. Undiluted samples, as well as samples with dilution factors of 2 and

10 were analyzed for their PFAS content in duplicate. From these results, the uncertainty in all analysis results due to the dilution steps could be estimated. Moreover, one blank sample containing 1 mL supernatant of centrifuged demiwater diluted 20 times was tested, to quantify the PFAS concentration due to environmental background pollution.

3.3.6 EC runs with PFAS and dissolved organic matter

The competition effect during the removal was assessed by treating demineralized water solutions containing both PFAS and humic acid. In biologically treated leachate from the Nauerna site of Afvalzorg, the total organic carbon concentration fluctuates between 51 and 95 mg/l. To approximate this TOC level, an initial humic acid concentration of 120 mg/l was used, corresponding to a carbon content of approximately 45 mg/l. Higher concentration levels are outside the solubility and UV detection range. The initial PFAS concentration was kept at 0.25 mmol/l. Initially, 1000 mL solution was prepared by diluting 100 mL PFOA or 200 mL PFOS stock solution. 2 g NaCl and 0.120 g humic acid were added.

The UV absorption of this initial solution was determined, and 1 mL was diluted 20 times and sent in for determination of the initial PFAS concentration. The remaining solution was divided over two reaction flasks and treated at a current density of 25 mA/cm^2 for 50 minutes, with all other process variables as described previously. After 5, 15 and 30 minutes, PFAS samples were collected similarly as in the runs without humic acid, but the UV absorption of the supernatant was determined before dilution. After 50 minutes, the reaction was stopped, and 150 mL solution was centrifuged for 8 minutes. The UV absorption of the supernatant was determined, after which 100 mL undiluted supernatant was sent to Eurofins for TOC analysis, and 20 mL for PFAS analysis.

3.3.7 EC runs with real wastewater

Four different types of wastewater obtained from Afvalzorg were tested in an identical set-up as the artificial solutions. The leachate water treatment plant (LWTP) present on the Nauerna site treats a combined influent, consisting of leachate water and runoff water. A process overview of this LWTP is given in Appendix 8. Untreated influent (Nauerna Inf) to this plant as well as treated effluent (Nauerna Eff) were tested for PFAS and TOC removal. Additionally, leachate from two compartments of another landfill managed by Afvalzorg was tested. This landfill is located on the Zeeasterweg and leachate from compartments 5 (Zee. 5) and 8 (Zee. 8) was tested. Finally, Zee. 5 water spiked with 0.15 mmol/l PFOA, PFBS and PFBA was tested.

2 g/L NaCl was added to all water types to improve conductivity. Initially, 100 mL of each water type was analyzed for initial TOC content, and 20 mL for initial PFAS content. After 5 and 25 minutes of treatment, 25 mL sample was extracted, centrifuged for 8 minutes at 3000 rpm and 20 mL undiluted supernatant was sent in for PFAS analysis. After the EC run, 100 mL supernatant was sent in for TOC analysis and 20 mL for PFAS analysis. All PFAS samples were tested for the concentrations of 38 different PFAS, amongst which were PFOS, PFOA, PFBS and PFBA, as specified in Appendix 7.

4. Results & Discussion

In this chapter, the obtained results for each part of the research are presented. The results of the laboratory experiments were used to calibrate and test the PHREEQC model. Therefore, the combined experimental and model results will be presented together for each part. Moreover, as the integration of the model and experimental results was an important part of the research, the presentation and discussion of the results are combined in one chapter. At the end of this chapter, in sections 4.9 and 4.10, the main uncertainties associated with the model and experimental results are outlined. Finally, section 4.11 serves to discuss some of the implications of the results.

Table 1: Constants in model for which optimization was necessary

Constant	Description/Equation	Value
k_0	Rate constants for Fe(II) oxidation, see Equation 2 (s^{-1} and $l^2mol^{-2}s^{-1}atm^{-1}$)	2.91e-9
k_1		1.33e12 or 8.33e13
$k_{diss,O2}$	Rate constant for O_2 dissolution (s^{-1}), Equation 11	0.012
$k_{diss,CO2}$	Rate constant for CO_2 dissolution (s^{-1}), Equation 11	0.0045
M_{HA}	Molar mass humate (g/mol)	332.11
Log(K) values for HA surface complexation	Hfo_wOH + HA^{-2} + H^+ = Hfo_wHA^- + H_2O Hfo_sOH + HA^{-2} + H^+ = Hfo_sHA^- + H_2O	80
	Hfo_wOH + HA^{-2} = Hfo_w$OHHA^{-2}$ Hfo_sOH + HA^{-2} = Hfo_s$OHHA^{-2}$	75
Log(K) values for PFOS surface complexation	Hfo_wOH + $Pfos^-$ + H^+ = Hfo_wPfos + H_2O Hfo_sOH + $Pfos^-$ + H^+ = Hfo_sPfos + H_2O	46
	Hfo_wOH + $Pfos^-$ = Hfo_w$OHPfos^-$ Hfo_sOH + $Pfos^-$ = Hfo_s$OHPfos^-$	42
Log(K) values for PFOA surface complexation	Hfo_wOH + $Pfoa^-$ + H^+ = Hfo_wPfoa + H_2O Hfo_sOH + $Pfoa^-$ + H^+ = Hfo_sPfoa + H_2O	23
	Hfo_wOH + $Pfoa^-$ = Hfo_w$OHPfoa^-$ Hfo_sOH + $Pfoa^-$ = Hfo_s$OHPfoa^-$	23
Log(K) values for PFBS surface complexation	Hfo_wOH + $Pfbs^-$ + H^+ = Hfo_wPfbs + H_2O Hfo_sOH + $Pfbs^-$ + H^+ = Hfo_sPfbs + H_2O	23
	Hfo_wOH + $Pfbs^-$ = Hfo_w$OHPfbs^-$ Hfo_sOH + $Pfbs^-$ = Hfo_s$OHPfbs^-$	26
Log(K) values for PFBA surface complexation	Hfo_wOH + $Pfba^-$ + H^+ = Hfo_wPfba + H_2O Hfo_sOH + $Pfba^-$ + H^+ = Hfo_sPfba + H_2O	23
	Hfo_wOH + $Pfba^-$ = Hfo_w$OHPfba^-$ Hfo_sOH + $Pfba^-$ = Hfo_s$OHPfba^-$	26
Log(K) values for HA speciation	$HumateH_2$ + H^+ = $HumateH_3^+$	5.71
	$HumateH_2$ = $Humate^{-2}$ + $2H^+$	-56.1
	H^+ + $Humate^{-2}$ = $HHumate^-$	33.1
Log(K) values for HA complexation to iron	Fe^{3+} + $Humate^{2-}$ = FeHumate+	58
	Fe^{2+} + $Humate^{2-}$ = FeHumate	47

Table 1 gives an overview of all optimized model constants. The validity of these constants is limited to the experimental conditions as employed in the current research. The model results presented in this thesis were all obtained using the parameter values as presented in this table, unless it is explicitly specified that a value was altered. For example, the values were varied in some cases to analyze the

sensitivity to certain parameters. Because PHREEQC uses atmosphere as unit for the pressure of gases, this unit is used rather than Pascal for reporting pressures, such that the values of all constants are consistent with how they are included in the model.

4.1 Optimization of kinetic gas dissolution constants

The pH-drop due to CO_2 dissolution was very fast. At a pH around 8.5, the pH decreased rapidly due to the low buffering capacity of the solution. As the exact time of NaOH addition was not identical for all runs, there was a high variability in the data. Nonetheless, a dissolution rate was established based on the data and $k_{diss,CO2}$ was estimated at 0.0045 s^{-1}, with a fit as shown in Appendix 11. From this plot, it could be observed that the sensitivity to the exact value was high for the calibration data fit. Nonetheless, the sensitivity of the final model to the exact value was relatively low, as long as the order of magnitude of $k_{diss,CO2}$ remained the same. Hence, the dissolution rate was assumed valid.

The oxidation rate of $Fe(II)SO_4$ under O_2 saturated conditions fitted the experimental data very well, see Appendix 12. Hence, the rate law from Singer and Stumm (1970)[57] and used in PHREEQC example 9 was maintained[56]. It should be noted that the effect of temperature on the predicted pH is relatively large in an unbuffered solution, because the dissociation constant of water is temperature-dependent. For a temperature difference of 5 °C, the pH difference could reach 0.14 pH-units. Nonetheless, the agreement of the literature rate law with the experimental data was sufficiently accurate to accept the literature rate law as valid. Furthermore, the predicted variability in oxidation rate due to pH by Morgan and Lahav was reproduced well by this model[55]. Although there was no exact agreement between their predictions and the currently established model, the spread in oxidation rate at different pH values was similar, which is illustrated in Appendix 13.

Finally, $k_{diss,O2}$ was established at 0.012 s^{-1}. Again, this value should be considered as an order of magnitude, as the exact value was highly dependent on the pressure of the aeration system, stirring rate, and temperature. Nevertheless, the sensitivity of the final model to the exact rate of oxygen dissolution was low. In all laboratory oxidation experiments, formation of orange $Fe(OH)_3$ precipitate was clearly observable within the first five minutes. This precipitation was included as an equilibrium step in PHREEQC, e.g. $Fe(OH)_3$ was assumed to precipitate instantaneously when its SI exceeds 0. This assumption was ratified by the high stirring rate, preventing mass transfer limitations, and the constant supersaturation due to the continuous formation of Fe^{2+} and OH^-.

4.2 Electrocoagulation experiments without pollutants

Formation of orange iron hydroxide precipitate was observable during the experiments. As expected, the formation of hydrogen gas in the reduction of water caused gas formation at the cathode. After 50 minutes treatment time, the formed flocs settled quickly after turning off the stirring and could easily be separated by filtration. Drying of the flocs was carried out on the filter paper, but this filter paper showed burn marks after being put in the oven. Hence, the measured weight data were corrected to exclude the effect of mass loss from the filter paper. Figure 7 shows the good agreement between the calculated mass of iron hydroxide and the measured data. The data shown are the measurements before oven drying, corrected for a remaining water content of 11.4%. This factor was calculated from the outlying measurement at 37.5 mA/cm2, because this precipitate was dried in an aluminum container and thus no mass loss due to burning or drying of the filter paper occurred.

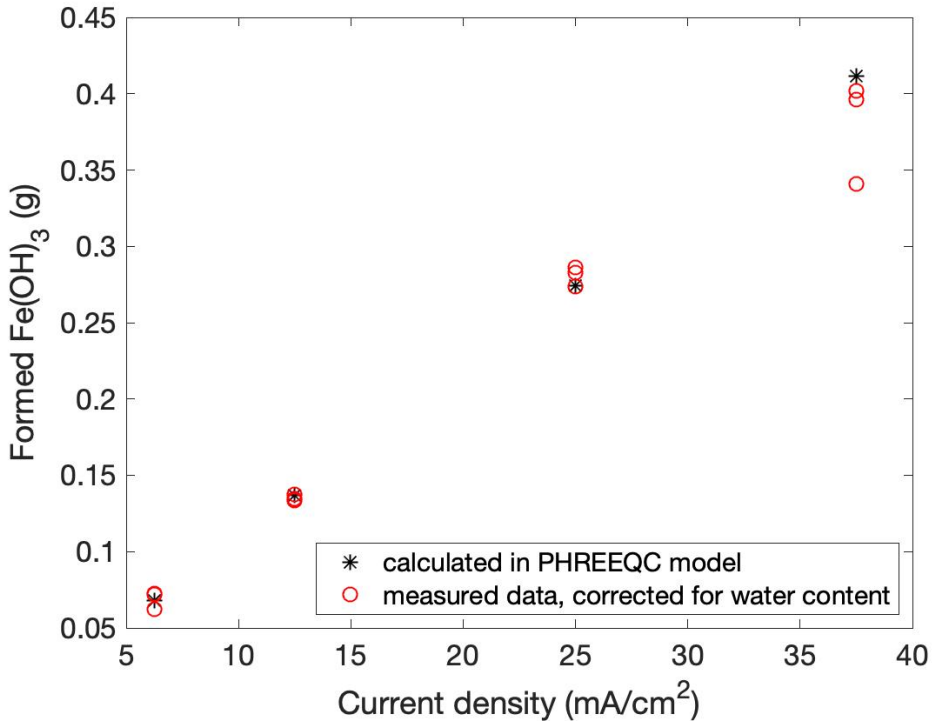

Figure 7: Comparison of calculated mass of iron hydroxide formed with experimental results at four different current densities after 50 minutes of treatment.

The outlying result at 37.5 mA/cm^2 was probably due to transferring of the precipitate from the filter paper to the aluminum container before weighing, during which a high yield loss occurred. Possible explanations for the differences in the remaining measurements include loss of yield in the filtration steps, or a higher mass of the precipitate due to a higher remaining water content. Moreover, crystal water is not accounted for in the calculated $Fe(OH)_3$ mass. Finally, small amounts of other precipitates are likely to form in the EC experiments as well, whereas the calculated mass was based on formation of $Fe(OH)_3$ only.

Despite these deviations, these results indicated that the model approximation of the $Fe(OH)_3$ formation was quite well. This was confirmed by good agreement between the mass loss of the electrodes after 50 minutes of treatment and the iron dissolution predicted by Faradays law, as shown in Figure 8. The measured mass loss was more often too high than too low, which confirmed the hypothesis of ferrous iron dissolution. Substituting Z = 3 in Faradays law (Equation 3) would lead to a lower electrode mass loss, which was not observed experimentally.

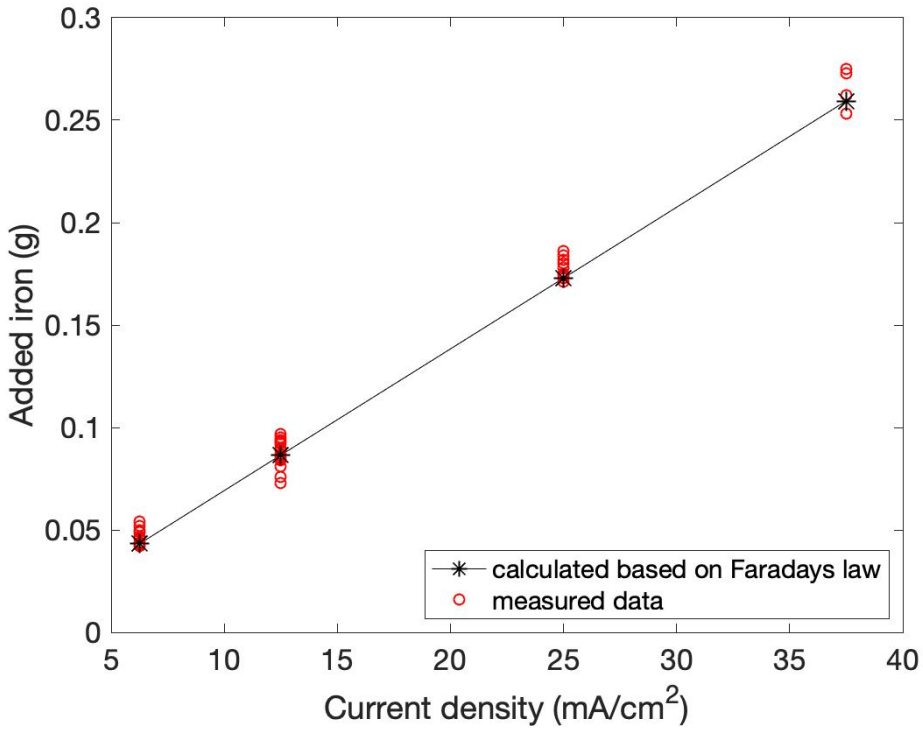

Figure 8: Comparison of mass loss of electrodes to predicted iron dissolution from Faradays law at four different current densities, all after 50 minutes of treatment time.

The agreement between the predicted pH and the measured data is shown in Figure 9. Overall, the variability of the pH increased at higher current densities. This was mostly an experimental limitation, as the voltage was less controlled at higher currents and the pH was measured potentiometrically. Due to the lower level of process control and higher rates of Fe^{2+} and OH^- formation, the pH measurement fluctuated strongly. Moreover, at high current densities, an initial drop in pH was observed in the experimental data, possibly due to alternative cathode reactions. Interestingly, an accurate agreement between the modelled and experimental pH data could only be achieved by increasing the previously checked literature rate constant for Fe(II) oxidation by a factor 60, to $8.33 * 10^{13}$ $l^2mol^{-2}s^{-1}atm^{-1}$.

Generally, kinetic constants only depend on temperature[72]. However, the presented rate law (Equation 2) is not elementary and describes a combination of processes[57]. The original rate constant ($1.33 * 10^{12}$ $l^2mol^{-2}s^{-1}atm^{-1}$ at 25 °C) represents Fe^{2+} oxidation at pH values above 4.5[57]. It worked well in the case of PHREEQC example 9 and the currently presented oxidation of $FeSO_4$, but failed to accurately predict the pH during electrocoagulation[56]. The temperature difference was not significant enough to explain this change in rate. Rate constants can also change when a process is catalyzed[72]. In the electrocoagulation experiments, polarization of the electrodes could lead to a change in activation energy for the oxidation process, which leads to a change in rate constant[72]. Moreover, Fe^{2+} ions adsorbed on the generated $Fe(OH)_3$ surface can release ions more easily due to a lower transition state energy, hence increasing the rate constant for oxidation[73].

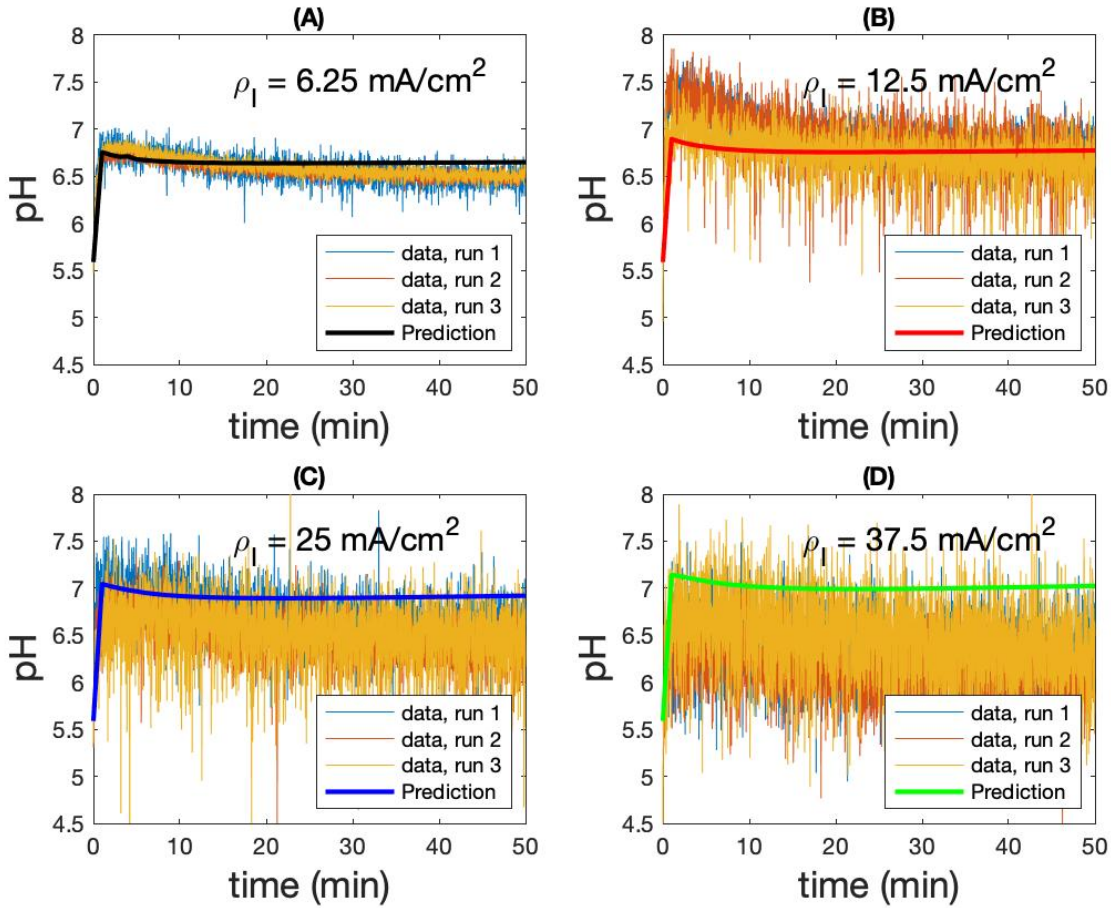

Figure 9: Comparison of predicted pH vs time during EC without pollutants to measured data at current densities of (A) 6.25 mA/cm², (B) 12.5 mA/cm², (C) 25 mA/cm² and (D) 37.5 mA/cm².

4.3 Electrocoagulation experiments with phosphate

As illustrated in Figure 10, the phosphate was removed within 15 minutes of treatment, which did not agree with the original model prediction using the literature adsorption constants. According to the database values, phosphate adsorption was prevented by the competition with Fe^{2+} for adsorption sites. Equilibrium constants for Fe^{2+} binding on Hfo surfaces were added to the Dzombak and Morel database by Appelo *et al.*, after they discovered the importance of Fe^{2+} sorption in certain environments[87]. The continuous supply of Fe^{2+} from the sacrificial anode ensured a relatively constant concentration level of this species in the current experiments, even though oxidation to Fe^{3+} is extremely fast at high pH. Hence, Fe^{2+} sorption on the Hfo surface is a probable phenomenon during EC with iron electrodes.

Nonetheless, it can also be expected that sorbed Fe^{2+} ions are oxidized to Fe^{3+} at a high rate. Moreover, it has been hypothesized that electron transfer between sorbed Fe^{2+} and the mineral surface may occur, leading to changes in the interfacial charge distribution[73]. These phenomena are better included in the CD-MUSIC model than in the classic Dzombak-Morel sorption model. Currently, the PO_4^{3-} removal data were fitted by the introduction of a new surface species (Equation 12), where Fe^{2+} and PO_4^{3-} are sorbed together at the same binding site. The sorbed Fe^{2+} increases the local surface charge and hence the binding affinity for phosphate. Introducing this surface species yielded a relatively accurate model result, although the initial removal and pH are not reproduced precisely.

$$\equiv FeOH^0 + PO_4^{3-} + Fe^{2+} \quad = \quad \equiv Fe(III)Fe(II)PO_4^0 \quad logK = 34.94$$

Equation 12: The compound on the right-hand-side is the newly introduced surface species for phosphate binding

Phosphate can precipitate with iron as Strengite ($FePO_4.2H_2O$), where iron is present as Fe(III), or with iron as Fe(II) in Vivianite ($Fe_3(PO_4)_2.8H_2O$). The redox conditions determine the stability of these minerals, and Vivianite only precipitates at highly reducing conditions. Theoretically, when the sum of the pe and the pH is higher than 17, $Fe(OH)_3$ precipitation dominates and thus fixes the solubility of Strengite[48]. In the current system, the pH + pe always exceeded 17, making $Fe(OH)_3$ precipitation dominant. However, as the system was also under kinetic control, coprecipitation of Strengite may remain possible.

This coprecipitation of Strengite is an alternative explanation for the high phosphate removal, rather than adsorption on the ferrihydrite surface[88]. Most likely, these two processes occurred together, and surface precipitation of Strengite might also play a role. The currently introduced co-adsorption of iron and phosphate approximately mimics surface precipitation. It is probable that a more accurate model representation could be obtained by inclusion of these processes. Merely allowing PHREEQC to precipitate Strengite did not yield the desired results. More advanced attempts to find better modelling methods were left for further research, as it was not within the scope of the current investigation.

The purpose of the phosphate removal experiments was to determine the accuracy of the surface site density. A reliable ratification of the literature values was impossible, due to the necessity of introducing an additional surface species for reproduction of the experimental data. As explained in section 2.9.1, a surface in PHREEQC is characterized by two types of surface sites. The range of surface densities reported in literature is between 0.001 and 0.01 mol/mol Fe for strong binding sites, and between 0.1 and 0.3 mol/mol Fe for weak binding sites[74]. Phosphate removal increased for an increased site density, but to obtain complete removal within 50 minutes the number of surface sites had to be increased unrealistically and the ratio between strong and weak sites could not be kept constant. Therefore, the literature values were accepted throughout this research and phosphate removal was represented by the introduction of an alternative surface species.

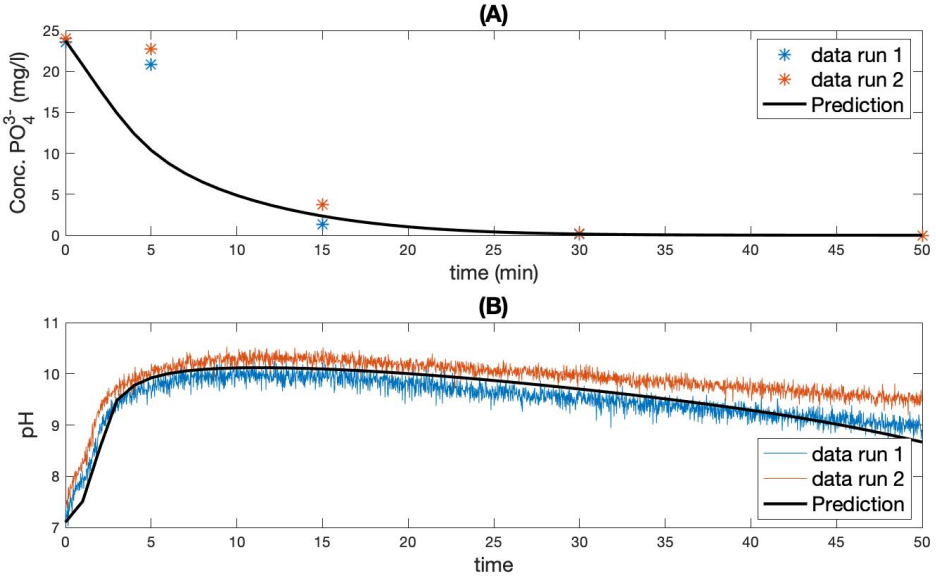

Figure 10: (A) Phosphate concentration and (B) pH versus time during phosphate removal.

4.4 ELECTROCOAGULATION EXPERIMENTS WITH ORGANIC MATTER

In the PHREEQC model, the humic species was assumed to be a diprotic acid. The initial pH values of the 30, 60 and 120 mg/l solution were 6.43 ± 0.16, 6.79 ± 0.12 and 7.126 ± 0.13, respectively. The initial pH values of 120 mg/L HA mixture with 108 mg/L PFOA or 115 mg/L PFOS were 4.95 and 7.00, respectively. The three pK_a values as listed in table 1 were found from a simple optimization script that minimized the sum of squared errors between the modeled and mean experimental pH values of these HA solutions. Accordingly, initial pH values of 6.38; 6.54; 6.71; 5.45 and 6.71 were found for the respective scenario's, which were deemed sufficiently close to the measured values. The UV absorption calibration curve, shown in Appendix 18, fitted the expected linear trend well.

Although the UV absorption of the samples at all timesteps in experiments without HA in solution was essentially negligible after centrifugation, the absorption initially increased steeply in the presence of HA to values outside of the range calibrated for HA concentration. This made an accurate determination of the HA concentration in solution at these timesteps impossible, as the high UV absorption was caused by the presence of iron rather than a higher HA concentration. Nonetheless, an almost complete removal of HA was achieved at all initial concentrations and current densities, as illustrated in Figure 11. From these data, log(K) values for the adsorption of HA on the ferric hydroxide surface were determined, and a relatively accurate model for the removal could be established.

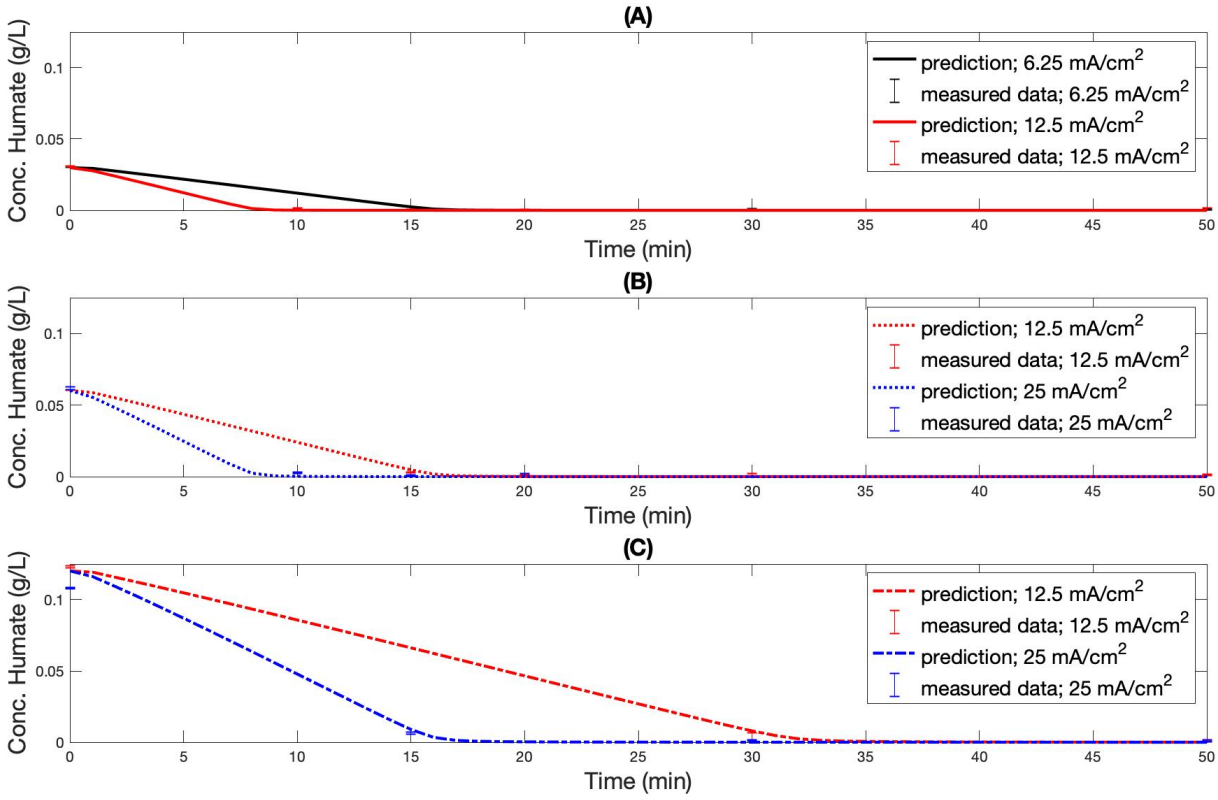

Figure 11: Humate removal with EC at initial concentrations of (A) 30 mg/L, (B) 60 mg/L and (C) 120 mg/L and different current densities. The concentration results are calculated from the UV absorption (λ = 254 nm) using the calibration curve given in Appendix 18. Data-points are represented by error bars located at the mean value of the three runs. The error bars include the standard deviation in the three parallel runs, as well as the standard deviation in the three parallel runs for determination of the blank absorption during EC. Measurements outside the calibration range at early timesteps of 5, 10 and 15 minutes are excluded from the plots.

The initial UV absorption was approximately 0.8 and 1.6 at a concentration of 30 and 60 mg/L HA, respectively. As illustrated in Figure 12, this absorption increased initially, before decreasing due to HA removal. The initial increase can be explained by two factors. First, iron binding by humic acid increases its UV absorption, as explained in section 2.6[67]. Secondly, as mentioned in section 2.5, complexation of humic molecules can disturb the precipitation of ferric hydroxide. Iron precipitation has been shown to decrease in the presence of humic acid due to stabilization of the colloidal iron particles[64]. If the absolute zeta-potential of particles is larger than 30 mV, the particles are considered stable and do not precipitate readily[9]. Which of these mechanisms was the leading cause for the high initial UV absorption could be evaluated based on the model results.

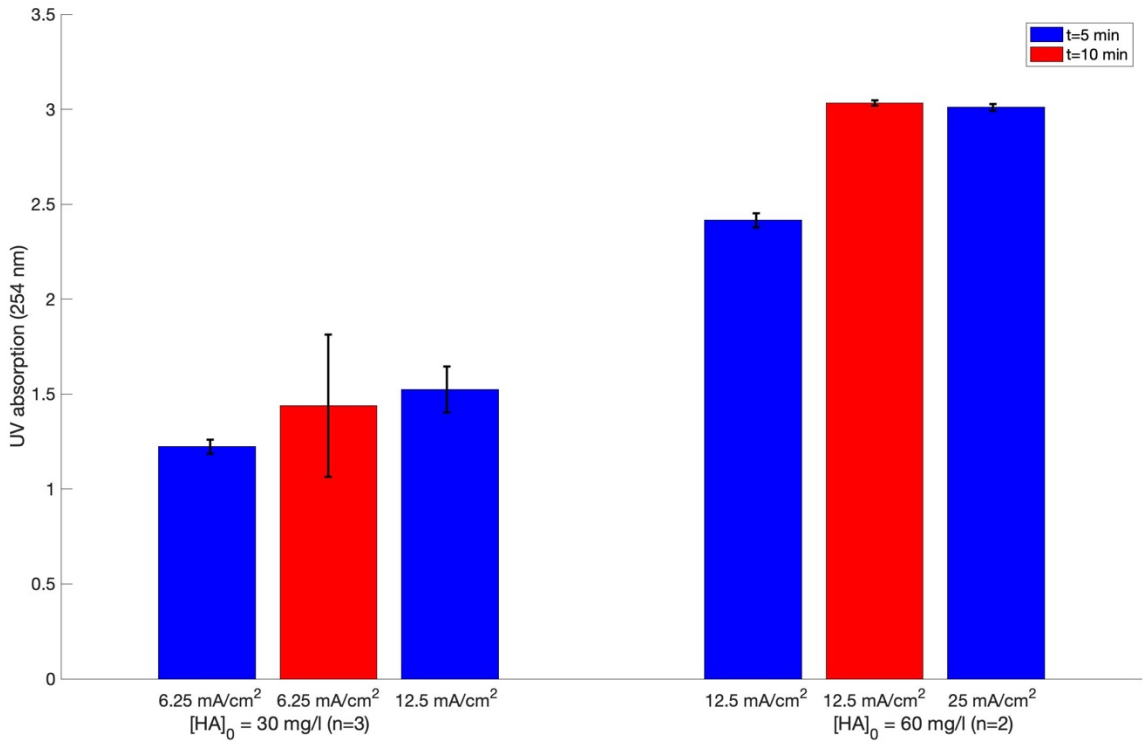

Figure 12: UV absorption at low time steps and different current densities. Only absorption values higher than the initial absorption are shown for each combination of experimental parameters, so the measurements after 10 minutes for 30 mg/l at 12.5 mA/cm² and 60 mg/L at 25 mA/cm² are calculated to concentrations and included in Figure 11.

Clear trends in the measured absorption were observable, as illustrated in Figure 11. The removal was about twice as slow when the initial concentration was doubled. Moreover, the removal could be accelerated by a factor two by doubling the current density. This indicated that the removal was directly proportional to the amount of iron added to the solution, as this is a linear function of both time and current density. Remarkably, the UV absorption at low timesteps also approximately doubles for a doubling of the current density and the initial concentration. Appendix 16 shows that initially, the average surface charge as well as the total surface and the total charged surface only depended on the current density, and not on the initial HA concentration. Hence, this increased UV absorption was most likely not caused by destabilization of iron hydroxide flocs, but by iron binding of the humic substances.

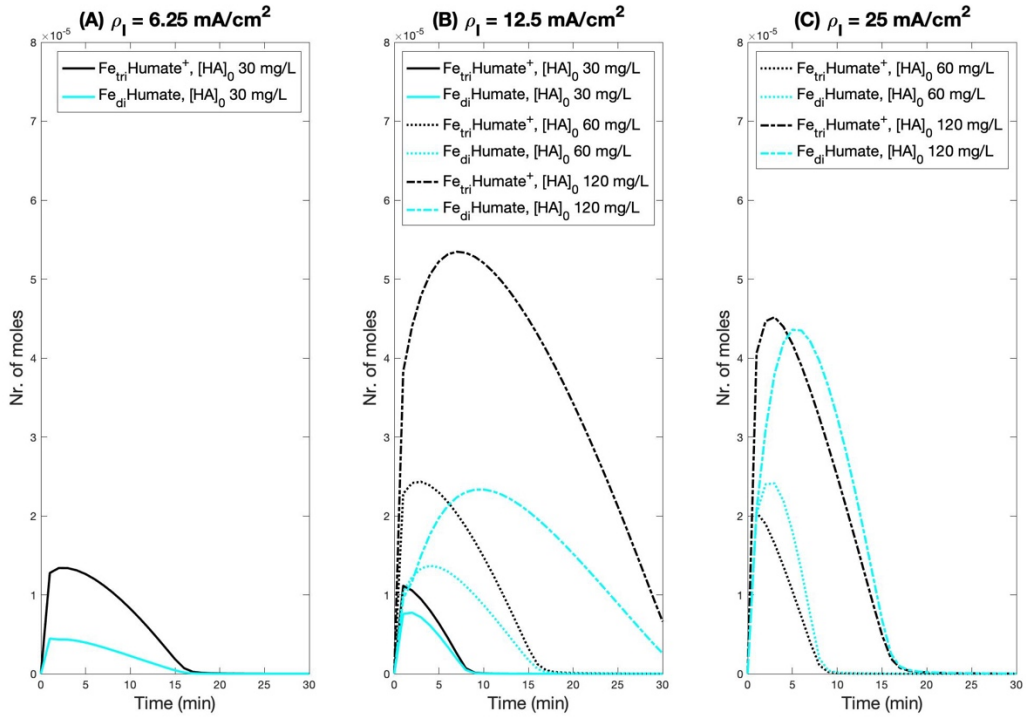

Figure 13: Total number of moles of iron-bound humate over time in EC with HA removal at different current densities and initial HA concentrations.

Figure 13 shows the amount of iron-bound humate over time in the EC experiments, according to the model. Based on the introduced association constants of ferrous and ferric iron with humate, it could be observed that initially, the HA indeed complexed with iron at low timesteps. After 15 minutes, however, all the humic acid is bound to the ferrous hydroxide surface and hence the absorption of centrifuged samples decreases. This confirms the hypothesis that the increased absorption was most likely indeed caused by iron binding to the HA, although destabilization of the flocs might still play a role. Notably, the results are highly dependent on the assumed molar mass of HA and the complexation constants, hence these variables should be verified. For the purposes of this thesis, accurately representing the removal rate sufficed, so this was deemed outside the scope of the current research.

An attempt to verify the results based on the UV absorption was established using the TOC measurements over time. In untreated samples, the TOC concentration corresponded linearly with the humic acid concentration, as was expected. This phenomenon is illustrated in Appendix 17 and indicated a mean mass-based carbon content of 36% in the humic acid. Figure 14 plots the determined TOC concentrations of the EC samples. In all runs, the measured TOC concentration decreased over time after the measurement at 5 minutes. Initially, the variation in the results is very high. However, as the removal progresses, the variation decreased steeply.

The initial concentrations of runs 1 and 2 at 12.5 mA/cm^2 shown in Figure 14 are the average of the centrifuged and uncentrifuged concentrations. No clear effect of centrifugation could be determined, as the centrifuged concentration was higher in one case, but lower in the other. A second attempt to determine TOC concentrations over time yielded similar results, with equally high variability. Despite the poor data quality, these measurements indeed verify the efficiency of EC towards humic acid removal, as the final TOC concentration measurements were all below the detection limit. No conclusions can be drawn on the initial removal due to the high variability between the runs.

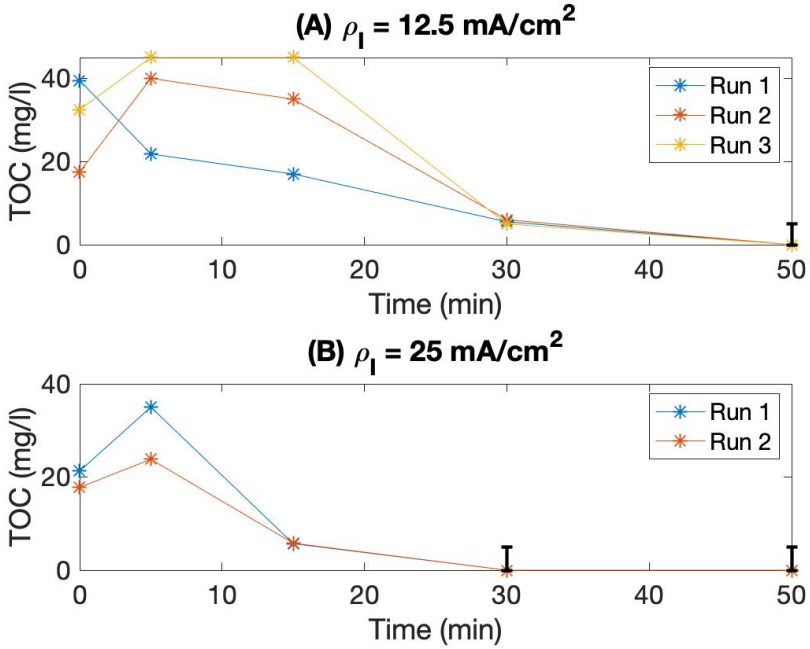

Figure 14: TOC measurements of EC samples during HA removal. The error bars indicate measurements below the limit of detection (5 mg/l).

In summary, due to experimental limitations, only the time required for complete removal of the humic acid could be determined. Accurate concentrations during the removal phase could neither be determined with UV spectrometry, nor with TOC measurements. Nonetheless, the time for total removal could be estimated relatively accurately with both methods. This required treatment time was proportional to the initial HA concentration and inversely proportional to the applied current density, as visible from Figure 11. These linear trends were reproduced very accurately by the model, indicating that the main mechanism for HA removal was indeed electrostatic adsorption.

4.5 Electrocoagulation experiments with PFAS

Concentrations of all PFAS in the blank sample were negligible. The concentrations of PFBA, PFBS, PFOA and PFOS in the samples that were tested to assess the effects of dilution, with dilution factors of 2 and 10, are given in Appendix 9. The concentrations calculated by multiplying the measured concentration in the diluted samples with the corresponding dilution factor are given in Appendix 10. From these calculated PFAS concentrations, the mean deviations from the concentrations measured in the undiluted samples were calculated as a percentage. These deviations are given in Appendix 10 and indicate the uncertainty due to dilution of the samples. As the deviation was different for each PFAS type, it was not due to measurement errors in the dilution steps. However, it should be noted that the solution was assumed to be homogeneous for all PFAS.

The absolute deviation between the PFOS concentration calculated from the diluted samples and the measured concentration in the undiluted samples was below 5 % for both dilution factors. This low deviation indicated that the effect of dilution on the PFOS measurements was small. For PFOA, PFBS and PFBA, absolute differences of at most 11.5, 9.1 and 18.6 % were found. Although the order of magnitude of the concentration measurements was thus correct, dilution may introduce a relatively large uncertainty in the concentration determinations for these species. This uncertainty should be

considered when evaluating the concentration results of these PFAS species. In all cases, the concentrations calculated from 10 times diluted samples were lower than those measured in the undiluted solution.

4.5.1 EC with PFOA

Whereas the flocs formed in EC without pollutants or EC with HA settled relatively quickly after the experiments, the flocs formed in the presence of PFOA floated on top of the solution. This could make the separation of flocs on an industrial scale problematic, but the flocs could still be settled by centrifugation. The UV absorption (254 nm) of all diluted centrifuged samples was negligible. In contrast to the literature conclusions, no significant PFOA removal was observed in the current experiments. Yang *et al.*[4] reported a removal of approximately 90% after 50 minutes treatment at 25 mA/cm^2, but the data in this thesis showed an approximate removal of at most 17%, see Figure 15. The removal and pH (Figure 16) could be reproduced well by the model with log(K) values for PFOA adsorption as reported in Table 1.

Explanations for the different results as compared to the literature were difficult to find. Aeration was not included in the experiments of Yang *et al.*[4], but similar results were obtained in additional experiments without aeration (data not shown). The stirring rate was controlled less accurately in the current set-up, but the high removal of PO_4^- and humate indicated good circumstances for coagulation and flocculation. Finally, Yang *et al.* used filtration rather than centrifugation to separate the flocs. They reported a negligible adsorption of PFAS in the used filters, so the difference between the methods should be unimportant. Industrially, centrifugation is a common method for post-treatment of EC effluent[40].

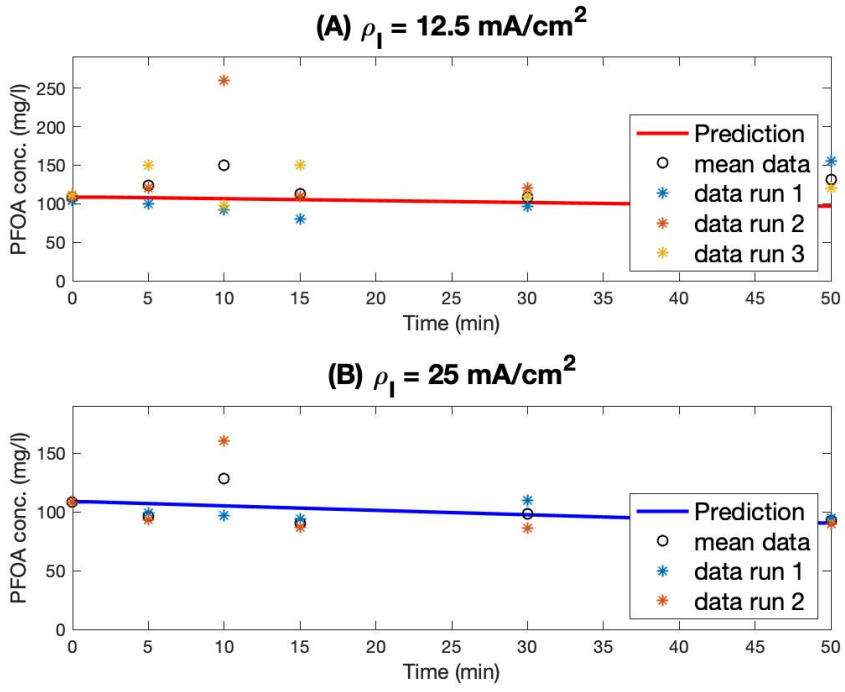

Figure 15: Results of PFOA removal experiments, model prediction and experimental data.

The variability in the concentration data was very high. As the initial concentrations were relatively close together, the variation in results originated from the EC treatment. The EC process is relatively uncontrolled, because small changes in experimental conditions cause large differences in pH or

$Fe(OH)_3$ precipitation. An additional error source was formed by the dilution of the samples. Moreover, the instrument calibration was for samples with significantly lower PFAS concentrations, requiring additional dilution before the measurements. Altogether, this created a high level of uncertainty. Nonetheless, the lack of samples with decreased concentrations ratified the conclusion that significant removal of PFOA did not occur under the current experimental circumstances.

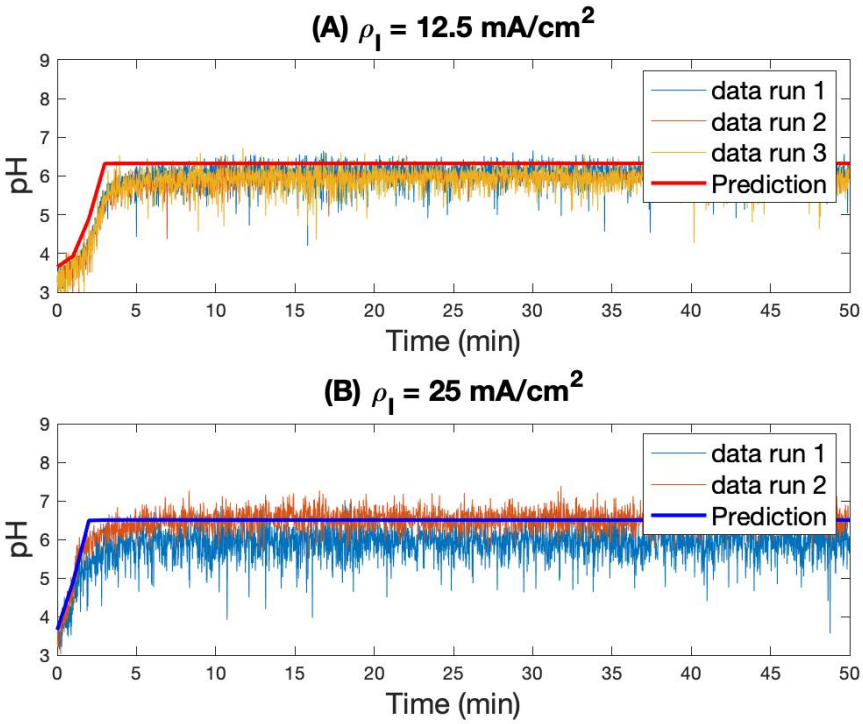

Figure 16: pH vs time during PFOA removal experiments at current densities of (A) 12.5 mA/cm² and (B) 25 mA/cm².

4.5.2 EC with PFOS

The flocs formed in EC with PFOS settled relatively easily after the experiments and the UV absorption (254 nm) of all diluted centrifuged samples was again negligible. The initial pH of the PFOA solution was low, since PFOA was dosed as an acid. Because PFOS is added as potassium salt, the initial pH was around 5.5 and thus similar to that of demineralized water. Accordingly, the increase in pH was less steep during PFOS removal than during PFOA removal. Except for these differences, no clear distinctions were observable during the experiments.

The PFOS removal started fast but stagnated around 72% after five minutes. This indicates that there was a change in binding affinity to the flocs, possibly because of the increased pH or a changed zeta-potential. Alternatively, it suggests another mechanism of PFOS removal than adsorption. In the current model, it was not possible to reproduce these experimental results. Although the predicted pH development was again relatively accurate, the removal continued to 100% rather than stagnating after five minutes. In EC, the number of surface sites increases linearly over time, due to the continuous precipitation of $Fe(OH)_3$. Despite the less favorable adsorption at increased pH, this rapid formation of new surface sites should cause a continued removal. The lack of such a dose-response relationship implied the likeliness of an alternative removal mechanism.

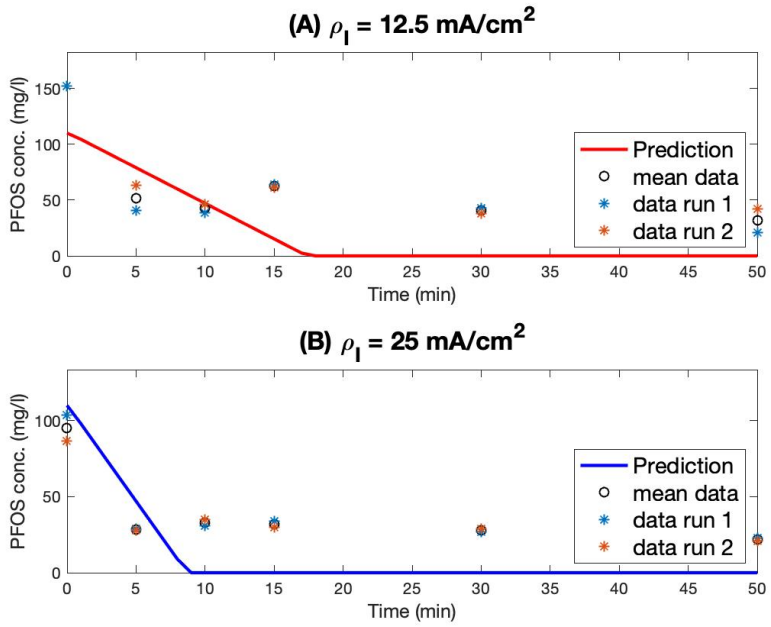

Figure 17: Results of PFOS removal experiments, model prediction and experimental data.

The mean initial concentration of all the runs with PFOS was 115.3 mg/L, hence this concentration was used for calculating the removal. At 12.5 mA/cm^2, the mean final removal was 72.7% (83.8 and 63.6 for run 1 and 2, respectively). At 25 mA/cm^2, the mean final removal was 81.1% (80.2 and 81.9, respectively) after fifty minutes of treatment. Similar to the results for PFOA, this differed from the literature values of approximately 80 % and 99 % removal at 12.5 mA/cm^2 and 25 mA/cm^2, respectively[4]. Also the behavior of the removal was different, since in literature the removal continued over time, while in the current results no significant further removal occurred after the first five minutes of treatment. Interestingly, a very recent research using PREC with Al-Zn electrodes also showed steep PFOS removal within 5 minutes of treatment[51].

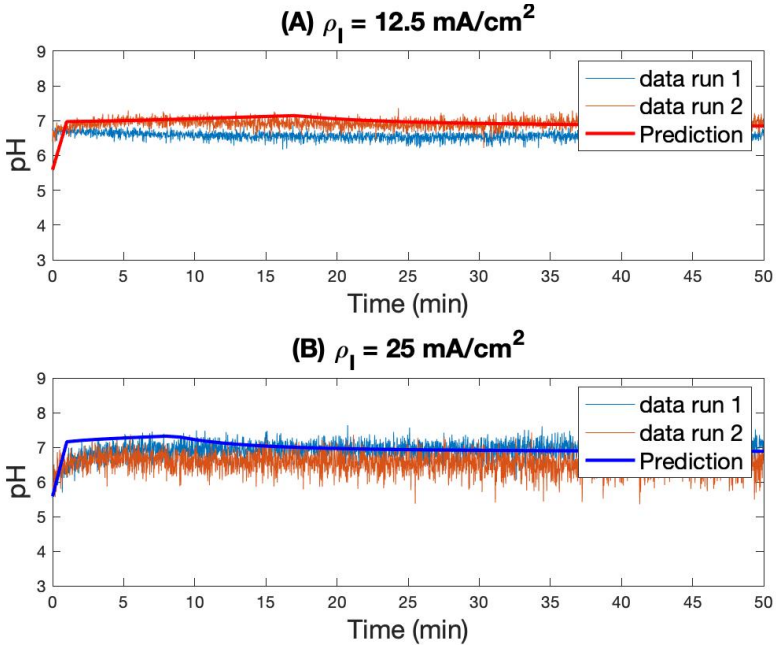

Figure 18: pH vs time during PFOS removal experiments at current densities of (A) 12.5 and (B) 25 mA/cm^2.

The sensitivity of the predicted removal to the exact values of the log(K) constants was low. For a $\log(K)_2$ and $\log(K)_3$ between 40 and 50, the predicted removal was identical, as illustrated in Appendix 14. Conversely, the predicted pH largely depended on the ratio between $\log(K)_2$ and $\log(K)_3$. If $\log(K)_2$ was higher than $\log(K)_3$, H^+ ions are consumed in the adsorption reactions. This resulted in an initially strongly increased pH, that decreased again over time. The magnitude of this pH peak increased for a larger difference between the two log(K) values. A pH peak was observed in the experimental results with humic acid, as will be illustrated in section 4.6.2 and Figure 21. Therefore, the currently chosen log(K) values also lead to a small peak. Appendix 14 illustrates which adapted log(K) values represent alternative pH behavior.

4.5.3 EC with PFBS and PFBA

Figure 19 summarizes the results of the simultaneous removal of PFBS and PFBA. The experimental results obtained for the PFBS and PFBA concentrations were implausible for three reasons. First of all, the aimed initial concentrations were 33 and 46 mg/L for PFBA and PFBS, respectively, whereas the measured concentrations were 92.5 and 127.5 mg/L. This difference of a factor three was too extreme to be caused by a measuring error during addition of the PFAS. Secondly, for one of the samples, very different concentrations were determined by Eurofins after reanalysis. First, concentrations below the detection limit of 0.2 mg/L were reported, but the reanalysis found concentrations of 38.5 mg/L PFBS and 26.5 mg/L PFBA. For the other samples, insufficient sample volume remained to reanalyze them.

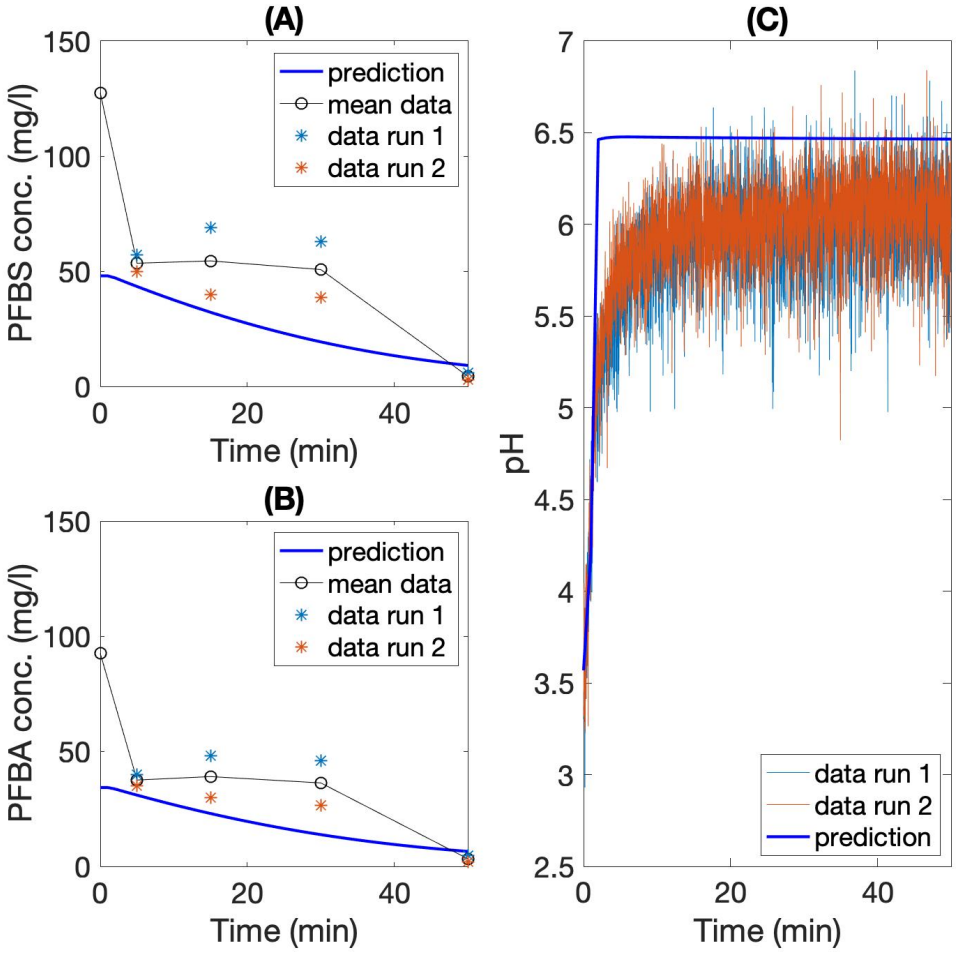

Figure 19: (A) PFBS and (B) PFBA concentrations and (C) pH during PFBA and PFBS removal experiments. The current density was 25 mA/cm² and all other experimental conditions were as before.

Finally, the removal would behave very inexplicably if these results are correct, as illustrated in Figure 19. In the first five minutes, the concentration of PFBA and PFBS decreased by approximately 50 %. Hereafter, it was constant until 30 minutes of treatment time. During the final 20 minutes, the removal then almost reached completion. If the measured results are correct, a mean removal of 96 % was reached for both PFBS and PFBA. However, it is deemed more probable that the initial and final concentration measurements were incorrect, and there was no significant removal at all. Repetition of these experiments is needed to verify the obtained results. Presently, these results were deemed too unreliable to be further included in the current research. Hence, all forthcoming conclusions will be based exclusively on the results for PFOS and PFOA removal.

The dilution factor applied to the sample at time 0 was 25, and that for the samples at times 5, 15 and 30 min was 10. The final sample was sent in undiluted. However, during the analysis stage at Eurofins, the samples were diluted further to obtain concentrations within the detection range of the analytical equipment. It was expected that Eurofins diluted the final sample more than the intermediate samples, and the initial sample less, to obtain concentrations within this detection range. However, possibly they erroneously applied their dilution factor used for the intermediate samples in the calculation of all of the reported concentrations. This would explain the inexplicable removal behavior, as well as the high reported initial concentrations. Because insufficient sample material remained, this hypothesis was impossible to verify, and these results were omitted from any further conclusions.

The experimental data could not be represented accurately by the current model. The pH prediction by PHREEQC matched the results significantly better when considering the aimed initial concentrations, instead of the measured ones. Accordingly, the aimed initial concentrations were used for the model prediction. Various different combinations of log(K) values for the adsorption reactions yielded similar removal results. As the removal of PFBS and PFBA was tested simultaneously, the log(K) values for one of the species also affected the removal of the other. Moreover, which sorption species was dominant for each PFAS type could not be determined. Because the reliability of the experimental data was deemed uncertain, no elaborate attempts to improve the model fit were carried out.

4.6 Electrocoagulation experiments with organic matter and PFAS: competition assessment

4.6.1 PFOA with HA

The UV absorption results indicated no significant influence of the presence of PFOA on the humic acid removal. Humic acid was still removed at the same rate as without PFOA in solution, and complete removal was achieved after 15 minutes of treatment. Interestingly, the final TOC concentrations (6.2 and 11 mg/L) were not in agreement with the final PFOA concentrations of 120 and 100 mg/L. The TOC content of PFOA is around 23 %, so TOC concentrations of at least 23 mg/L would be expected at these PFOA concentrations. If there is also still any HA remaining, the measured TOC concentrations should be even higher. In literature, a good correlation between TOC removal and PFOA degradation by gamma-ray irradiation was shown, indicating that TOC should indeed include PFOA[89].

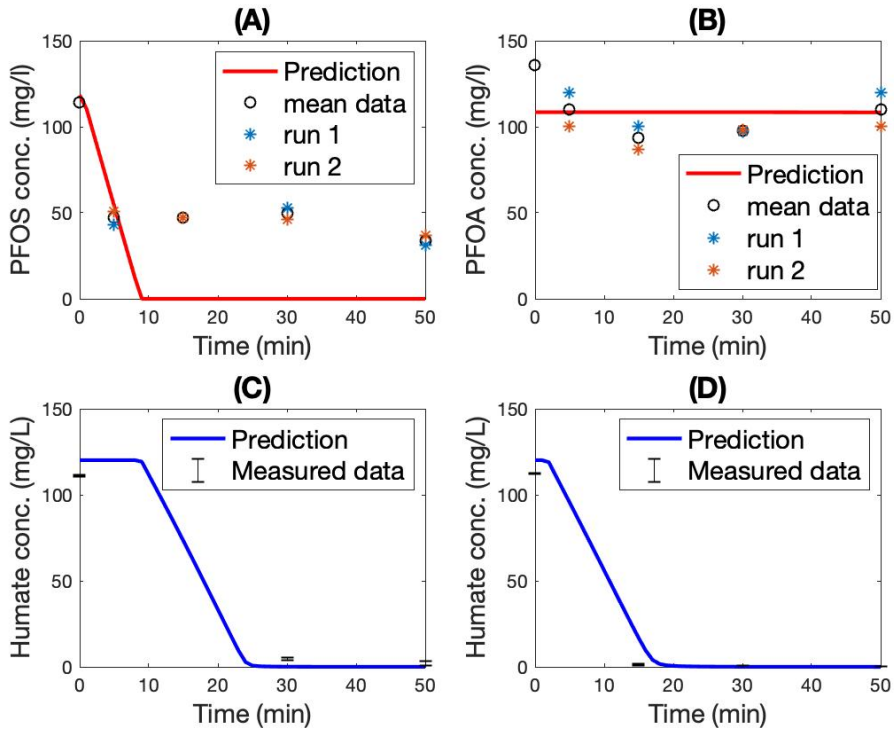

Figure 20: Results of simultaneous HA and PFAS removal. (A) PFOS removal with HA; (B) PFOA removal with HA; (C) HA removal with PFOS; (D) HA removal with PFOA. The HA concentration results are calculated from the UV absorption (λ = 254 nm) using the calibration curve given in Appendix 18. Data-points are represented by error bars located at the mean value of the three runs. The error bars include the standard deviation in the three parallel runs, as well as the standard deviation in the three parallel runs for determination of the blank absorption during EC. Measurements outside the calibration range at early timesteps of 5, 10 and 15 minutes are excluded from the plots. All tests were carried out at 25 mA/cm², with all other conditions as before.

TOC determination was performed by the complete oxidation of the acidified sample and determining the amount of CO_2 formed. From the amount of CO_2, the TOC concentration of the sample can be calculated using a calibration curve[90]. If the oxidation method used does not fully oxidize all PFAS in solution, the resulting TOC concentration is too low. As PFAS are notably difficult to oxidize fully, this is a probable explanation for the disagreement between the TOC and PFAS results. Measuring the TOC concentration of PFOA and PFOS solutions with known concentrations in duplicate also gave inconclusive results, confirming that not all PFAS was included in the TOC measurements. For PFOA, approximately 20% of the TOC was measured (19.1 % and 22.3 %, respectively). For PFOS, this was 36 % (32.6 % and 39.3 %, respectively).

If 20 % of the final PFOA concentration was measured as TOC in these experiments, that would lead to TOC concentrations of 5.2 and 1.4 mg/L originating from humic acid. These results are highly speculative, because it remains uncertain which fraction of PFOA is included exactly in the TOC results. Nonetheless, it confirmed that significant HA removal occurs, as the initial TOC concentration was roughly 43 mg/L. Therefore, it is reasonable to conclude that HA removal was indeed unaffected by the presence of PFOA as co-solute.

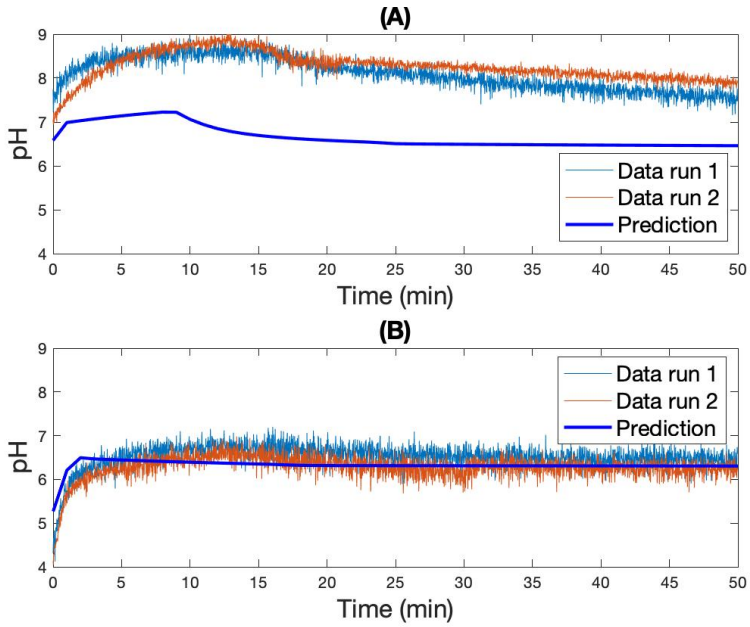

Figure 21: pH during simultaneous removal of HA with (A) PFOS and (B) PFOA. The current density was 25 mA/cm² and all other parameters were as before.

The model predicted no PFOA removal, due to the competition for adsorption sites by HA. The data also showed low removal of PFOA, although the variability between the results was again high. This made drawing reliable conclusions from the laboratory data difficult. Moreover, the measured initial concentration was much higher than that of all other PFOA runs. The initial concentration was only measured once, rather than in duplicate. If this concentration is accurate, removal of PFOA did occur. However, the initial PFOA concentration was close to 108 mg/L in all other tests, so this initial concentration measurement is probably incorrect. The pH prediction was relatively accurate, although the initial pH was slightly off. This was probably due to the inaccurate definition of the humic acid species in the model database.

4.6.2 PFOS with HA

In contrast with PFOA, the presence of PFOS affected the removal of humic acid. In all other tests with 120 mg/L HA at 25 mA/cm², almost complete removal of HA was achieved within 15 minutes. In the presence of PFOS, however, the UV absorption remained very high. Determination of an accurate HA concentration was impossible, because complexation with iron occurred and the UV absorption exceeded the calibrated range. Nonetheless, this indicated that PFOS was removed preferentially to humic acid and competed with HA for the adsorption sites, which was confirmed by the unaffected initial PFOS removal. The final PFOS concentration was slightly higher than in the experiments without HA, corresponding to a mean removal of 70.4 % rather than 81.1 %.

The presence of PFOS thus impeded HA removal, whereas the removal of PFOS was relatively unaffected by HA as co-solute. If adsorption is involved in the removal of PFOS, this indicates that the sorption of PFOS was more favorable than that of HA. However, the initial TOC concentration of the sample associated with HA was only approximately 43 mg/L. The TOC concentration in all real leachate samples tested varied between 51 and 470 mg/L. Thus, higher concentrations of HA must be tested to assess the generalizability of this more favorable PFOS sorption. Moreover, it should be determined

whether the slightly increased remaining concentration of PFOS was due to the presence of HA, or due to the normal variability in the final concentration.

The final TOC concentrations for runs 1 and 2 were 4.8 and 4.3 mg/L, respectively. The TOC content of PFOS is 19.2 % by mass, and the final PFOS concentrations were 31 and 37 mg/L. Assuming that 36% of the PFOS TOC is included in these measurements, see section 4.6.1, the final TOC concentrations originating from HA were 2.7 and 1.7 mg/L. It should again be noted that the uncertainty in these values is high, but they indicated that HA removal was successful, despite the retardation effect caused by the presence of PFOS.

Although the trend in pH was reproduced by the model, there was a difference of about 1 pH unit. The pH behavior was different from other experiments. A clear maximum in pH was reached, after which the pH decreased again. This is probably explained by the change from PFOS removal to HA removal. The model results clearly indicated that HA removal only occurs after significant PFOS removal. Moreover, competition for adsorption sites with Fe^{2+} occurred. Adsorption of Fe^{2+} increased once HA and PFOS adsorption have stabilized, resulting in a slowly decreasing pH due to H^{+} release. The magnitude of this pH peak strongly depended on the ratio between $\log(K)_2$ and $\log(K)_3$ for the different surface species related to PFOS adsorption, as explained in section 4.5.2.

4.7 Effect of pH on surface characteristics

The most apparent explanation for the constant PFOS concentration after an initial fast removal phase is a prohibited further removal by the increased pH. At a high pH, the surface charge of the binding sites may change from positive to negative, thereby preventing further PFOS sorption. To test this hypothesis, the modelled surface composition as it remained after 50 minutes treatment was equilibrated with solutions at different pH values. The surface without pollutants, as well as with PFOS and PFOA were simulated and the surface charge and corresponding potential were plotted versus pH, as shown in Figure 22. The remaining PFAS concentration after equilibration was also plotted for each pH value.

The surface charge of the $Fe(OH)_3$ flocs formed without pollutants indeed decreased for higher pH, but only dropped below zero for a pH above 11. The pH in the PFOS removal experiments only increased from 5.6 to approximately 7. With the currently defined binding constants, the surface was negatively charged in the presence of PFOS and PFOA at all pH values exceeding 2. This was due to the binding of these compounds, which leads to a decreasing surface charge. Theoretically, PFOA binding was strongly favored at low pH, resulting in lower surface charges for decreasing pH. However, in practice $Fe(OH)_3$ dissolves at low pH, so this is of limited applicability. PFOS was fully removed at all pH values with the currently defined binding constants. Decreased binding constants lead to incomplete removal at increasing pH but could not represent the initial fast removal (data not shown).

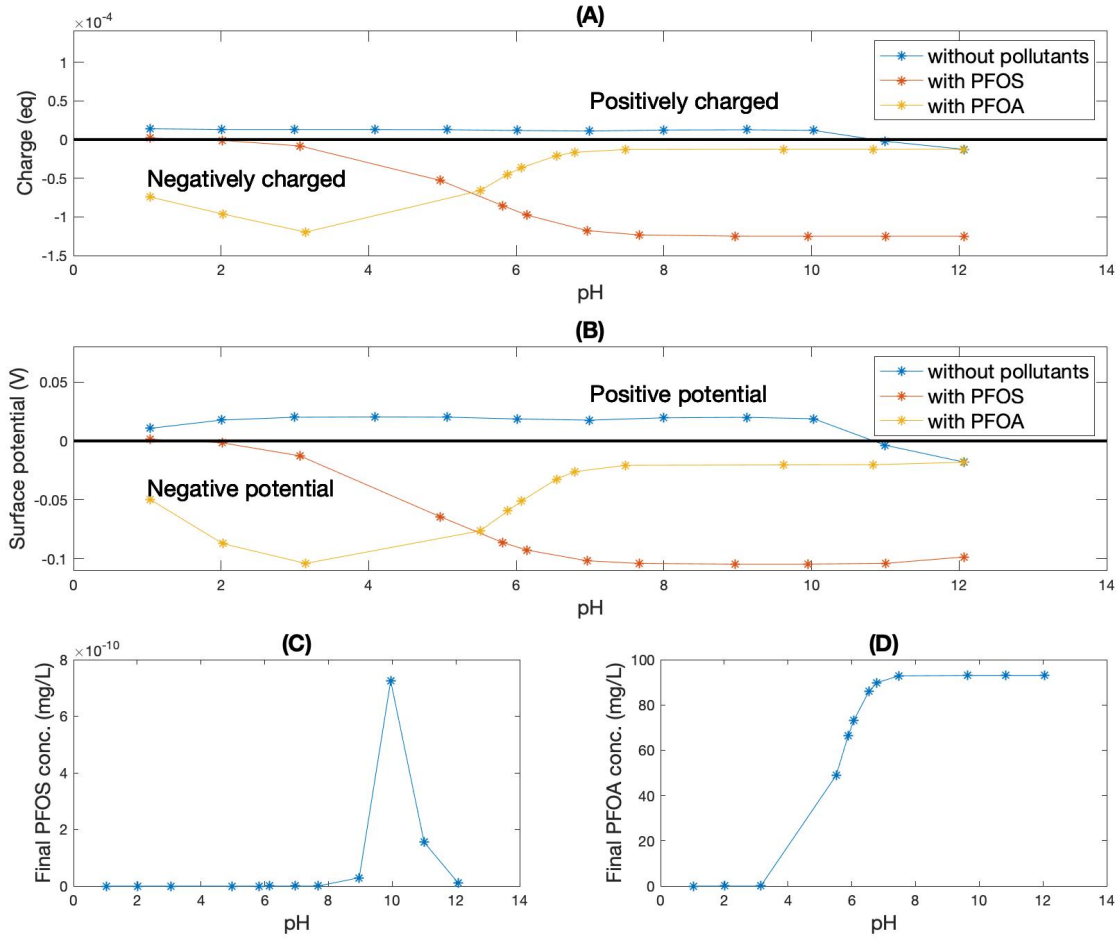

Figure 22: (A) Final surface charge, (B) surface potential (ψ), (C) final PFOS concentration and (D) final PFOA concentration versus pH. ψ is the surface potential as used in Equation 5 for the calculation of the activity corrections.

4.8 Changes in the linear/branched PFOS ratio during treatment

PFOS exists mostly in the linear form, where all non-terminal carbon atoms are attached to only 2 other carbons. However, branched isomers also exist and were detected in the artificial wastewater. The results so far were all summations of the branched and linear isomer concentrations. The ratio between these two isomers was expected to remain constant, unless one isomer is removed preferentially. For preferential removal of the linear isomer, the ratio linear/branched was expected to decrease over time. A decreasing ratio was observed in the experiments, but the trend was not entirely as expected from the concentration determinations. In all experiments, the total PFOS concentration decreased steeply in the first five minutes, as did the linear/branched ratio. Then, both the concentration and the ratio were relatively constant until 30 minutes. Whereas the concentration did not decrease significantly at 50 minutes, the ratio decreased further.

The decrease in linear/branched ratio was clearly not linearly related to treatment time, but neither was the removal. However, the ratio was also not merely correlated with the removal extent. Instead, the dilution factor of the samples seems to be important for the linear/branched ratio, as illustrated in Figure 23. All samples at time 0 were diluted 20 times, and all final samples were sent in undiluted. The samples at intermediate times were all diluted 10 times. The large difference between the initial ratio and that during treatment could be due to preferential removal of linear PFOS, but the difference between the intermediate and final samples remains unexplained. This could indicate that the integration of the mass spectrometry peaks corresponding to linear and branched PFOS is erroneous.

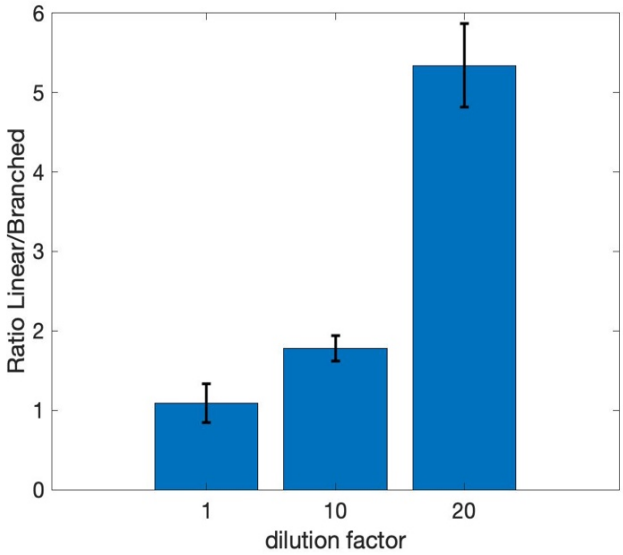

Figure 23: Ratio of linear:branched PFOS. A dilution factor of 1 corresponds to all final samples, a dilution factor of 10 to all samples at time 5, 10, 15 and 30 minutes, and a dilution factor of 20 to the initial concentration determinations.

For all wastewater samples, the UV absorption as well as the TOC concentration clearly decreased over time, as illustrated in Figure 24 and Appendix 19. The decrease in UV absorption is due to removal of other compounds than PFAS, as PFAS is not UV-active. Both results showed a high level of reproducibility between the runs, indicating that EC is a reliable treatment method for TOC and color removal. The UV absorption most likely originates from organic matter, as especially aromatic compounds are known to be highly colored.[86] However, also the presence of metals may lead to UV absorption. PFAS were not UV active, so the decrease in UV absorption is not related to PFAS removal.

The Nauerna influent and effluent as well as the Zeeasterweg 5 samples became a light orange suspension during treatment. The light orange color is probably explained due to the mixed formation of white $CaCO_3$ (lime) and orange $Fe(OH)_3$. The Zeeasterweg 8 sample turned black within the first five minutes of treatment, but the color decreased to a light brown over time. Lime formation was observed, and a dense foam formed on top of the liquid. The final precipitate was very difficult to remove from the reactor walls and the electrodes, possibly making EC a less useful treatment technique for this wastewater.

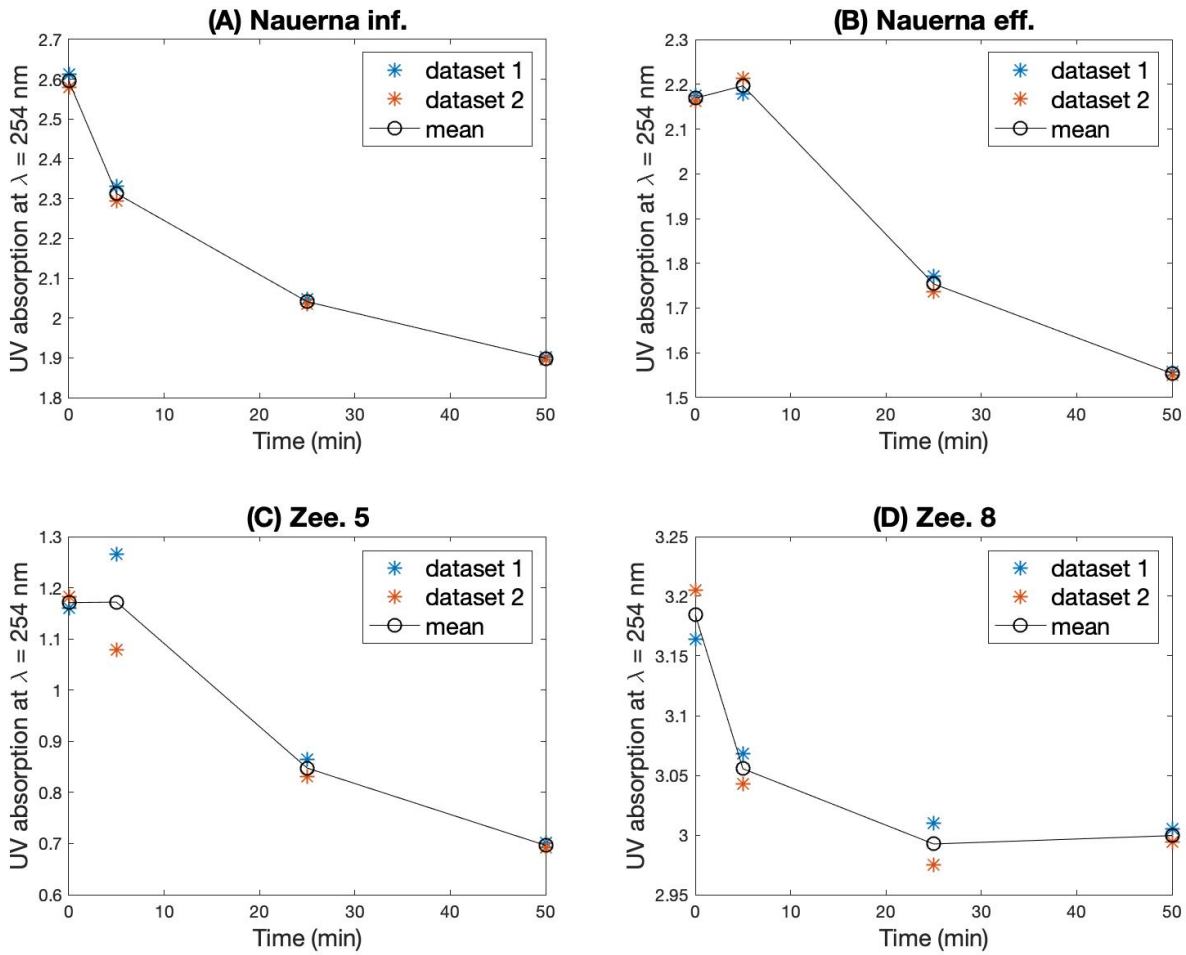

Figure 24: UV absorption over time during EC treatment of real wastewater. All tests were performed at 25 mA/cm², with all other conditions as before.

All measurable PFAS concentrations over time during EC treatment of the real wastewater samples are given in Appendix 20a-d. Only the species that were present at a detectable concentration in at least one sample are shown. For PFOS and PFOA, it is likely that external pollution occurred during the treatment. Their concentrations fluctuated strongly and sometimes even increased with treatment time. PFAS are known to adsorb to glass, and although all material was thoroughly rinsed with demiwater before use, traces of PFOA and PFOS were probably still present in the reactor vessel or measurement equipment. Except for traces of PFBA in the Nauerna effluent, no other PFAS were detected at quantifiable levels in the Nauerna water samples, so no statements on PFAS removal can be made.

Perfluorobutanesulfonylamide(N-methyl)acetate (MeFBSAA) was detected in both the Zee. 5 and Zee. 8 wastewaters. Although the results are inconclusive, concentrations were seen to decrease in some of the runs, indicating that EC could be a suitable treatment technique for this compound. However, further tests are needed to achieve reproducibility and confirm the removal. Perfluoropentanoic acid (PFPeA) and PFBS were also detected in Zee. 8 water, but except for negligible concentrations in the final sample of run 1, no significant removal was detected for either.

The results of the experiments with Zee 5. water spiked with PFOA, PFBS and PFBA (Appendix 21, Figure 25) were clearer. Interestingly, Perfluoroheptanoic acid (PFHpA) and Perfluorohexanoic acid (PFHxA) were detected in these samples, although they were not in the unspiked Zee. 5 water. These compounds were removed during treatment, but the variability between the runs was high. Conversely,

the results for the samples with added PFAS were relatively similar for both runs. For all compounds, the removal was highest after five minutes of treatment (23.3 %, 24.7 % and 26.0 % for PFBA, PFOA and PFBS, respectively), after which the concentration increased again. This is in accordance with the earlier results for PFOS removal, where most of the removal was reached in the first five minutes. The difference in pH results was partly due to the withdrawal of relatively high sample volumes, which skewed the results.

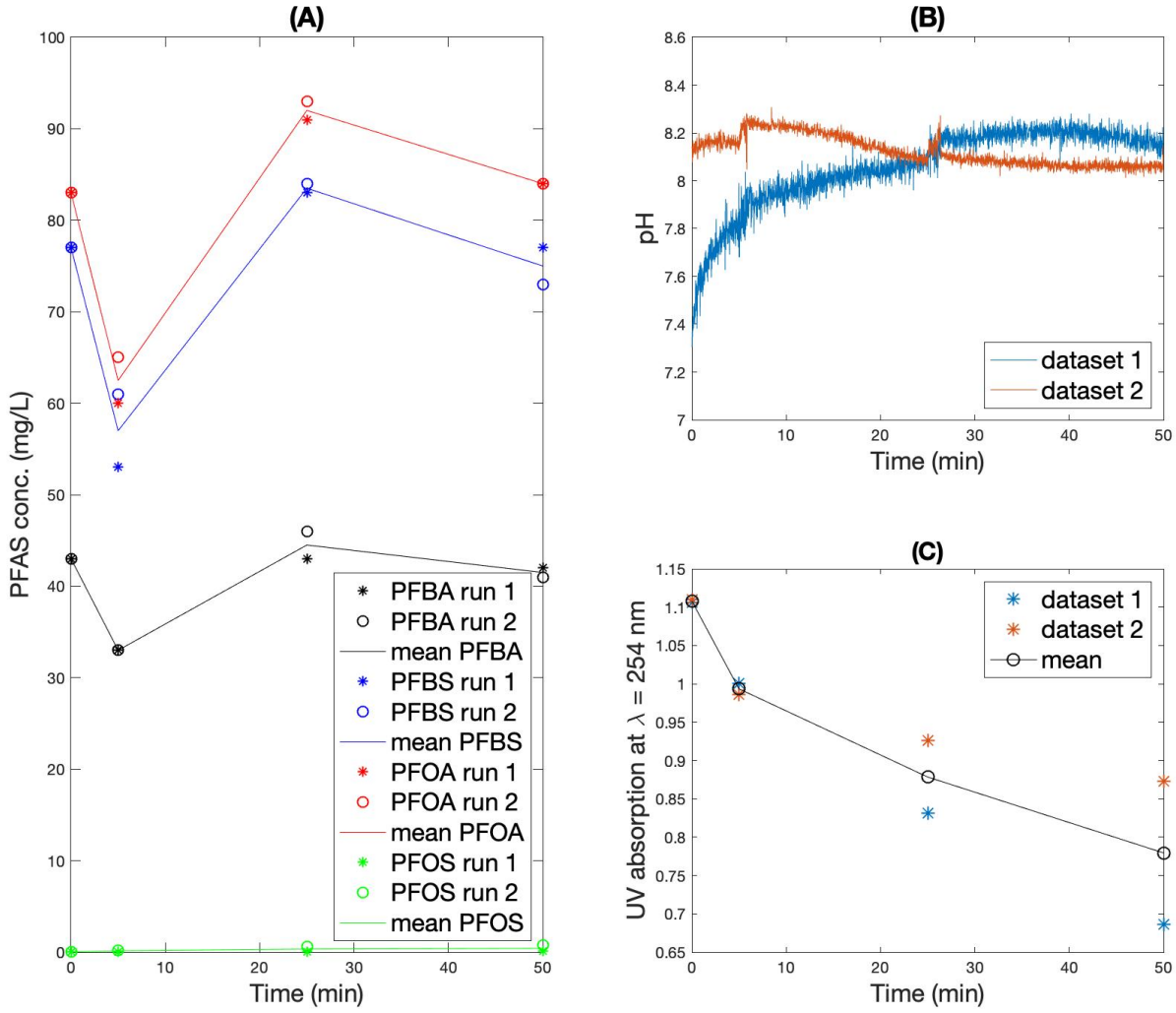

Figure 25: (A) PFAS concentrations, (B) pH and (C) UV absorption versus time during the treatment of Zee. 5 leachate with PFOA, PFBS and PFBA added before treatment. The current density was 25 mA/cm² and all other conditions were as defined previously.

The final TOC concentrations were 66 and 68 mg/L. This was higher than the initial TOC concentration of the unspiked Zee. 5 water, which was 51 mg/L. Initial concentrations of the spiked water were not measured, and neither were the detected fractions of TOC originating from PFBS and PFBA. Based on a TOC content of 23.2, 16.0 and 22.5 % for PFOA, PFBS and PFBA, respectively, the expected final TOC concentrations originating from PFAS were 41.4 and 40.6 mg/L. As it is not certain what percentage of this TOC is detected by the measurement technique, no definite conclusions on the TOC removal can be drawn. Comparing Figure 24 to Figure 25 shows that the decrease in UV absorption is slightly less for the spiked Zee. 5 water, but also this difference is not significant.

4.9 Model uncertainties

4.9.1 Determination of CO_2 and O_2 dissolution rates

Naturally, the determined kinetic constants depend heavily on experimental conditions such as stirring rate and the shape of the flask. The pressure of the aeration system was also an important variable, which was not controlled very accurately in the current research. Therefore, the determined values should be considered to give an order of magnitude only. Although the pH predicted by the final electrocoagulation model was sensitive to these values, the sensitivity of the removal prediction was lower. Hence, for the purpose of modelling removal efficiencies over time, these gas dissolution rates are not very relevant as long as oxygen is non-limiting.

4.9.2 Equilibrium versus non-equilibrium processes

PHREEQC is a very useful program for calculating equilibrium compositions of aqueous solutions, but including kinetic processes is less straightforward. All calculations in PHREEQC are based on equilibrium, except if kinetic rate laws are explicitly included. In the current model, kinetics were only included for the addition of iron based on Faradays law, the dissolution of CO_2 and O_2 and the oxidation of Fe(II) to Fe(III). Hence, processes like precipitation and adsorption were allowed to go to their equilibrium state immediately, without kinetic limitations. For precipitation, the kinetics were probably mostly relevant in the beginning of the treatment, when the supersaturation with respect to $Fe(OH)_3$ was not extremely high yet.

For adsorption, the relevance of kinetic limitations was less clear. The solution was continuously stirred and aerated, which minimized mass transfer limitations. Nonetheless, concentration gradients were expected to exist on the molecular scale near the $Fe(OH)_3$ surfaces. Concentration differences were also expected in the vicinity of the electrodes. Continuous formation of Fe^{2+} and OH^- takes place at the anode and the cathode, respectively. Although the solution was stirred, it remained probable that most $Fe(OH)_3$ still precipitated in this region, where the PFAS concentration might be different than the bulk concentration. If generalizable adsorption parameters are required, exclusion of these effects from their calibration is necessary.

The manually defined adsorption log(K) constants currently include these kinetic effects, as they were defined based on data that included kinetic processes. Hence, the adsorption constants are not expected to apply outside the currently defined system. Moreover, complexation of PFAS to iron in solution is ignored in the present model. As these molecules are oppositely charged, their complex formation is to be expected, but the extent of complex formation is unclear. Inclusion of accurate binding equations may lead to different adsorption constants that fit the data. The same holds for micelle formation of the PFAS molecules. Overall, more laboratory experiments under varying circumstances are needed to determine the log(K) values more accurately.

4.10 Experimental uncertainties

4.10.1 Determination of Humate concentration

Determination of the humic acid concentration based on the UV absorption could only be performed reliably after almost complete removal of the humic acid, because iron complexation changed the absorption curve. Nonetheless, these results proved equally valuable as the TOC measurements, because the variability of the TOC measurements was very high. The variability in UV absorption of the

samples outside the calibration range was actually very low, so this was most likely an analytical limitation. According to the NeN norms used for the determination of TOC, the standard intralaboratory variability is at most 5.5 %[90]. The current variability exceeded this uncertainty. However, both the TOC and the UV results indicated that the time needed for complete removal increases linearly for increasing initial concentration or decreasing current density, which was represented accurately by the model.

4.10.2 Inconsistencies in PFAS concentration results

An important limitation in the current research was the outsourcing of the PFAS- and TOC analyses to Eurofins laboratory. Although their professionalism is beyond dispute, in-house analyses remain preferable, since the time between sample collection and analysis can be minimized. The waiting time could currently reach up to four weeks, hence adapting the research methods to unexpected results was impossible. Finally, observing and managing inconsistencies during analysis was impossible with outsourced analyses, as was re-doing a certain analysis. Inconsistencies in the determined PFBS and PFBA concentrations were already outlined in section 4.5.3. The three most relevant remaining uncertainties related to the PFAS concentrations received from Eurofins will be elaborated upon below.

First, the initial PFAS concentrations measured by Eurofins varied widely between some of the runs, even though the solutions were made by diluting the same stock solution. The stock solutions were stirred before the dilution, so concentration gradients within the stock should be negligible. The solubility of PFOA far exceeded the concentration in the stock solution, so the initial PFOA concentration was expected to be constant between the runs. This expectation was true for all runs, except for the tests with PFOA and HA. Since the PFOA concentration in the solution with PFOS and HA was negligible, the high PFOA level did not originate from the HA. Hence, it was deemed a measurement error and the removal was calculated based on the expected initial concentration.

The PFOS potassium salt was very hygroscopic and thus difficult to dissolve, leading to the possibility of an inhomogeneous stock solution. The high variability in the measured initial concentrations could thus be accurate. Nonetheless, the model predictions and calculated removal rates were based on the expected initial concentration, as the initial concentrations remain uncertain. Moreover, the stock concentration exceeded the solubility of the PFOS potassium salt, so all PFOS should have been dissolved. The variability in concentration level of the treated samples between the runs was small in most cases. Nevertheless, these results should be treated with caution, as the removal might be higher or lower than stated if the initial concentration was in fact different.

A second complication was the inconsistency between the TOC and PFAS concentration measurements. As mentioned in section 4.6.1, the TOC measurements did not include the TOC originating from PFAS completely, implying that either the TOC or the PFAS results were wrong. It is assumed that the TOC measurements were incomplete, since the measured TOC level of solutions with known PFAS concentration were also too low. The reasoning behind this assumption was discussed in more detail in section 4.6. However, it is also a remote possibility that all measured PFAS levels were incorrect. This hypothesis is less likely, because the initial concentrations measured for PFOS and PFOA were in the range of the expected values, as were the results of the diluted PFAS stock solution.

Thirdly, the change in ratio between the branched and the linear form of PFOS was also difficult to explain, as discussed in section 4.8. A correlation between this ratio and the applied dilution factor was found, which indicated that the dilution steps may have introduced a significant uncertainty. However,

the effect of dilution on the linear/branched ratio was not observed for the results of the diluted stock solutions (Appendix 9). Possibly, the large change in ratio after 5 minutes of treatment was thus merely caused by a preferential removal of the linear isomer. Then, the change in ratio after 30 minutes of treatment was part of the natural fluctuations in this ratio, as no significant further removal was observed after this time.

4.11 IMPLICATIONS OF RESULTS

First of all, the presented results suggest that PFOS is removed more efficiently than PFOA under the examined conditions. PFOS is a slightly larger molecule than PFOA, as can be seen from Figure 1. This larger size could contribute to the improved removal, due to an increased attraction between the PFOS molecule and the flocs. However, as *Yang et al*. suggested electrostatic adsorption to be the main mechanism of removal[4], it is more probable that the difference in removal efficiency originates from the lower pKa value of PFOS as compared to PFOA, caused by its different headgroup. It should be noted that *Yang et al*. also reported a significantly higher PFOA removal than was found in the current research[4], so the lower pKa value may not be a complete explanation for the difference in removal.

Another important implication of all aforementioned results is that the mechanism of PFOS removal is probably not strictly limited to electrostatic adsorption. Reproducing the fast initial removal was only possible with high equilibrium constants for adsorption on the Hfo surface. However, stagnation of the removal after five minutes indicates that these high binding constants cannot be accurate. Appropriately decreasing the log(K) values lead to an accurate prediction of the final concentration, but not of the initial removal. An alternative removal mechanism consists of coprecipitation of PFOS, e.g. it is incorporated in the initially formed $Fe(OH)_3$ flocs. Alternatively, charge neutralization of PFOS molecules by the formed iron ions could lead to their aggregation and direct precipitation.

The occurrence of a different mechanism of PFOS removal would also explain the low impact of humic acid as co-solute, since competition for the adsorption sites is irrelevant if PFOS is not electrostatically adsorbed. However, the humic acid removal fits the electrostatic adsorption model well, as shown by the linear decrease of the removal time for an increasing current or decreasing initial concentration. The retardation of humic acid removal in the presence of PFOS was fittingly explained by the involvement of competition for the adsorption sites. Accordingly, electrostatic adsorption of PFOS would be involved in the removal process. Alternatively, the presence of PFOS prohibits the removal of HA through another mechanism.

Including different forms of precipitating iron-PFOS species in the model was possible and lead to the experimentally observed final equilibrium concentration remaining in solution. The level of this equilibrium concentration depended on the equilibrium constant, as well as on the exact definition of the species. However, the initial removal was still not as fast as observed in the laboratory data. Moreover, high equilibrium constants were again needed to overcome the dominance of $Fe(OH)_3$ precipitation. Combinations of the different removal mechanisms could also be incorporated but lead to many different unknown parameters for which optimization is necessary. As independent datasets were not available for the optimization of all parameters, this was excluded from the current research.

An alternative explanation for the disagreement between the model and experimental results is the occurrence of a mass transfer limitation. As mentioned in section 2.7, the cell potential and current intensity suffice for accurate representation of the process rate in EC systems limited by overpotential.

Currently, the model only includes these variables in its parameterization of the EC procedure. The simulated results for EC without pollutants, EC with HA removal and EC with PFOA removal matched the experimental data well. Hence, it could be hypothesized that these systems were indeed limited by overpotential and mass transfer limitations were negligible.

Conversely, the PFOS removal was not represented well by the model. Section 2.7 also described the necessity of including the Nernst-Planck equation (Equation 4) to parameterize EC limited by mass transfer in the boundary layers of the electrodes. Optionally, a detailed inclusion of this equation would indeed yield better model results. Most probably, the system was initially limited by overpotential, causing the fast initial removal phase. At a given moment hereafter, mass transfer limitations may have developed in the vicinity of the electrodes, thereby significantly slowing down any further removal. A detailed description of the ion flux near the electrodes would be needed to represent this phenomenon. Prior to complicating the model by the inclusion of this limiting equation, tests at lower current intensity could be carried out to decrease the overpotential and see if the limiting process is indeed altered.

5. CONCLUSION

The first aim of the present research was to investigate the effect of organic co-solutes on the removal of PFAS using electrocoagulation with iron electrodes. The second objective was to simulate this process in a computational model. In this chapter, the core findings are briefly repeated and their implications are discussed. The chapter also serves to reflect on the position of the presented work within the current state-of-the-art. Moreover, for both research goals, the extent of their realization will be substantiated. Finally, suggestions for improvement and recommendations for further research are listed and discussed.

One of the major results of this research was that it did not confirm the high PFAS removal efficiency as observed in previous studies. In general, therefore, the results opposed the high effectiveness of electrocoagulation as a treatment technology for PFAS removal. Specifically, the robustness of the treatment was refuted, as the differences in experimental conditions between this work and the work of Yang *et al.*[4] were small, but their results were not reproduced. These differences in results indicated that the treatment efficiency is sensitive to changes in certain process conditions, such as the aeration rate or the method of floc separation. Taken together, these findings have significant implications for the implementation of electrocoagulation aimed at PFAS removal on larger scales, where the process control is expected to be even more complex.

Because the removal efficiency of PFAS with EC was lower than expected, an accurate determination of the effect of organic co-solutes was difficult. Nonetheless, a thorough literature search indicated this work to be the first that directly compared PFAS removal rates in the presence or absence of organic co-solutes under otherwise identical experimental conditions. PFOA removal was not significant with or without HA as additional solute. Conversely, this study identified a significant PFOS removal within 5 minutes treatment time both with and without HA, and it revealed a decreased removal rate of HA in the presence of PFOS. These findings suggest that PFOS is removed preferentially to HA. However, more diverse experimental conditions must be tested to generalize this conclusion, such as other initial concentrations for PFOS and HA.

This study was the first of its kind in its utilization of the PHREEQC software for modelling electrocoagulation as a treatment technique for PFAS removal. It showed that PHREEQC has a promising capability of reproducing experimental electrocoagulation data. The established model could represent electrocoagulation without pollutants accurately, as well as PO_4^{3-} removal and humic acid removal. The results of the tests with PFOA were also simulated well. Another promising use of the model is the identification of the dominant mechanism in the removal of a specific pollutant. The results of the PFOS removal experiments could not be reproduced accurately by the model, which indicated that the mechanism of PFOS removal was not limited to electrostatic adsorption.

The current study was limited by the absence of in-house analysis equipment for determining aqueous PFAS concentrations. This deficiency restricted the number of PFAS analyses that could be executed and weakened the reliability of the results. Consequently, the quality of the data was insufficient for irrefutable determination of all required model variables. An additional uncontrolled factor was the possibility of environmental PFAS contamination during sample handling or storage. Moreover, the model excluded the evaluation of aspects such as PFAS-iron binding, aqueous micelle formation and complexation of PFAS to humic acid. Finally, the generalizability of the results to other organic co-solutes is disputable, as only one type of organic matter was tested.

Notwithstanding these limitations, this work enhanced the understanding of electrocoagulation as a means for PFAS removal from leachate water. The created PHREEQC model establishes a quantitative framework for detecting the interaction between different pollutants during electrocoagulation. This approach will prove useful in expanding the understanding of how the electrocoagulation process can be optimally controlled for removal of PFAS. Repetition of the current experiments with different combinations of process variables and in-house analysis of the PFAS samples could enable the determination of more accurate model parameters. Eventually, the current model could then be used to predict removal efficiencies from different wastewater compositions or to facilitate upscaling to an industrial size.

More broadly, further experimental investigations are needed to determine the exact removal rate of PFOS in the first five minutes of treatment. Moreover, accurate determination of the HA concentration during its removal are required. Eventually, optimization of the initial pH, stirring rate, aeration pressure or other process variables for more efficient removal are recommended. The applicability of sorption constants determined under equilibrium conditions is to be assessed, such that co-solutes for which literature sorption constants exist can be included in the model. Finally, extensive optimization of all model parameters with CPU-intensive methods such as Monte Carlo could transform the current model into an extremely valuable research tool, for which the groundwork has been laid in the present work.

6. REFERENCES

(1) Zhang, C.; Peng, Y.; Ning, K.; Niu, X.; Tan, S.; Su, P. Remediation of Perfluoroalkyl Substances in Landfill Leachates by Electrocoagulation. *Clean - Soil, Air, Water* 2014, *42* (12), 1740–1743.

(2) Kucharzyk, K. H.; Darlington, R.; Benotti, M.; Deeb, R.; Hawley, E. Novel Treatment Technologies for PFAS Compounds: A Critical Review. *J. Environ. Manage.* 2017, *204*, 757–764.

(3) Lau, C.; Anitole, K.; Hodes, C.; Lai, D.; Pfahles-Hutchens, A.; Seed, J. Perfluoroalkyl Acids: A Review of Monitoring and Toxicological Findings. *Toxicol. Sci.* 2007, *99* (2), 366–394.

(4) Yang, B.; Han, Y.; Yu, G.; Zhuo, Q.; Deng, S.; Wu, J.; Zhang, P. Efficient Removal of Perfluoroalkyl Acids (PFAAs) from Aqueous Solution by Electrocoagulation Using Iron Electrode. *Chem. Eng. J.* 2016, *303*, 384–390.

(5) Ramakrishnan, A.; Blaney, L.; Kao, J.; Tyagi, R. D.; Zhang, T. C.; Surampalli, R. Y. Emerging Contaminants in Landfill Leachate and Their Sustainable Management. *Environ. Earth Sci.* 2015, *73* (3), 1357–1368.

(6) Wei, Z.; Xu, T.; Zhao, D. Treatment of Per- And Polyfluoroalkyl Substances in Landfill Leachate: Status, Chemistry and Prospects. *Environ. Sci. Water Res. Technol.* 2019, *5* (11), 1814–1835.

(7) Li, P.; Zhi, D.; Zhang, X.; Zhu, H.; Li, Z.; Peng, Y.; He, Y.; Luo, L.; Rong, X.; Zhou, Y. Research Progress on the Removal of Hazardous Perfluorochemicals: A Review. *J. Environ. Manage.* 2019, *250* (February), 109488.

(8) Ilhan, F.; Kurt, U.; Apaydin, O.; Gonullu, M. T. Treatment of Leachate by Electrocoagulation Using Aluminum and Iron Electrodes. *J. Hazard. Mater.* 2008, *154* (1–3), 381–389.

(9) Moussa, D. T.; El-Naas, M. H.; Nasser, M.; Al-Marri, M. J. A Comprehensive Review of Electrocoagulation for Water Treatment: Potentials and Challenges. *J. Environ. Manage.* 2017, *186*, 24–41.

(10) Holt, P. K.; Barton, G. W.; Mitchell, C. A. Deciphering the Science behind Electrocoagulation to Remove Suspended Clay Particles from Water. *Water Sci. Technol.* 2004, *50* (12), 177–184.

(11) Graça, N. S.; Ribeiro, A. M.; Rodrigues, A. E. Modeling the Electrocoagulation Process for the Treatment of Contaminated Water. *Chem. Eng. Sci.* 2019, *197*, 379–385.

(12) Essadki, A. H.; Gourich, B.; Azzi, M.; Vial, C.; Delmas, H. Kinetic Study of Defluoridation of Drinking Water by Electrocoagulation/Electroflotation in a Stirred Tank Reactor and in an External-Loop Airlift Reactor. *Chem. Eng. J.* 2010, *164* (1), 106–114.

(13) Lu, J.; Wang, Z.; Ma, X.; Tang, Q.; Li, Y. Modeling of the Electrocoagulation Process: A Study on the Mass Transfer of Electrolysis and Hydrolysis Products. *Chem. Eng. Sci.* 2017, *165*, 165–176.

(14) Mahinroosta, R.; Senevirathna, L. A Review of the Emerging Treatment Technologies for PFAS Contaminated Soils. *J. Environ. Manage.* 2020, *255* (June 2019), 109896.

(15) Lin, H.; Wang, Y.; Niu, J.; Yue, Z.; Huang, Q. Efficient Sorption and Removal of Perfluoroalkyl Acids (PFAAs) from Aqueous Solution by Metal Hydroxides Generated in Situ by Electrocoagulation. *Environ. Sci. Technol.* 2015, *49* (17), 10562–10569.

(16) Kabdaşlı, I.; Arslan-Alaton, I.; Ölmez-Hancı, T.; Tünay, O. Electrocoagulation Applications for Industrial Wastewaters: A Critical Review. *Environ. Technol. Rev.* 2012, *1* (1), 2–45.

(17) Stefanakis, A.; Akratos, C. S.; Tsihrintzis, V. A. Treatment of Special Wastewaters in VFCWs. In *Vertical Flow Constructed Wetlands*; 2014; pp 145–164.

(18) NV Afvalzorg Holding. Over Afvalzorg https://www.afvalzorg.nl/over-afvalzorg/ (accessed Nov 18, 2019).

(19) John Smit. *Beschrijving Pwzi Nauerna*; 2017.

(20) EColoRO BV. *Elektrocoagulatie Voor Metaalverwijderingsinstallatie - Afvalzorg Deponie N.V. Nauerna*; 2018.

(21) Rijkswaterstaat; Ministerie van Infrastructuur en Waterstaat. *Watervergunning Ten Behoeve van Afvalzorg Deponie B.V.*; 2019; pp 1–33.

(22) Merino, N.; Qu, Y.; Deeb, R. A.; Hawley, E. L.; Hoffmann, M. R.; Mahendra, S. Degradation and Removal Methods for Perfluoroalkyl and Polyfluoroalkyl Substances in Water. *Environ. Eng. Sci.* 2016, *33* (9), 615–649.

(23) Lau, C. Chapter 1 Perfluorinated Compounds: An Overview. In *Toxicological Effects of Perfluoroalkyl and Polyfluoroalkyl Substances*; 2015.

(24) Rodricks, J. L. B. and J. V. Chapter 15 Human Health Risk Assessment of Perfluoroalkyl Acids. In *Toxicological Effects of Perfluoroalkyl and Polyfluoroalkyl Substances*; 2015.

(25) Kudo, N. Chapter 6 Metabolism and Pharmacokinetics. In *Toxicological Effects of Perfluoroalkyl and Polyfluoroalkyl Substances*; 2015.

(26) De Witt, J. C. Chapter 18 Conclusions and Recommendations. In *Toxicological Effects of Perfluoroalkyl and Polyfluoroalkyl Substances*; 2015.

(27) Pancras, T.; van Bentum, E.; Slenders, H. *Poly- En Perfluor Alkyl Stoffen (PFAS): Kennisdocument over Stofeigenschappen, Gebruik, Toxicologie, Onderzoek En Sanering van PFAS in Grond En Grondwater*; 2018.

(28) Horst, J.; McDonough, J.; Ross, I.; Dickson, M.; Miles, J.; Hurst, J.; Storch, P. Water Treatment Technologies for PFAS: The Next Generation. *Groundw. Monit. Remediat.* 2018, *38* (2), 13–23.

(29) Huang, S.; Jaffé, P. R. Defluorination of Perfluorooctanoic Acid (PFOA) and Perfluorooctane Sulfonate (PFOS) by Acidimicrobium Sp. Strain A6. *Environ. Sci. Technol.* 2019.

(30) Guo, B.; Zeng, J.; Brusseau, M. L. A Mathematical Model for the Release, Transport, and Retention of Per- and Polyfluoroalkyl Substances (PFAS) in the Vadose Zone. *Water Resour. Res.* 2020, 1–25.

(31) Chen, W.; Zhang, X.; Mamadiev, M.; Wang, Z. Sorption of Perfluorooctane Sulfonate and Perfluorooctanoate on Polyacrylonitrile Fiber-Derived Activated Carbon Fibers: In Comparison with Activated Carbon. *RSC Adv.* 2017, *7* (2), 927–938.

(32) Shih, K.; Wang, F. Adsorption Behavior of Perfluorochemicals (PFCs) on Boehmite: Influence of Solution Chemistry. *Procedia Environ. Sci.* 2013, *18*, 106–113.

(33) Gao, X.; Chorover, J. Adsorption of Perfluorooctanoic Acid and Perfluorooctanesulfonic Acid to Iron Oxide Surfaces as Studied by Flow-through ATR-FTIR Spectroscopy. *Environ. Chem.* 2012, *9* (2), 148–157.

(34) Wang, X.; Chen, J.; Wang, D.; Dong, S.; Hao, J.; Hoffmann, H. Monitoring the Different Micelle

Species and the Slow Kinetics of Tetraethylammonium Perfluorooctane-Sulfonate by 19F NMR Spectroscopy. *Adv. Colloid Interface Sci.* 2017, *246* (May), 153–164.

(35) Ramprasad, C.; Sona, K.; Afridhi, M.; Kumar, R.; Gopalakrishnan, N. Comparative Study on the Treatment of Landfill Leachate by Coagulation and Electrocoagulation Processes. *Nat. Environ. Pollut. Technol.* 2019, *18* (3), 845–856.

(36) Behbahani, M.; Alavi Moghaddam, M. R.; Arami, M. A Comparison between Aluminum and Iron Electrodes on Removal of Phosphate from Aqueous Solutions by Electrocoagulation Process. *Int. J. Environ. Res.* 2011, *5* (2), 403–412.

(37) Nguyen, D. D.; Ngo, H. H.; Guo, W.; Nguyen, T. T.; Chang, S. W.; Jang, A.; Yoon, Y. S. Can Electrocoagulation Process Be an Appropriate Technology for Phosphorus Removal from Municipal Wastewater? *Sci. Total Environ.* 2016, *563–564*, 549–556.

(38) Vik, E. A.; Carlson, D. A.; Eikum, A. S.; Gjessing, E. T. Electrocoagulation of Potable Water. *Water Res.* 1984, *18* (11), 1355–1360.

(39) Li, L.; Van Genuchten, C. M.; Addy, S. E. A.; Yao, J.; Gao, N.; Gadgil, A. J. Modeling As(III) Oxidation and Removal with Iron Electrocoagulation in Groundwater. *Environ. Sci. Technol.* 2012, *46* (21), 12038–12045.

(40) Hakizimana, J. N.; Gourich, B.; Chafi, M.; Stiriba, Y.; Vial, C.; Drogui, P.; Naja, J. Electrocoagulation Process in Water Treatment: A Review of Electrocoagulation Modeling Approaches. *Desalination* 2017, *404*, 1–21.

(41) Liu, Y.; Hu, X. M.; Zhao, Y.; Wang, J.; Lu, M. X.; Peng, F. H.; Bao, J. Removal of Perfluorooctanoic Acid in Simulated and Natural Waters with Different Electrode Materials by Electrocoagulation. *Chemosphere* 2018, *201*, 303–309.

(42) Islam, S. M. D.-U. Electrocoagulation (EC) Technology for Wastewater Treatment and Pollutants Removal. *Sustain. Water Resour. Manag.* 2019, *5* (1), 359–380.

(43) Nayak, B. A Review of Electrocoagulation Process for Wastewater Treatment. *Int. J. ChemTech Res.* 2018, *11* (3), 289–302.

(44) Baudequin, C.; Couallier, E.; Rakib, M.; Deguerry, I.; Severac, R.; Pabon, M. Purification of Firefighting Water Containing a Fluorinated Surfactant by Reverse Osmosis Coupled to Electrocoagulation-Filtration. *Sep. Purif. Technol.* 2011, *76* (3), 275–282.

(45) Lin, H.; Wang, Y.; Niu, J.; Yue, Z.; Huang, Q. SI Efficient Sorption and Removal of Perfluoroalkyl Acids (PFAAs) from Aqueous Solution by Metal Hydroxides Generated in Situ by Electrocoagulation. *Environ. Sci. Technol.* 2015, *49* (17), 10562–10569.

(46) Adyel, T. M.; Rahman, S. H.; Zaman, M. M.; Sayem, H. M.; Khan, M.; Abdul Gafur, M.; Islam, S. M. N. Reuse Feasibility of Electrocoagulated Metal Hydroxide Sludge of Textile Industry in the Manufacturing of Building Blocks. *J. Waste Manag.* 2013, *2013* (May 2014), 1–9.

(47) Mansouri, K.; Ibrik, K.; Bensalah, N.; Abdel-Wahab, A. Anodic Dissolution of Pure Aluminum during Electrocoagulation Process: Influence of Supporting Electrolyte, Initial PH, and Current Density. *Ind. Eng. Chem. Res.* 2011, *50* (23), 13362–13372.

(48) Lindsay, W. L.; Vlek, P. L. G. Phosphate Minerals. In *Minerals in soil environments*; 1977; pp 639–670.

(49) Brett, C. M. A.; Brett, A. M. O. 7. Electrochemical Experiments. In *Electrochemistry : principles, methods, and applications*; Oxford University Press, 1993; pp 129–150.

(50) Bratby, J. *Coagulation and Flocculation in Water and Wastewater Treatment*, 3rd ed.; IWA Publishing, 2016.

(51) Bao, J.; Yu, W. J.; Liu, Y.; Wang, X.; Liu, Z. Q.; Duan, Y. F. Removal of Perfluoroalkanesulfonic Acids (PFSAs) from Synthetic and Natural Groundwater by Electrocoagulation. *Chemosphere* 2020, *248*, 125951.

(52) Lakshmanan, D.; Clifford, D. A.; Samanta, G. Ferrous and Ferric Ion Generation during Iron Electrocoagulation. *Environ. Sci. Technol.* 2009, *43* (10), 3853–3859.

(53) Dubrawski, K. L.; Mohseni, M. In-Situ Identification of Iron Electrocoagulation Speciation and Application for Natural Organic Matter (NOM) Removal. *Water Res.* 2013, *47* (14), 5371–5380.

(54) Sasson, M. Ben; Calmano, W.; Adin, A. Iron-Oxidation Processes in an Electroflocculation (Electrocoagulation) Cell. *J. Hazard. Mater.* 2009, *171* (1–3), 704–709.

(55) Morgan, B.; Lahav, O. The Effect of PH on the Kinetics of Spontaneous Fe(II) Oxidation by O2 in Aqueous Solution - Basic Principles and a Simple Heuristic Description. *Chemosphere* 2007, *68* (11), 2080–2084.

(56) Parkhurst, D. L.; Appelo, C. a. J. Description of Input and Examples for PHREEQC Version 3 — A Computer Program for Speciation , Batch-Reaction , One-Dimensional Transport , and Inverse Geochemical Calculations. In *U.S. Geological Survey Techniques and Methods, book 6, chapter A-43*; 2013.

(57) Singer, P.; Stumm, W. Acidic Mine Drainage: The Rate-Determining Step. *Science (80-.).* 1970, *167* (3921), 1121–1123.

(58) Zaleschi, L.; Teodosiu, C.; Cretescu, I.; Rodrigo, M. A. A Comparative Study of Electrocoagulation and Chemical Coagulation Processes Applied for Wastewater Treatment. *Environ. Eng. Manag. J.* 2012, *11* (8), 1517–1525.

(59) Harif, T.; Khai, M.; Adin, A. Electrocoagulation versus Chemical Coagulation: Coagulation/Flocculation Mechanisms and Resulting Floc Characteristics. *Water Res.* 2012, *46* (10), 3177–3188.

(60) Wang, Y.; Zhang, P.; Pan, G.; Chen, H. Ferric Ion Mediated Photochemical Decomposition of Perfluorooctanoic Acid (PFOA) by 254 Nm UV Light. *J. Hazard. Mater.* 2008, *160* (1), 181–186.

(61) Park, S.; Zenobio, J. E.; Lee, L. S. Perfluorooctane Sulfonate (PFOS) Removal with Pd0/NFe0 Nanoparticles: Adsorption or Aqueous Fe-Complexation, Not Transformation? *J. Hazard. Mater.* 2018, *342*, 20–28.

(62) Kang, K. H.; Shin, H. S.; Park, H. Characterization of Humic Substances Present in Landfill Leachates with Different Landfill Ages and Its Implications. *Water Res.* 2002, *36* (16), 4023–4032.

(63) Gagliano, E.; Sgroi, M.; Falciglia, P. P.; Vagliasindi, F. G. A.; Roccaro, P. Removal of Poly- and Perfluoroalkyl Substances (PFAS) from Water by Adsorption: Role of PFAS Chain Length, Effect of Organic Matter and Challenges in Adsorbent Regeneration. *Water Res.* 2020, *171*, 115381.

(64) Qiao, J.; Jiang, Z.; Sun, B.; Sun, Y.; Wang, Q.; Guan, X. Arsenate and Arsenite Removal by FeCl

3 : Effects of PH, As/Fe Ratio, Initial As Concentration and Co-Existing Solutes. *Sep. Purif. Technol.* 2012, *92*, 106–114.

(65) Al-Qodah, Z.; Al-Shannag, M.; Bani-Melhem, K.; Assirey, E.; Yahya, M. A.; Al-Shawabkeh, A. Free Radical-Assisted Electrocoagulation Processes for Wastewater Treatment. *Environ. Chem. Lett.* 2018, *16* (3), 695–714.

(66) Dia, O.; Drogui, P.; Buelna, G.; Dubé, R.; Ihsen, B. S. Electrocoagulation of Bio-Filtrated Landfill Leachate: Fractionation of Organic Matter and Influence of Anode Materials. *Chemosphere* 2017, *168*, 1136–1141.

(67) Tipping, E.; Campbell, P. G. C.; Harrison, R. M. *Cation Binding by Humic Substances*; 2002.

(68) Liu, Z. P.; Wu, W. H.; Shi, P.; Guo, J. S.; Cheng, J. Characterization of Dissolved Organic Matter in Landfill Leachate during the Combined Treatment Process of Air Stripping, Fenton, SBR and Coagulation. *Waste Manag.* 2015, *41*, 111–118.

(69) Schuricht, F.; Borovinskaya, E. S.; Reschetilowski, W. Removal of Perfluorinated Surfactants from Wastewater by Adsorption and Ion Exchange — Influence of Material Properties, Sorption Mechanism and Modeling. *J. Environ. Sci. (China)* 2017, *54*, 160–170.

(70) Koopal, L. K.; Saito, T.; Pinheiro, J. P.; Van Riemsdijk, W. H. Ion Binding to Natural Organic Matter: General Considerations and the NICA-Donnan Model. *Colloids Surfaces A Physicochem. Eng. Asp.* 2005, *265* (1–3), 40–54.

(71) Borkovec, M.; Westall, J. Solution of the Poisson-Boltzmann Equation for Surface Excesses of Ions in the Diffuse Layer at the Oxide-Electrolyte Interface. *J. Electroanal. Chem.* 1983, *150* (1–2), 325–337.

(72) Atkins, P. *Physical Chemistry 10th Edition*; 2014.

(73) Hiemstra, T.; Van Riemsdijk, W. H. A Surface Structural Approach to Ion Adsorption: The Charge Distribution (CD) Model. *J. Colloid Interface Sci.* 1996, *179* (2), 488–508.

(74) Dzombak, D.; Morel, F. *Surface Complexation Modelling: Hydrous Ferric Oxide*; John Wiley & Sons, 1990.

(75) Orsi, M. Molecular Dynamics Simulation of Humic Substances. *Chem. Biol. Technol. Agric.* 2014, *1* (1), 1–14.

(76) Groenenberg, J. E.; Koopmans, G. F.; Comans, R. N. J. Uncertainty Analysis of the Nonideal Competitive Adsorption - Donnan Model: Effects of Dissolved Organic Matter Variability on Predicted Metal Speciation in Soil Solution. *Environ. Sci. Technol.* 2010, *44* (4), 1340–1346.

(77) Weber, T.; Allard, T.; Tipping, E.; Benedetti, M. F. Modeling Iron Binding to Organic Matter. *Environ. Sci. Technol.* 2006, *40* (24), 7488–7493.

(78) Lenoir, T.; Matynia, A.; Manceau, A. Convergence-Optimized Procedure for Applying the NICA-Donnan Model to Potentiometric Titrations of Humic Substances. *Environ. Sci. Technol.* 2010, *44* (16), 6221–6227.

(79) Milne, C. J.; Kinniburgh, D. G.; Van Riemsdijk, W. H.; Tipping, E. Generic NICA - Donnan Model Parameters for Metal-Ion Binding by Humic Substances. *Environ. Sci. Technol.* 2003, *37* (5), 958–971.

(80) Dudal, Y.; Gérard, F. Accounting for Natural Organic Matter in Aqueous Chemical Equilibrium

Models: A Review of the Theories and Applications. *Earth-Science Rev.* 2004, *66* (3–4), 199–216.

(81) Kac, F. U.; Kobya, M.; Gengec, E. Removal of Humic Acid by Fixed-Bed Electrocoagulation Reactor: Studies on Modelling, Adsorption Kinetics and HPSEC Analyses. *J. Electroanal. Chem.* 2017, *804* (October), 199–211.

(82) Charlton, S. R.; Parkhurst, D. L. Modules Based on the Geochemical Model PHREEQC for Use in Scripting and Programming Languages. *Comput. Geosci.* 2011, *37* (10), 1653–1663.

(83) Meeussen, J. C. L. Orchestra: An Object-Oriented Framework for Implementing Chemical Equilibrium Models. *Environ. Sci. Technol.* 2003, *37* (6), 1175–1182.

(84) Thermo Fisher Scientific. Hach Lange™ Cuvettesten fosfaat ortho/totaal.

(85) Brock, O.; Helmus, R.; Kalbitz, K.; Jansen, B. Non-Target Screening of Leaf Litter-Derived Dissolved Organic Matter Using Liquid Chromatography Coupled to High-Resolution Mass Spectrometry (LC-QTOF-MS). *Eur. J. Soil Sci.* 2019, No. December 2018, 1–13.

(86) Weishaar, J. L.; Aiken, G. R.; Bergamaschi, B. A.; Fram, M. S.; Fujii, R.; Mopper, K. Evaluation of Specific Ultraviolet Absorbance as an Indicator of the Chemical Composition and Reactivity of Dissolved Organic Carbon. *Environ. Sci. Technol.* 2003, *37* (20), 4702–4708.

(87) Appelo, C. A. J.; Van Der Weiden, M. J. J.; Tournassat, C.; Charlet, L. Surface Complexation of Ferrous Iron and Carbonate on Ferrihydrite and the Mobilization of Arsenic. *Environ. Sci. Technol.* 2002, *36* (14), 3096–3103.

(88) Zhang, T.; Ding, L.; Ren, H.; Guo, Z.; Tan, J. Thermodynamic Modeling of Ferric Phosphate Precipitation for Phosphorus Removal and Recovery from Wastewater. *J. Hazard. Mater.* 2010, *176* (1–3), 444–450.

(89) Zhang, Z.; Chen, J. J.; Lyu, X. J.; Yin, H.; Sheng, G. P. Complete Mineralization of Perfluorooctanoic Acid (PFOA) by γ-Irradiation in Aqueous Solution. *Sci. Rep.* 2014, *4*, 1–6.

(90) Normcommissie 390 147 "Waterkwaliteit." *NEN-EN 1484: Guidelines for the Determination of TOC and DOC*; 1997.

(91) Wypych, G. 1 - PHOTOPHYSICS. In *Handbook of Material Weathering (Sixth Edition)*; ChemTec Publishing, 2018; pp 1–26.

7. Acknowledgements

Most importantly, I would like to thank my supervisors Timo Heimovaara, Julia Gebert, Bas Heijman and John Smit for their helpful insights and useful advice in the completion of this thesis. Further, I want to thank all the people who assisted me in the lab at the TU Delft and who allowed me to continue working during the strange times of Covid-19, especially Jolanda and Marc. My father deserves to be accredited for helping me with the design aspects of this thesis. Finally, I want to thank my friends and family for nodding appreciatively when I was overenthusiastic about either my pH-meter or the joy of finding an accurate model parameter. I promise to expand my range of conversation topics again.

8. APPENDICES

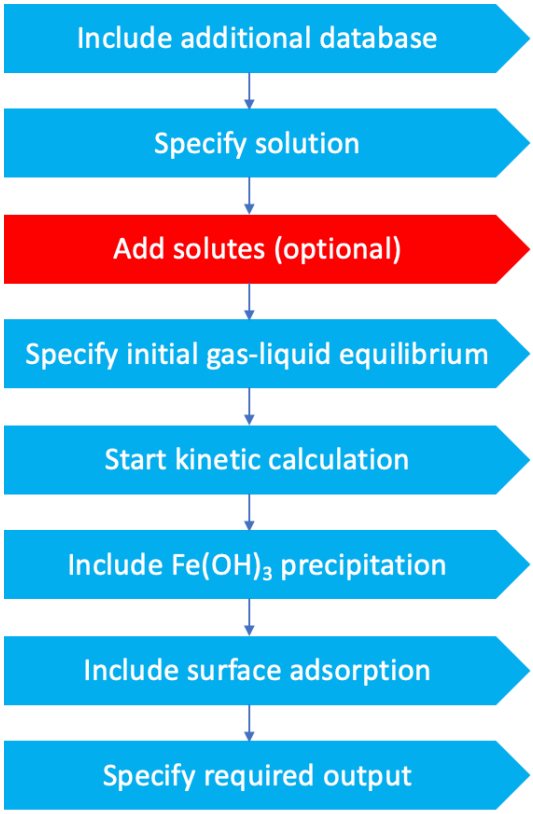


```
INCLUDE$ mySolutionSpecies.phr

INCLUDE$ ../PhreeqC/inputfiles/mySolution.phr

SAVE Solution 1
END

USE Solution 1
REACTION 1
INCLUDE$ PFAS.phr
1 moles

EQUILIBRIUM_PHASES 1
INCLUDE$ EquilibriumPhases.phr

SAVE Solution 1
END

USE Solution 1

INCLUDE$ ../PhreeqC/inputfiles/myKinetics.phr

EQUILIBRIUM_PHASES 1
MyFerrihydrite 0 0

INCLUDE$ ../PhreeqC/inputfiles/mySurface.phr
SAVE Solution 1

SELECTED_OUTPUT
     -file FeECwithPFAS.out
     -equilibrium_phases MyFerrihydrite
     -totals Pfoa Pfos Pfba Pfbs
USER_PUNCH
     -headings mins Hfo_wOHPfoa- Hfo_wOPfoa Hfo_wOFe_diOH Hfo_wOHPfos- Hfo_wOPfos HfoCharge
 10 PUNCH SIM_TIME / 60
 20 PUNCH MOL("Hfo_wOHPfoa-")
 30 PUNCH MOL("Hfo_wPfoa")
 40 PUNCH MOL("Hfo_wOFe_diOH")
 50 PUNCH MOL("Hfo_wOHPfos-")
 60 PUNCH MOL("Hfo_wPfos")
 70 PUNCH EDL("charge","Hfo")
END
```

Appendix 1: PHREEQC Pseudocode and summarized actual code. PFAS.phr and EquilibriumPhases.phr determine the initial PFAS concentration and gas saturation, respectively. These files are controlled from the MATLAB environment.

```
SOLUTION_MASTER_SPECIES (Adapted from Walinder 2016)
#element_name master_species    alk     gfw_formula     element_gfw
Pfba            Pfba-           0.0     C4F7O2H         214.0384
#Pfpea          Pfpea-          0.0     C5F9O2H         264.0459
#Pfhxa          Pfhxa-          0.0     C6F11O2H        314.0534
#Pfhpa          Pfhpa-          0.0     C7F13O2H        364.0609
Pfoa            Pfoa-           0.0     C8F15O2H        414.0684
#Pfna           Pfna-           0.0     C9F17O2H        464.0759
#Pfda           Pfda-           0.0     C10F19O2H       514.0834
#Pfunda                 Pfunda-         0.0     C11F21O2H       564.0909
#Pfdoda                 Pfdoda-         0.0     C12F23O2H       614.0984
Pfbs            Pfbs-           0.0     C4F9SO3H        300.0996
#Pfhxs          Pfhxs-          0.0     C6F13SO3H       400.1146
Pfos            Pfos-           0.0     C8F17SO3H       500.1296
#Fosa           Fosa-           0.0     C8F17SO2NH2     499.1448
#Pfteda                 Pfteda-         0.0     C14F27O2H       714.1134
Fe_di           Fe_di+2         0       Fe_di           55.847
Fe_tri          Fe_tri+3        0       Fe_tri          55.847
Charn           Charn-          0.0     Charn           1
Charp           Charp+          0.0     Charp           1
Humate          HumateH2        0.0     C10H11.54O10.89N0.23S0.09 332.11
#Redox uncoupled gases
Hdg             Hdg     0       Hdg             2.016 # H2 gas
Oxg             Oxg     0       Oxg             32 # O2 gas
Mtg             Mtg     0       Mtg             16.032 # CH4 gas
Sg              H2Sg    1.0     H2Sg            34.08
Ntg             Ntg     0       Ntg             28.0134 # N2 gas

SOLUTION_SPECIES
Fe_di+2 = Fe_di+2
        log_k   0.0
Fe_tri+3 = Fe_tri+3
        log_k   0.0
HumateH2 = HumateH2
        log_k   0.0
HumateH2 + H+ = HumateH3+
        INCLUDE$ logKHA1.phr
HumateH2 = Humate-2 + 2H+
        INCLUDE$ logKHA2.phr
H+ + Humate-2 = HHumate-
        INCLUDE$ logKHA3.phr
Fe_tri+3 + Humate-2 = Fe_triHumate+
        INCLUDE$ logKFetriHA.phr
Fe_di+2 + Humate-2 = Fe_diHumate
        INCLUDE$ logKFediHA.phr
Charn- = Charn-
        log_k 0.0
Charp+ = Charp+
        log_k 0.0
Charp+ + e- = Charp
        log_k 10
```

```
#
# Fe+2 species
#
Fe_di+2 + H2O = Fe_diOH+ + H+
        log_k   -9.397
        delta_h 55.81 kJ
Fe_di+2 + 2H2O = Fe_di(OH)2 +2H+
        log_k -20.494
        delta_h 119.62 kJ
Fe_di+2 + 3H2O = Fe_di(OH)3- + 3H+
        log_k -28.991
        delta_h 126.43 kJ
#
#... and also other Fe+2 species
#
Fe_di+2 + Cl- = Fe_diCl+
        log_k   0.14
```

```
Fe_di+2 + CO3-2 = Fe_diCO3
        log_k   4.38
Fe_di+2 + HCO3- = Fe_diHCO3+
        log_k   2.0
Fe_di+2 + SO4-2 = Fe_diSO4
        log_k   2.25
        delta_h 3.230   kcal
Fe_di+2 + HSO4- = Fe_diHSO4+
        log_k   1.08
Fe_di+2 + 2HS- = Fe_di(HS)2
        log_k   8.95
Fe_di+2 + 3HS- = Fe_di(HS)3-
        log_k   10.987
Fe_di+2 + H+ + PO4-3 = Fe_diHPO4 #Minteq
        log_k 15.975
Fe_di+2 + 2H+ + PO4-3 = Fe_diH2PO4+ #Minteq
        log_k 22.273
Fe_di+2 + F- = Fe_diF+
        log_k   1.0
#
# Fe+3 species
#
Fe_tri+3 + H2O = Fe_triOH+2 + H+
        log_k   -2.19
        delta_h 10.4    kcal
#
#... and also other Fe+3 species
Fe_tri+3 + 2 H2O = Fe_tri(OH)2+ + 2 H+
        log_k   -4.594
        delta_h 0 kJ
Fe_tri+3 + 3 H2O = Fe_tri(OH)3 + 3 H+
        log_k   -12.56
        delta_h 24.8    kcal
Fe_tri+3 + 4 H2O = Fe_tri(OH)4- + 4 H+
        log_k   -21.588
        delta_h 31.9    kcal
```

```
2 Fe_tri+3 + 2 H2O = Fe_tri2(OH)2+4 + 2 H+
        log_k   -2.854
        delta_h 13.5    kcal
3 Fe_tri+3 + 4 H2O = Fe_tri3(OH)4+5 + 4 H+
        log_k   -6.288
        delta_h 14.3    kcal
Fe_tri+3 + Cl- = Fe_triCl+2
        log_k   1.48
        delta_h 5.6     kcal
Fe_tri+3 + 2 Cl- = Fe_triCl2+
        log_k   2.13
Fe_tri+3 + 3 Cl- = Fe_triCl3
        log_k   1.13
Fe_tri+3 + SO4-2 = Fe_triSO4+
        log_k   4.04
        delta_h 3.91    kcal
Fe_tri+3 + HSO4- = Fe_triHSO4+2
        log_k   2.48
Fe_tri+3 + 2 SO4-2 = Fe_tri(SO4)2-
        log_k   5.38
        delta_h 4.60    kcal
Fe_tri+3 + 2H+ + PO4-3 = Fe_triH2PO4+2
        log_k 23.8515
Fe_tri+3 + H+ + PO4-3 = Fe_triHPO4+
        log_k 22.292
        delta_h -30.54 kJ

Fe_tri+3 + F- = Fe_triF+2
        log_k   6.2
        delta_h 2.7     kcal
Fe_tri+3 + 2 F- = Fe_triF2+
        log_k   10.8
        delta_h 4.8     kcal
```

```
Fe_tri+3 + 3 F- = Fe_triF3
        log_k   14.0
        delta_h 5.4     kcal


#PFAS species
Pfos- = Pfos-
        log_k 0.0
Pfos- + H+ = PfosH
        log_k -0.14
Pfoa- = Pfoa-
        log_k 0.0
Pfoa- + H+ = PfoaH
        log_k 0.2
Pfba- = Pfba-
        log_k 0.0
Pfba- + H+ = PfbaH
        log_k -0.05
Pfbs- = Pfbs-
        log_k 0.0
Pfbs- + H+ = PfbsH
        log_k -0.14
```

```
# redox-uncoupled gases
Hdg = Hdg # H2
        -dw      5.13e-9
        -Vm 6.52  0.78  0.12 # supcrt
Oxg = Oxg # O2
        -dw      2.35e-9
        -Vm  5.7889  6.3536  3.2528  -3.0417  -0.3943 # supcrt
Mtg = Mtg # CH4
        -dw   1.85e-9
        -Vm   9.01  -1.11  0  -1.85  -1.50 # ref. 1 + Hnedkovsky et al., 1996, JCT 28, 125
Ntg = Ntg # N2
        -dw      1.96e-9
        -Vm 7 # Pray et al., 1952, IEC 44. 1146
H2Sg = H2Sg # H2S
        -dw      2.1e-9
        -Vm  7.81  2.96  -0.46 # supcrt

SURFACE_SPECIES
# Iron, strong site: Appelo, Van der Weiden, Tournassat & Charlet, EST 36, 3096
        Hfo_sOH + Fe_di+2 = Hfo_sOFe_di+ + H+
        -log_k  -0.95

# Iron, weak site: Liger et al., GCA 63, 2939, re-optimized for D&M
        Hfo_wOH + Fe_di+2 = Hfo_wOFe_di+ + H+
        -log_k  -2.98

       Hfo_wOH + Fe_di+2 + H2O = Hfo_wOFe_diOH + 2H+
        -log_k 11.55

# Carbonate: Van Geen et al., 1994 reoptimized for D&M model
#
        Hfo_wOH + CO3-2 + H+ = Hfo_wCO3- + H2O
        -log_k  12.56

        Hfo_wOH + CO3-2 + 2H+= Hfo_wHCO3 + H2O
        -log_k  20.62

        Hfo_wOH + Fe_di+2 + PO4-3  = Hfo_wFe_diPO4 + OH-
        -log_k 34.94


# PFOA Species
Hfo_wOH + Pfoa- + H+ = Hfo_wPfoa + H2O
INCLUDE$ mylogK2a.phr

Hfo_sOH + Pfoa- + H+ = Hfo_sPfoa + H2O
INCLUDE$ mylogK2a.phr
```

```
Hfo_wOH + Pfoa- = Hfo_wOHPfoa-
INCLUDE$ mylogK3a.phr

Hfo_sOH + Pfoa- = Hfo_sOHPfoa-
INCLUDE$ mylogK3a.phr
```

```
# PFOS Species
Hfo_wOH + Pfos- + H+ = Hfo_wPfos + H2O
INCLUDE$ mylogK2s.phr

Hfo_sOH + Pfos- + H+ = Hfo_sPfos + H2O
INCLUDE$ mylogK2s.phr

Hfo_wOH + Pfos- = Hfo_wOHPfos-
INCLUDE$ mylogK3s.phr

Hfo_sOH + Pfos- = Hfo_sOHPfos-
INCLUDE$ mylogK3s.phr

# PFBA Species
Hfo_wOH + Pfba- + H+ = Hfo_wPfba + H2O
INCLUDE$ mylogK2a.phr

Hfo_sOH + Pfba- + H+ = Hfo_sPfba + H2O
INCLUDE$ mylogK2a.phr

Hfo_wOH + Pfba- = Hfo_wOHPfba-
INCLUDE$ mylogK3a.phr

Hfo_sOH + Pfba- = Hfo_sOHPfba-
INCLUDE$ mylogK3a.phr

# PFBS Species
Hfo_wOH + Pfbs- + H+ = Hfo_wPfbs + H2O
INCLUDE$ mylogK2s.phr

Hfo_sOH + Pfbs- + H+ = Hfo_sPfbs + H2O
INCLUDE$ mylogK2s.phr

Hfo_wOH + Pfbs- = Hfo_wOHPfbs-
INCLUDE$ mylogK3s.phr

Hfo_sOH + Pfbs- = Hfo_sOHPfbs-
INCLUDE$ mylogK3s.phr

# HUMATE Species
Hfo_wOH + Humate-2 + H+ = Hfo_wHumate- + H2O
INCLUDE$ mylogKHA2.phr

Hfo_sOH + Humate-2 + H+ = Hfo_sHumate- + H2O
INCLUDE$ mylogKHA2.phr

Hfo_wOH + Humate-2 = Hfo_wOHHumate-2
INCLUDE$ mylogKHA3.phr

Hfo_sOH + Humate-2 = Hfo_sOHHumate-2
INCLUDE$ mylogKHA3.phr
```

```
PHASES
# redox-uncoupled gases
Oxg(g)
        Oxg = Oxg
        -analytic -7.5001 7.8981e-3 0.0 0.0 2.0027e5
        -T_c  154.6 ; -P_c   49.80 ; -Omega 0.021
Hdg(g)
        Hdg = Hdg
        -analytic   -9.3114    4.6473e-3   -49.335    1.4341    1.2815e5
        -T_c  33.2 ; -P_c   12.80 ; -Omega -0.225
```

```
Ntg(g)
        Ntg = Ntg
        -analytic -58.453 1.81800e-3  3199  17.909 -27460
        T_c  126.2 ; -P_c   33.50 ; -Omega 0.039
Mtg(g)
        Mtg = Mtg
        -log_k -2.8
        -analytic   10.44  -7.65e-3  -6669  0  1.014e6 # CH4 solubilities 25 - 100°C
        -T_c  190.6 ; -P_c   45.40 ; -Omega 0.008

# Minerals
MyFerrihydrite
        Fe_tri(OH)3 + 3H+  = Fe_tri+3 + 3H2O
        log_k 3.191
        delta_h -73.373 kcal
MyPFOSFerrihydrite
        Fe_tri(OH)2Pfos + 2H+ = Fe_tri+3 + 2H2O + Pfos-
        log_k -10
MySiderite
        Fe_diCO3 = Fe_di+2 + CO3-2
        log_k -10.24
        delta_h -16 kJ
MyFe(OH)2
        Fe_di(OH)2 + 2H+ = Fe_di+2 + 2H2O
        log_k 13.564
        delta_h -0
MyGoethite
        Fe_triOOH + 3H+ = Fe_tri+3 + 2H2O
        log_k 0.491
        delta_h -0 kJ
MyMaghemite
        Fe_tri2O3 + 6H+ = 2Fe_tri+3 + 3H2O
        log_k -1.418
        delta_h -128.987 kJ
MyMagnetite
        Fe_tri2Fe_diO4 + 8H+ = Fe_di+2 + 2 Fe_tri+3 + 4 H2O
        log_k 3.4028
        delta_h -313.92 kJ
MyFe2(OH)8
        Fe_tri2Fe_di(OH)8 + 8 H+ = 2Fe_tri+3 + Fe_di+2 + 8H2O
        log_k 20.222
        delta_h -0 kJ
```

```
MyFe(OH)2.7Cl.3
        Fe_tri(OH)2.7Cl.3 + 2.7H+ = Fe_tri+3 + 2.7H2O + 0.3Cl-
        log_k -3.04
        delta_h -0 kJ
MyStrengite
        Fe_triPO4:2H2O = Fe_tri+3 + PO4-3 + 2H2O
        log_k -26.4
        delta_h 8.8701 kJ
MyVivianite
        Fe_di3(PO4)2:8H2O = 3Fe_di+2 + 2PO4-3 + 8H2O
        log_k -36
        delta_h -0 kJ
Fix_H+
        H+ = H+
        log_k 0.0
# Attempt to model PFOS precipitation incorporated in iron mineral
MyFePfos
#       Fe_triPfos3 = Fe_tri+3 + 3Pfos-
#       log_k -32
        Fe_diPfos2 = Fe_di+2 + 2Pfos-
        log_k -12.6

END
```

```
RATES

OLDFe_di_ox #From example 9
  -start
  10  Fe_di = TOT("Fe_di")
  20  if (Fe_di <= 0) then goto 200
  30  p_o2 = 10^SI("O2(g)")
  31  k0 = 2.91e-9
  32  k1 = 8.33e13 #original constant: 1.33e12
  40  mymoles = (k0 + k1 * (ACT("OH-"))^2 * p_o2) * Fe_di * TIME
  200 SAVE mymoles
  -end

Faraday
  -start
  10 REM Parms(1) = rho_I
  20 eta_Fe = 0.996
  30 F = 96485 #Faraday's constant, C/mol
  50 Z=2 #Valence number
  60 A_el = 8 #Electrode area, cm2
  70 I = A_el*PARM(1)
  80 r_m = I/(F*Z)*eta_Fe;
  100 moles = r_m*TIME
  200 SAVE moles
  -end
CO2_Dissolution
-start
        10 k_diss = PARM(1) #kinetic constant for CO2 dissolution
        20 SI_CO2 = SI("CO2(g)")
        30 C_CO2 = (10^SI_CO2)/29 #Kh = 29 (Henry constant CO2)
        35 C_sat = (10^PARM(2))/29
        36 n = 1
        40 rate = (C_sat - C_CO2)^n*k_diss
        100 moles = rate*TIME
        110 save moles
-end

O2_Dissolution
-start
        10 k_diss =  PARM(1) #kinetic constant for O2 dissolution
        20 SI_O2 = SI("O2(g)")
        30 C_O2 = (10^SI_O2)/770 #Kh = 770
        35 C_sat = (10^PARM(2))/770
        36 n = 1
        50 rate = k_diss*(C_sat-C_O2)^n
        100 moles = rate*TIME
        110 save moles
```

Appendix 2: mySolutionSpecies.phr – Additional database file specifying manually included species and rates.

```
SOLUTION 1
units mg/l
Temp 20
Na 787
Cl 1213
-water 0.50
```

Appendix 3: mySolution.phr – Included file that specifies the initial solution for all EC experiments.

```
KINETICS 1
Faraday
        INCLUDE$ rhoI.phr
        -formula Fe_di+2 1.0 OH- 2 Hdg 1 H2 1 H2O -2
OLDFe_di_ox
        -formula  Fe_di+2  -1.0  Fe_tri+3  1.0
CO2_Dissolution
        -formula HCO3- 1 H+ 1 H2O -1
INCLUDE$ myKCO2.phr
O2_Dissolution
        -formula O2 1
INCLUDE$ myKO2.phr
-steps 3000 in 50
-step_divide 500

INCREMENTAL_REACTIONS true
```

Appendix 4: myKinetics.phr – Included file that specifies the kinetic calculation to be executed by PHREEQC. Rates are specified in mySolutionSpecies.phr, Appendix 2. The files rhoI.phr, myKCO2.phr and myKO2.phr are included from the MATLAB environment and specify the current density, kinetic constant for CO_2 dissolution and kinetic constant for O_2 dissolution, respectively.

```
SURFACE 1
Surface name   #connected phase        -    #sites (mol/mol)   mineral area (m2/mol)
Hfo_wOH         MyFerrihydrite    equilibrium_phase     0.2           5.33E+04
Hfo_sOH         MyFerrihydrite    equilibrium_phase     0.005
-equilibrate 1
-sites_units density
```

Appendix 5: mySurface.phr – Included file that specifies the surface used for the adsorption calculations. The surface is connected to the $Fe(OH)_3$ equilibrium phase. All values are at their default literature value, as obtained from Dzombak and Morel[74].

JSW STEEL LIMITED

Vijayanagar Works, PO: Vidyanagar, Village : Tornagallu,Dist: Bellary,Karnataka-583275,INDIA
Regd. Office: JSW Centre, Bandra Kurla Complex, Bandra (East), Mumbai-400051.

MILL TEST/ INSPECTION CERTIFICATE (According to EN 10204 - 3.1)

TO,
ROBA METALS B.V
ZOMERDIJK, 0000 AA
NL

TC No / 0400923298 _ 40 / 7020005490
Date 27.12.2018

Product: Cold Rolled Annealed, Skinpassed & Oiled									Chemical Composition & Mechanical Properties											
									C %	Mn %	S %	P %	Si %	Al %	N %	YS MPa	UTS MPa	EL %	Ra µm	GL mm	Hard HRB
Specification : EN 10130_2006 DC01							MIN	⟶	-	-	-	-	-	-	-	280	270	28 (M)	0.80		
							MAX	⟶	0.1200	0.600	0.0450	0.045	-	-	0.0060	280	410	-	1.30		
Cast/Heat No.	Coil No.	T	X	W (mm)	X	L	Net Wt.	Gross Wt.	C %	Mn %	S %	P %	Si %	Al %	N %	YS MPa	UTS MPa	EL %	Ra µm	GL mm	Hard HRB
A400154	HC14422000	2.000	X	1000.0	X	Coil	9.060	9.130	0.035	0.210	0.008	0.014	0.013	0.058	0.0036	224	340	40.10	1.25	80MM	54.00
A400154	HC14421000	2.000	X	1000.0	X	Coil	8.700	8.770	0.035	0.210	0.008	0.014	0.013	0.058	0.0036	224	340	40.10	1.25	80MM	54.00
A400302	HC27221000	2.000	X	1000.0	X	Coil	8.885	8.950	0.034	0.210	0.008	0.016	0.009	0.058	0.0034	221	338	37.00	1.15	80MM	53.00
A400302	HC27222000	2.000	X	1000.0	X	Coil	9.185	9.255	0.034	0.210	0.008	0.016	0.009	0.058	0.0034	221	338	37.00	1.15	80MM	53.00
B400297	HC30831000	2.000	X	1000.0	X	Coil	8.845	8.910	0.035	0.220	0.008	0.009	0.011	0.060	0.0040	214	335	41.30	1.01	80MM	49.00
B400297	HC30832000	2.000	X	1000.0	X	Coil	9.200	9.270	0.035	0.220	0.008	0.009	0.011	0.060	0.0040	214	335	41.30	1.01	80MM	49.00
Total Weight in Metric Tonnes							53.875	54.285												
Total no of Batches							6													

Appendix 6: Steel characteristics (Inspection certificate)

10:2 fluorotelomer sulfonic acid
2H,2H,3H,3H-perfluoro-undecanoic acid
4:2 fluorotelomer sulfonic acid
6:2 fluorotelomer sulfonic acid
7H-perfluoroheptanoic acid (HPFHpa)
8:2 fluorotelomer phosphate diester (8:2 diPAP)
8:2 fluorotelomer unsaturated carbonic acid
8:2 fluorotelomer sulfonic acid (8:2)
ADONA
F53B (9Cl-PF3ONS)
N-methyl perfluorooctanesulfonamide (MeFOSA)
N-methyl perfluorooctanesulfonamide
PFOA branched
PFOS branched
perfluoro-1-octanesulfonamide-Ethylacetate (PFOSAA)
perfluoro-3,7-dimethyloctanoic acid
perfluoro-n-butanoic acid (PFBA)
perfluoro-n-decanoic acid (PFDeA)
perfluoro-n-heptanoic acid (PFHpa)
perfluoro-n-hexanoic acid (PFHxA)
perfluoro-n-nonanoic acid (PFNA)
perfluoro-n-octanoic acid (PFOA)
perfluorobutane sulfonamide (PFBSA)
perfluorobutanesulfonate (PFBS)
perfluorodecanesulfonate (PFDS)
perfluorododecanoic acid (PFDoDA)
perfluoroheptanesulfonate (PFHpS)
perfluorohexanesulfonate (PFHxS)
perfluorooctanesulfonamide (EtFOSA)
perfluorooctanesulfonamide (PFOSA)
perfluorooctanesulfonic acid (PFOS)
perfluoroohexadecanoic acid (PFHxDA)
perfluorooooctadecanoic acid (PFODA)
perfluoropentanesulfonate (PFPeS)
perfluoropentanoic acid(PFPeA)
perfluorotetradecanoic acid (PFTeDA)
perfluorotridecanoic acid (PFTrDA)
perfluoroundecanoic acid (PFUnDA)
n-Methylperfluoro-1-butanesulfonamide (MePFBSA)
perfluorobutanesulfonylamide(N-methyl)acetate (MeFBSAA)
sum PFOA
sum PFOS

Appendix 7: List of analyzed PFAS species

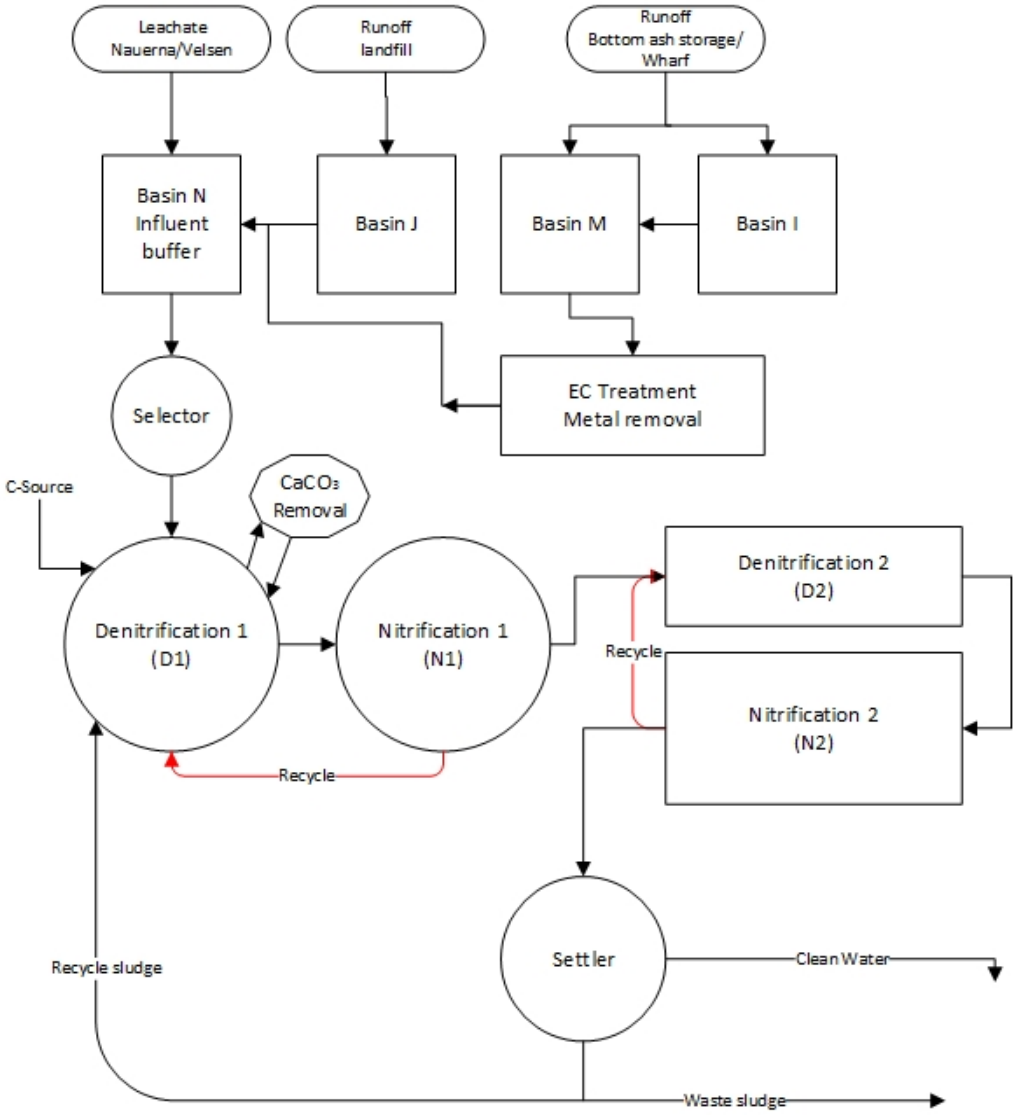

Appendix 8: Process overview of the leachate water treatment plant (LWTP). The main goal of the treatment is nitrogen removal, but two runoff streams are also treated for heavy metal removal in an EC set-up. The influent and effluent from this treatment plant were tested for PFAS removal in the current research.

	PFAS type	Conc. (mg/L)		Conc. (mg/L)		Conc. (mg/L)	
	Dilution factor:	1		2		10	
PFOS	Perfluorooctane sulfonic acid (PFOS)	93	95	48	48	8.8	9.3
	PFOS branched	18	18	8.7	9	1.7	1.7
	sum PFOS	110	110	57	57	10	11
PFOA	Perfluorooctanoic acid (PFOA)	85	81	40	39	7.2	7.5
	PFOA branched	0.14	0.12	0.12	0.12	<0.02	<0.02
	sum PFOA	85	81	40	39	7.2	7.5
PFBS	Perfluorobutane sulfonic acid (PFBS)	33	33	18	18	3.2	3.1
PFBA	Perfluorobutanoic acid (PFBA)	36	34	15	15	2.9	2.8

Appendix 9: Measured concentrations of all PFAS species in diluted samples of a stock solution.

		Measured concentration * dilution factor (mg/L)			
	dilution factor	sample 1	sample 2	mean	Deviation from undiluted (%)
PFOS (sum)	1	110	110	110	
	2	114	114	114	3.64
	10	100	110	105	-4.55
PFOA (sum)	1	85	81	83	
	2	80	78	79	-4.82
	10	72	75	73.5	-11.45
PFBS	1	33	33	33	
	2	36	36	36	9.09
	10	32	31	31.5	-4.55
PFBA	1	36	34	35	
	2	30	30	30	-14.29
	10	29	28	28.5	-18.57

Appendix 10: Calculated deviations in the measured concentration due to dilution.

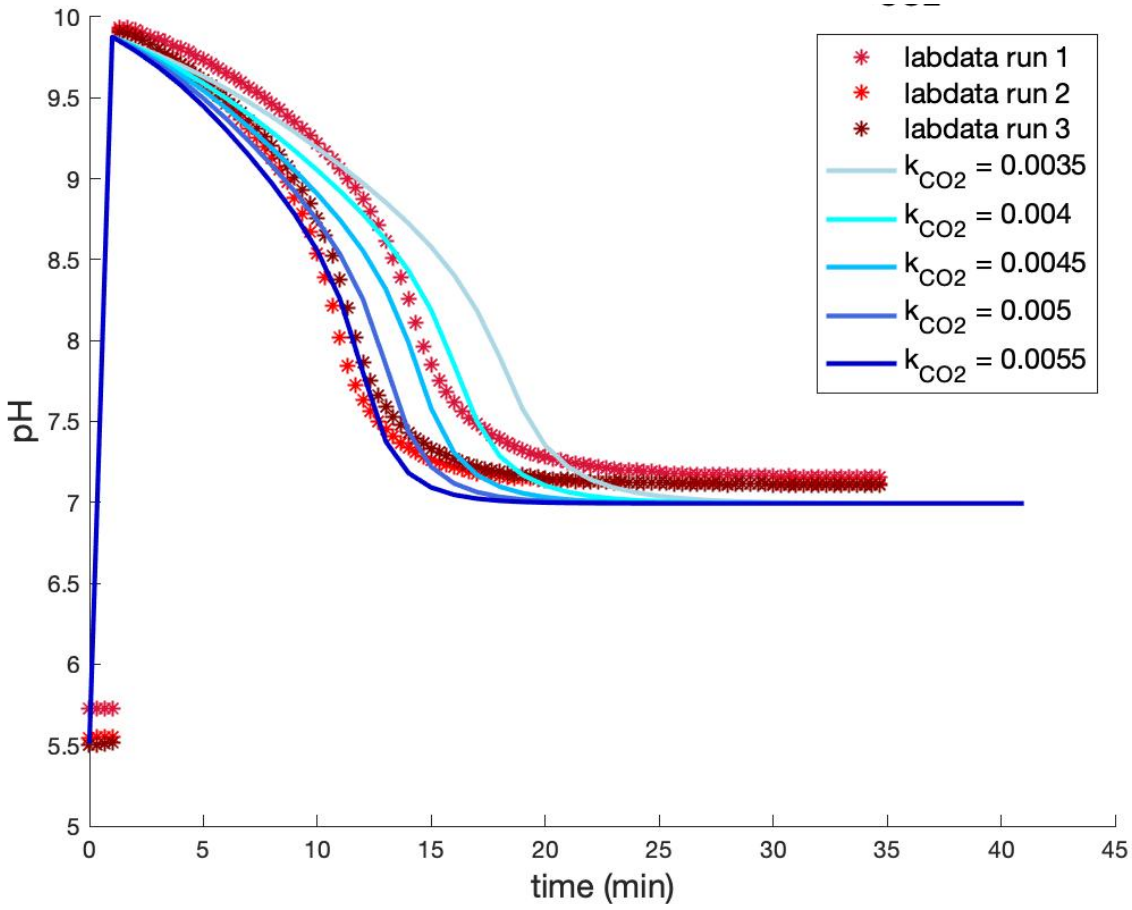

Appendix 11: pH over time in the determination of the CO_2 dissolution kinetics by addition of NaOH.

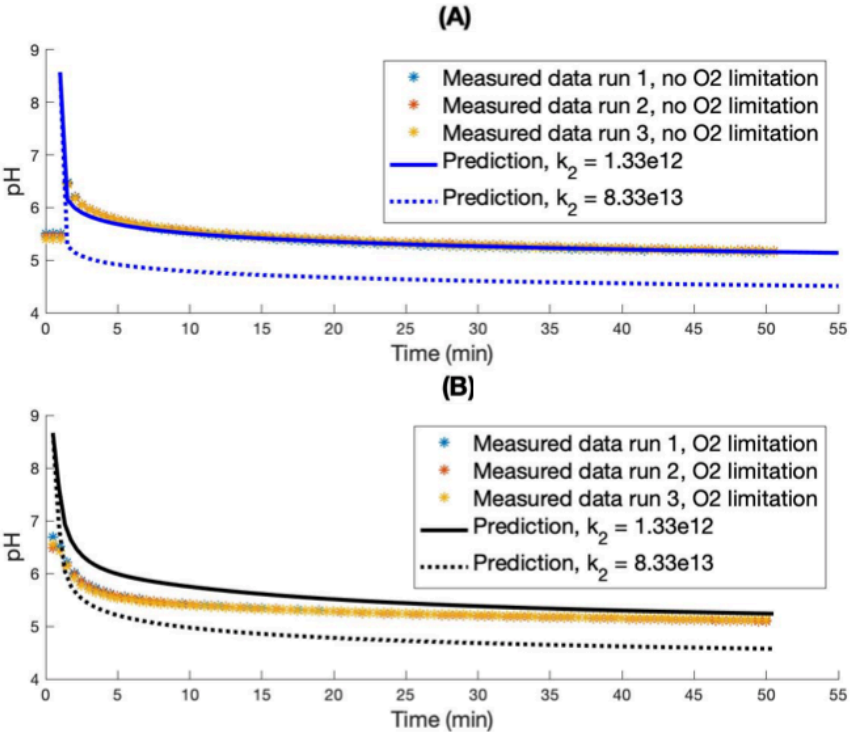

Appendix 12: pH vs time in $FeSO_4$ oxidation, (A) with and (B) without O_2 limitation, and the corresponding model fits with different kinetic constants (k_2) for Fe(II) oxidation.

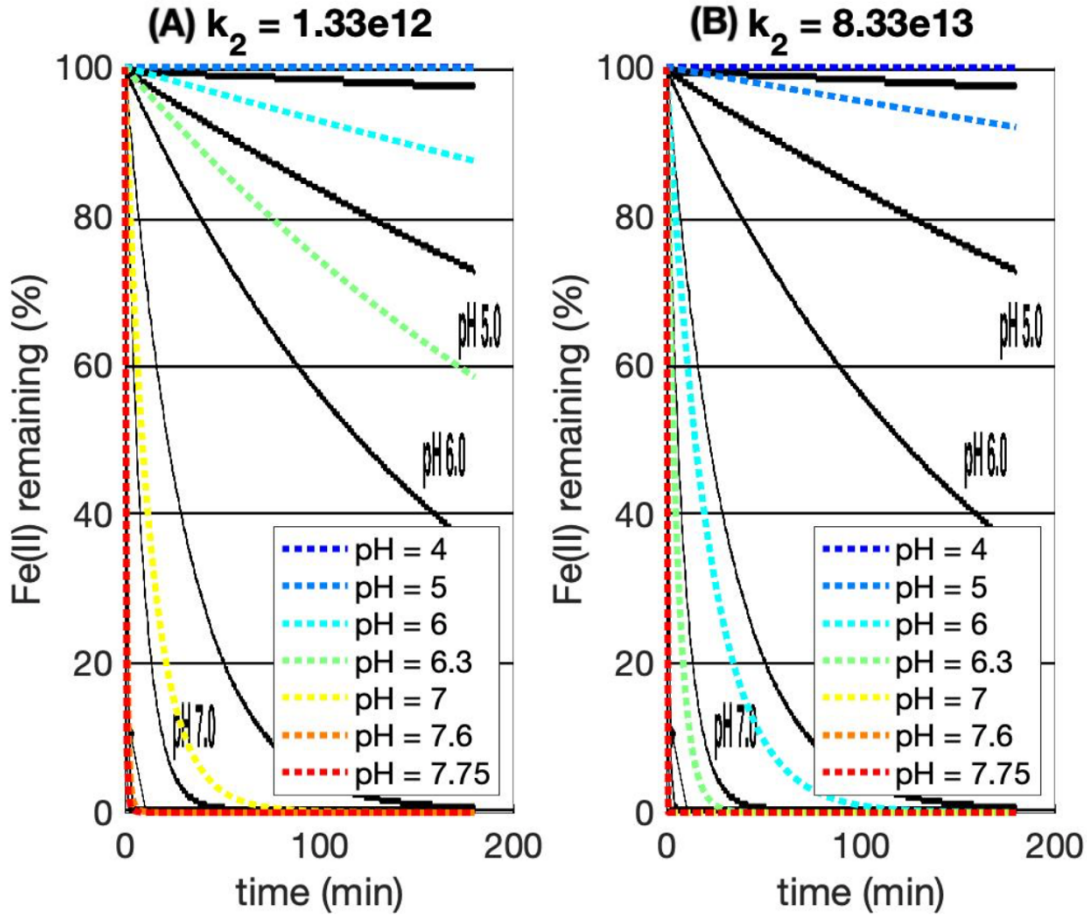

Appendix 13: Literature prediction of the effect of pH on Fe(II) oxidation[55] (solid black lines), as well as prediction found by the current model (dotted colored lines) with two different values for the kinetic constant k_2.

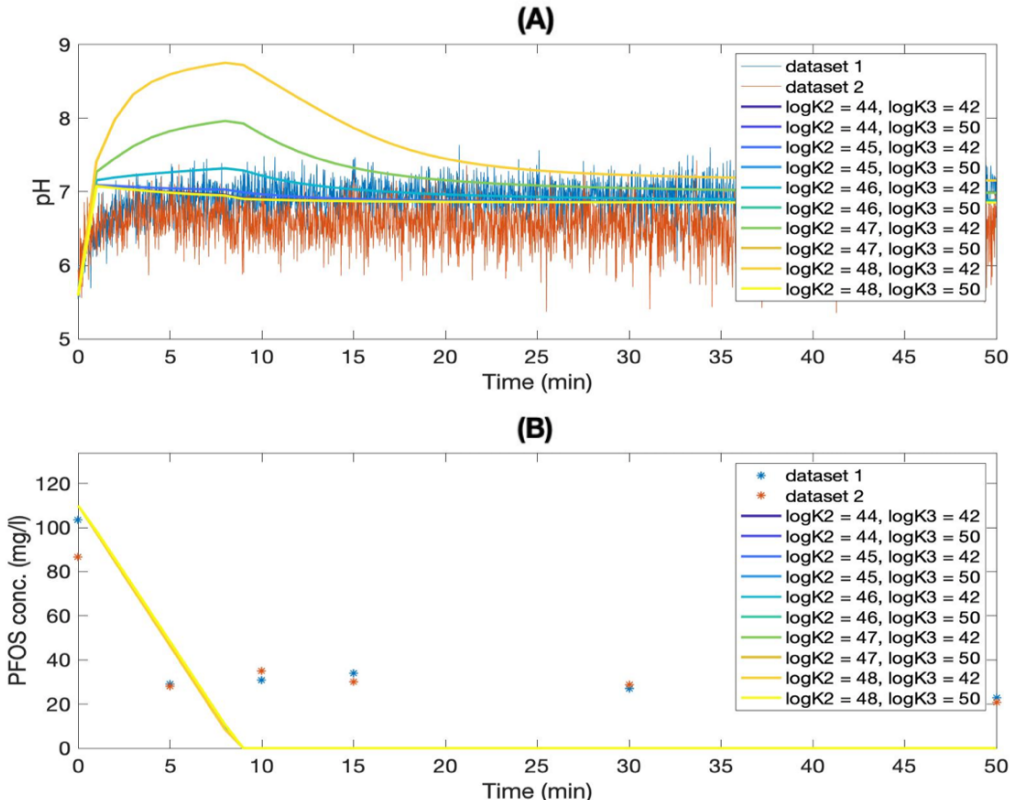

Appendix 14: (A) pH and (B) PFOS concentration model predictions for different log(K) values for PFOS binding. A peak in pH occurs when $log(K)_2$ is higher than $log(K)_3$, and the magnitude of the peaks increases for a larger difference in values. The removal results are constant for all tested combinations of log(K) values.

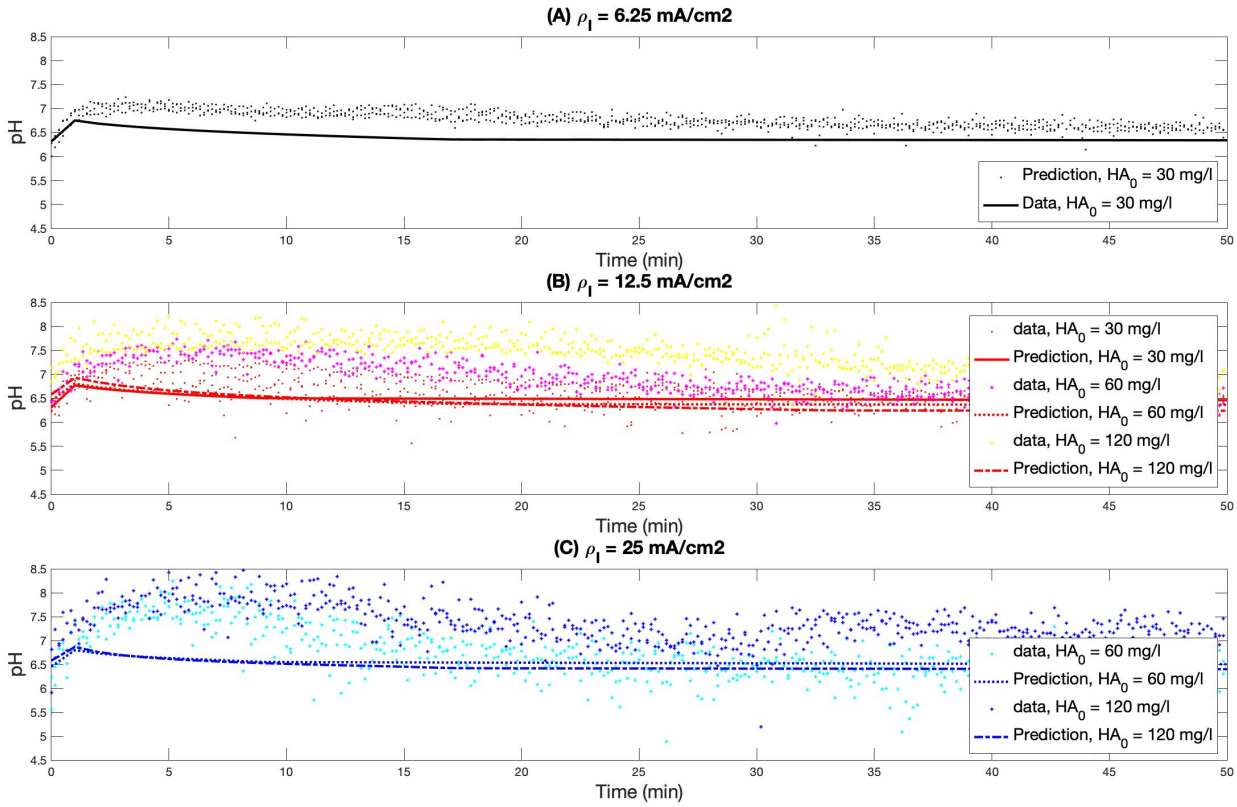

Appendix 15: pH vs time in EC experiments with removal of humic acid at different current densities and initial HA concentrations.

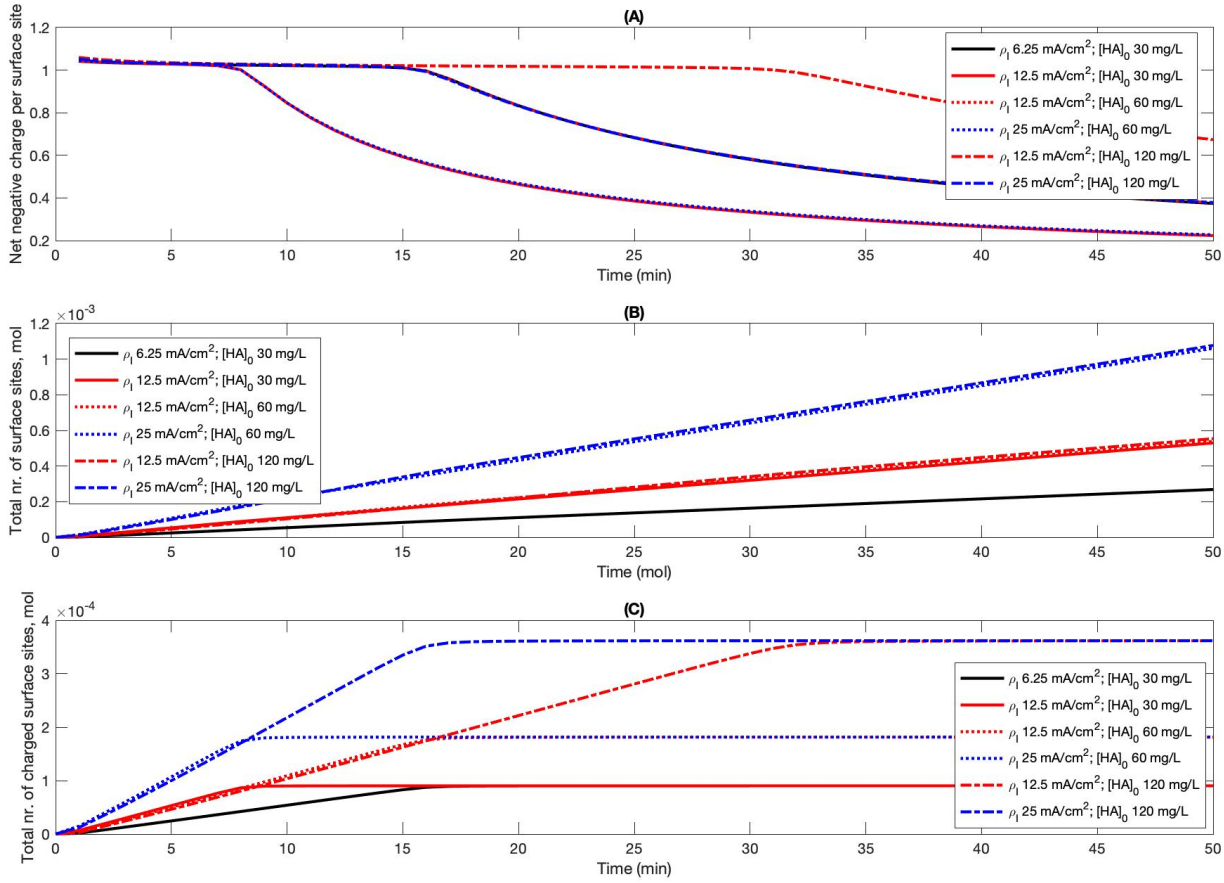

Appendix 16: (A) Average charge per surface site, (B) total number of surface sites and (C) total nr. of charged surface site over time during EC experiments with HA.

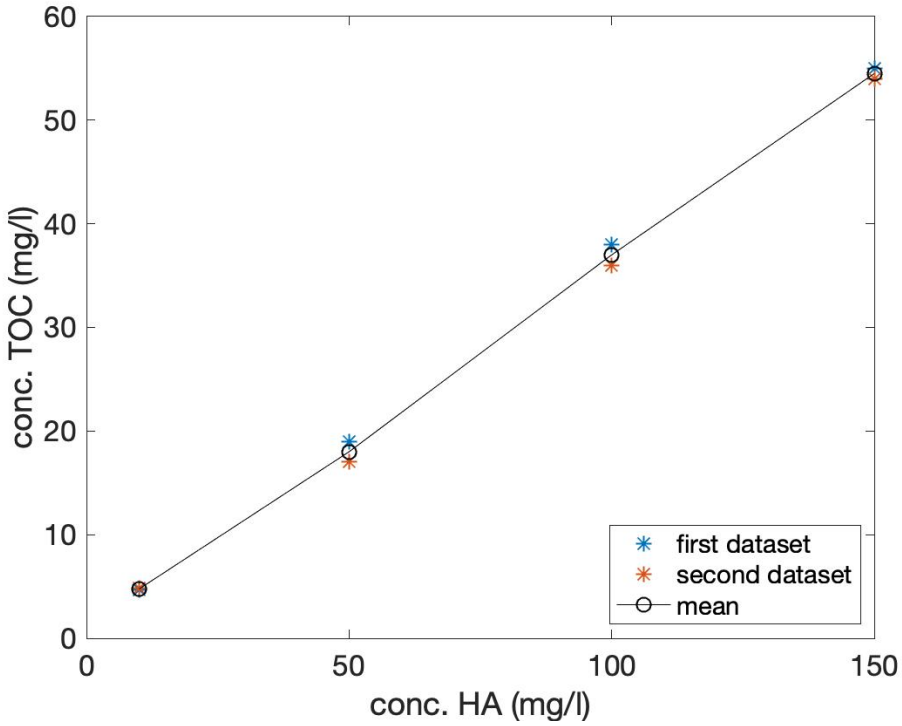

Appendix 17: Calibration of TOC data with HA concentration by means of measurements of humic acid solutions with known concentrations

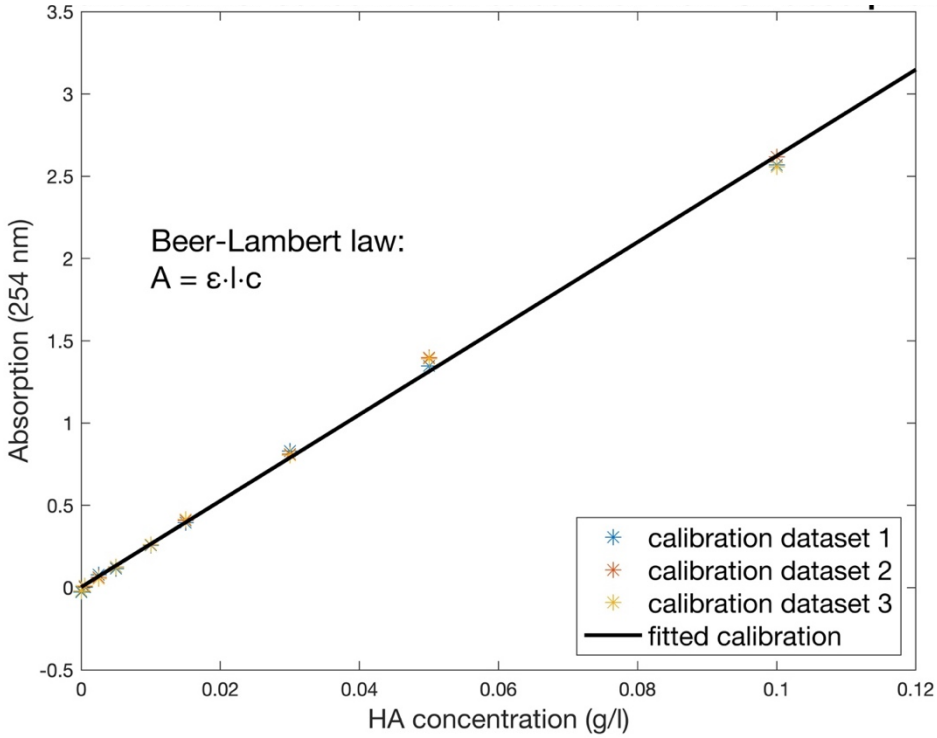

Appendix 18: Calibration curve for calculation of HA concentration from UV absorption at 254 nm. The Beer-Lambert law predicts a linear correlation between absorption and concentration, hence the dataset is fitted to a linear curve[91].

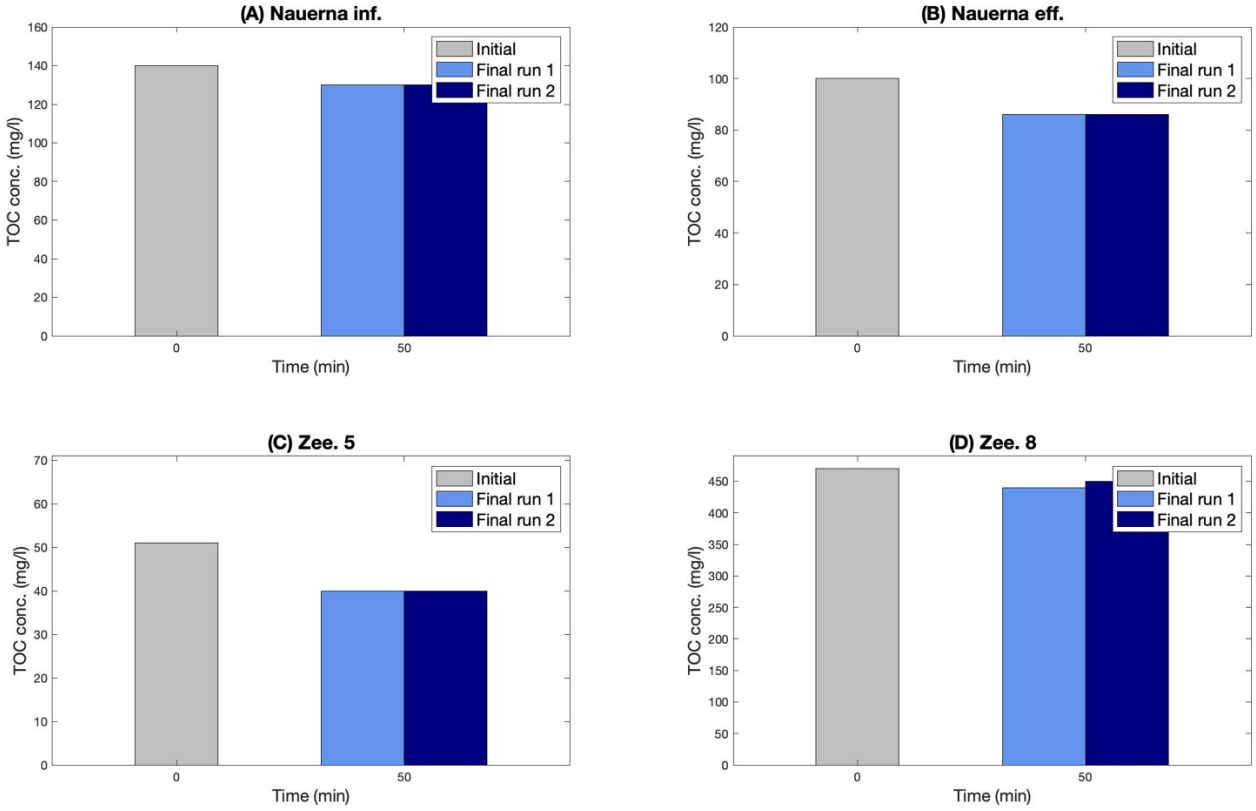

Appendix 19: Initial and final TOC concentration of the real wastewater samples.

a) Nauerna Influent – PFAS concentrations (µg/L)	0 min	5 min		25 min		50 min	
		Run a	Run b	Run a	Run b	Run a	Run b
PFOA branched	<2	<20	<20	<20	<20	<20	<20
PFOS branched	<2	46	<20	97	<20	70	<20
PFBA	<2	<20	<20	<20	<20	<20	<20
Perfluoroheptanoic acid (PFHpa)	<2	<20	<20	<20	<20	<20	<20
Perfluorohexanoic acid (PFHxA)	<2	<20	<20	<20	<20	<20	<20
Perfluoooctanoic acid (PFOA)	7.1	<20	<20	<20	<20	<20	<20
Perfluorobutane sulfonamide (PFBSA)	<2	<20	<20	<20	<20	<20	<20
PFBS	<2	<20	<20	<20	<20	<20	<20
perfluoro-1-decane sulfonic acid (PFDS)	<2	<20	<20	<20	<20	<20	<20
perfluoro-1-octane sulfonic acid (PFOS)	<2	230	82	430	110	350	<20
perfluoro-1-hexane sulfonic acid (PFHxDA)	2.4	<20	<20	<20	<20	<20	<20
Perfluoropentanoic acid (PFPeA)	<2	<20	<20	<20	<20	<20	<20
perfluorobutanesulfonylamide(N-methyl)acetate (MeFBSAA)	<2	<20	<20	<20	<20	<20	<20
sum PFOA	8	28	28	28	28	28	28
sum PFOS	3	280	96	530	120	420	28

b) Nauerna Effluent – PFAS concentrations (µg/L)	0 min	5 min		25 min		50 min	
		Run a	Run b	Run a	Run b	Run a	Run b
PFOA branched	<20	<2	<2	<20	<2	<20	<2
PFOS branched	<20	<2	<2	<20	<2	<20	<2
PFBA	<20	<2	2.7	<20	2.8	23	3.6
Perfluoroheptanoic acid (PFHpa)	<20	<2	<2	<20	<2	<20	<2
Perfluorohexanoic acid (PFHxA)	<20	<2	<2	<20	<2	<20	2.7
Perfluoooctanoic acid (PFOA)	<20	<2	11	<20	37	<20	46
Perfluorobutane sulfonamide (PFBSA)	<20	<2	<2	<20	<2	<20	<2
PFBS	<20	<2	<2	<20	<2	<20	<2
perfluoro-1-decane sulfonic acid (PFDS)	<20	<2	<2	<20	<2	<20	<2
perfluoro-1-octane sulfonic acid (PFOS)	<20	<2	2.9	<20	5.8	<20	2.8
perfluoro-1-hexane sulfonic acid (PFHxDA)	<20	<2	<2	<20	<2	<20	2.2
Perfluoropentanoic acid (PFPeA)	<20	<2	<2	<20	<2	<20	<2
perfluorobutanesulfonylamide(N-methyl)acetate (MeFBSAA)	<20	<2	<2	<20	<2	<20	<2
sum PFOA	28	3	12	28	38	28	47
sum PFOS	28	3	4	28	7	28	4

c) Zee. 5 – PFAS concentrations (µg/L)	0 min	5 min		25 min		50 min	
		Run a	Run b	Run a	Run b	Run a	Run b
PFOA branched	<2	<2	<2	<2	<2	<2	<2
PFOS branched	<2	<2	<2	<2	<2	<2	<2
PFBA	<2	2.5	<2	<2	2	<2	2.2
Perfluoroheptanoic acid (PFHpa)	<2	<2	<2	<2	<2	<2	<2
Perfluorohexanoic acid (PFHxA)	<2	<2	<2	<2	<2	2.3	<2
Perfluoooctanoic acid (PFOA)	<2	<2	<2	<2	<2	<2	<2
Perfluorobutane sulfonamide (PFBSA)	<2	<2	<2	<2	<2	<2	<2
PFBS	<2	<2	<2	<2	<2	<2	<2
perfluoro-1-decane sulfonic acid (PFDS)	<2	<2	<2	<2	<2	<2	<2
perfluoro-1-octane sulfonic acid (PFOS)	<2	35	3	<2	<2	18	<2

perfluoro-1-hexane sulfonic acid (PFHxDA)	<2	<2	<2	<2	<2	2.5	2.3
Perfluoropentanoic acid (PFPeA)	<2	<2	3.3	<2	<2	<2	<2
perfluorobutanesulfonylamide(N-methyl)acetate (MeFBSAA)	<2	6.6	8.9	<2	4	5.7	3.8
sum PFOA	3	3	3	3	3	3	3
sum PFOS	3	36	4	3	3	19	3

d) Zee. 8 – PFAS concentrations (µg/L)	**0 min**	**5 min**		**25 min**		**50 min**	
		Run a	**Run b**	**Run a**	**Run b**	**Run a**	**Run b**
PFOA branched	<2	<2	<2	<2	<2	<2	<2
PFOS branched	<2	<2	<2	<2	<2	<2	<2
PFBA	8.2	8.5	13	12	12	<2	13
Perfluoroheptanoic acid (PFHpa)	4.7	5.3	3.1	6.6	4.4	<2	3.5
Perfluorohexanoic acid (PFHxA)	16	12	17	22	14	<2	14
Perfluoooctanoic acid (PFOA)	<2	<2	10	<2	42	<2	48
Perfluorobutane sulfonamide (PFBSA)	<2	<2	<2	2.2	<2	<2	<2
PFBS	14	14	16	21	14	<2	13
perfluoro-1-decane sulfonic acid (PFDS)	<2	<2	<2	<2	<2	<2	<2
perfluoro-1-octane sulfonic acid (PFOS)	<2	<2	<2	<2	<2	<2	<2
perfluoro-1-hexane sulfonic acid (PFHxDA)	<2	<2	<2	<2	<2	<2	<2
Perfluoropentanoic acid (PFPeA)	7.2	8.4	7.3	9.7	6.6	<2	6.3
perfluorobutanesulfonylamide(N-methyl)acetate (MeFBSAA)	66	58	72	110	66	<2	79
sum PFOA	3	3	11	3	43	3	49
sum PFOS	3	3	3	3	3	3	3

Appendix 20a-d: PFAS concentrations in EC-treated real wastewater. a: Nauerna influent; b: Nauerna effluent; c: Zee. 5; d: Zee. 8.

Zee. 5 spiked with PFAS - concentrations (µg/L)	**0 min**	**5 min**		**25 min**		**50 min**	
		Run a	**Run b**	**Run a**	**Run b**	**Run a**	**Run b**
PFBA	43000	33000	33000	43000	46000	42000	41000
Perfluoroheptanoic acid (PFHpa)	76	43	26	33	47	48	35
Perfluorohexanoic acid (PFHxA)	63	39	42	61	<20	40	36
PFBS	77000	53000	61000	83000	84000	77000	73000
sum PFOA	83000	60000	65000	91000	93000	84000	84000
sum PFOS	28	67	240	77	610	100	730

Appendix 21: PFAS concentrations during treatment of Zee 5 wastewater with PFOA, PFBA and PFBS added.